

Department of Physics and Astronomy
University of Heidelberg

Diploma thesis
in Physics

submitted by
Niels Lörch

born in Karlsruhe
2010

A study of open quantum systems

This diploma thesis has been carried out by Niels Lörch
at the
Institut für Theoretische Physik der Universität Heidelberg
under the supervision of
Herrn Dr. Sandro Wimberger
and at the
Centre for Quantum Technologies in Singapore
under the supervision of
Herrn Prof. Dr. Berthold-Georg Englert

(A study of open quantum systems):

In the system we are studying in the first part of this thesis a Bose-Einstein condensate is loaded into the ground state of a one dimensional optical lattice. Acceleration of the lattice causes Landau-Zener like tunneling to higher energy bands at avoided crossings. This tunneling is the process we want to study. After the first Bloch period the condensate also populates higher bands and can tunnel back to the ground state, causing a difference between the short time and long time decay rate. We establish a Floquet theory based model to describe and manipulate this difference for various parameters of the lattice acceleration and the potential depth.

A system of three spin- $\frac{1}{2}$ -atoms allows the construction of a qubit - in the subspace of total angular momentum $j = \frac{1}{2}$ - that is not affected by any magnetic field activity on the magnetic moments of the atoms, provided that all three atoms experience the same magnetic field. If, however, there are stray fields of different direction or strength at the sites of the atoms, the qubit will slowly decohere. It is the objective of the second part of this thesis to examine the decoherence process and to establish the conditions, under which the lifetime of the qubit is sufficiently long for practical uses.

(Eine Untersuchung offener Quantensysteme):

Im ersten Teil dieser Arbeit untersuchen wir ein Bose-Einstein-Kondensat, das in den Grundzustand eines eindimensionalen optischen Gitters gebracht wird. Wenn man das Gitter beschleunigt kann das Kondensat am Rand der Brillouin Zone in höhere Energiebänder tunneln. Diesen Prozess wollen wir untersuchen und mit dem Landau-Zener Modell vergleichen. Nach der ersten Blochperiode bevölkert das Kondensat bereits höhere Bänder und kann wieder zurück in den Grundzustand tunneln, wodurch eine Differenz zwischen der Kurz- und Langzeiterfallsrate entstehen kann. Wir schlagen ein Modell auf Grundlage der Floquet Theorie vor, um diese Differenz für verschiedene Einstellungen der Gitterbeschleunigung und Potentialtiefe zu beschreiben.

In einem System aus drei Spin- $\frac{1}{2}$ -Atomen kann man ein qubit im Unterraum mit Drehmoment $j = \frac{1}{2}$ konstruieren, das von der Wirkung eines äußeren Magnetfelds auf die magnetischen Momente der Atome nicht beeinflusst wird, wenn die Feldstärke bei allen Atomen den gleichen Wert hat. Wenn es aber Streufelder verschiedener Richtung oder Stärke am Ort der Atome gibt, zerfällt das qubit langsam mit der Zeit. Im zweiten Teil dieser Arbeit wird der Dekohärenzprozess dieses Systems untersucht um herauszufinden, unter welchen Bedingungen die Lebensdauer des qubits lange genug für praktische Anwendungen ist.

Acknowledgements

I would like to thank Berge Englert and Sandro Wimberger for their great support and very helpful supervision of this diploma thesis and for being always ready to discuss with me about and teach me physics. I also want to thank Ghazal Tayebirad, Han Rui, Jun Suzuki and Ng Hui Khoo for the very good team work and cooperation throughout this project. Many thanks to Andreas Keil, Benoît Grémaud, Christian Miniatura, Christian Scheelen, Dario Poletti, Ennio Arimondo, John Goold, Klaus Mølmer, Lu Yin, Lü Xin, Marek Kuś, Patrick Plötz, Reinhard Werner, Susanne Pielawa and Syed Assad for their contribution of advice, discussions and ideas which were indispensable to make progress. I thank the Studienstiftung des deutschen Volkes, the Centre for Quantum Technologies in Singapore and the Institut für Theoretische Physik in Heidelberg for financial support. For the fantastic time they showed me in Singapore, I want to thank Berge Englert, his group and CQT for making me feel always very welcome and at home.

Inhaltsverzeichnis

1. Introduction	11
I. Landau-Zener tunneling in an optical lattice	15
2. Preliminaries	17
2.1. Abstract	17
2.2. Experimental setup	17
2.3. The quasi free particle model for periodic lattices	18
2.4. Comparison to 2×2 matrix model	19
2.5. Floquet's Theorem	20
2.6. Vitanov's paper	21
2.7. Niu and Raizen's paper	23
2.7.1. Introduction	23
2.7.2. Basic calculation	23
2.7.3. First approximation	25
2.7.4. Second approximation	26
2.7.5. Simplification of the integral	27
2.7.6. Summary: Results obtained	29
3. Methods, results and comparison to experiment	31
3.1. Notation	31
3.2. Comparison to the Pisa experiment	32
3.2.1. Lattice off	33
3.2.2. Switching on the lattice	33
3.2.3. Switching on the acceleration	34
3.2.4. Diabatic basis	34
3.2.5. Adiabatic basis	34
3.2.6. Comparability to experiment	36
3.3. Numerical Calculation and Implementation in MATLAB	38
3.3.1. How to choose M_1 and M_2	38
3.4. Resonances of γ and Z	39
3.4.1. Definition and Calculation of γ and Z	39
3.4.2. Explanation for the behavior of γ and Z	43
3.4.3. Manipulation of the resonances	49

II. Quantum storage in a decoherence-free subspace	53
4. Introduction and Preliminaries	55
4.1. Abstract	55
4.2. Motivation	55
4.3. Construction of the decoherence-free qubit	55
4.4. Time evolution of the setup	56
4.5. Methods for stabilization	58
4.5.1. Zeno effect	58
4.5.2. Stabilization by overall B-field	59
4.6. Summary	59
5. Methods, results and possible experiment	61
5.1. Master equation method	61
5.2. Spatially uncorrelated noise	64
5.2.1. Unstabilized setup	64
5.2.2. Zeno effect	65
5.2.3. Bias magnetic field	66
5.2.4. Conclusion	67
5.3. Spatially correlated noise	67
5.3.1. The gradient	67
5.3.2. Limitations of the linear model	69
5.3.3. Expansion point method	71
5.3.4. 2-point-correlation model	72
5.3.5. Unstabilized setup	72
5.3.6. Bias magnetic field	73
5.4. Different number of atoms	73
5.4.1. Four atoms	73
5.4.2. Two atoms	75
5.5. Numerical analysis	75
5.5.1. Method	75
5.5.2. Error estimation	76
5.5.3. Comparison to analytical equation	77
5.5.4. Strongly time correlated noise	78
5.6. Internal interaction	79
6. Entanglement in 2-qubit master equations	85
6.1. Motivation	85
6.2. White noise limit of unitary evolution...	85
6.2.1. ...cannot entangle if:	85
6.2.2. ...does entangle:	87
6.3. Inhibition of entanglement by noise	88

7. Conclusion and Outlook

91

1. Introduction

The experimental control of atoms in optical lattices has improved in recent years, which makes it possible to manipulate and study atomic quantum systems at an increasingly high level of precision [1, 2]. In this Diplom thesis we investigate two such open systems, in which the fidelity (survival probability) of the respective initial state decays due to a coupling to an external perturbation.

In the first part of the thesis, which was conducted in cooperation of Sandro Wimberger's group in Heidelberg with the experimental group of Ennio Arimondo in Pisa, we study the time evolution of a Bose-Einstein condensate (BEC) loaded into a one-dimensional optical lattice. Such systems are studied for their own purpose and are also used to simulate solid state systems that are not yet within the same level of experimental control. In the Pisa experiment [2, 3] it is possible to tune down the atom-atom interaction in the BEC to realize an effective one particle model. In addition, the experimentalists can achieve a very narrow probability distribution in momentum space, much smaller than the size of a Brillouin-zone. The BEC is initially distributed tightly around the center of the lowest energy band. In analogy to the behavior of electrons in a solid, adiabatic acceleration of the lattice causes Bloch oscillations [4, 5] of the condensate. A fast acceleration increases the diabatic coupling to higher bands, causing a decay of the ground state amplitude [2]. This is the decay process we want to study.

A similar experiment with a broad quasi-momentum distribution of a few Brillouin zones has been conducted with cold atoms [6, 7]. In the Pisa BEC experiment with its very narrow quasi-momentum distribution even the tunneling process occurring when the condensate is at the edge of the Brillouin zone can be resolved in time. That is one of the reasons why the earlier theory developed in [7] cannot be used for this setup, see section 2.7. We propose a different theoretical description in this thesis.

Denoting the potential height and wavenumber of the laser with V and k_L , the lattice acceleration with a and the atomic mass with m , the Hamiltonian of the system is

$$H = \int_{-\infty}^{\infty} dp \frac{1}{2m} (p + mat)^2 |p\rangle \langle p| + \int_{-\infty}^{\infty} dx V \cos(2k_L x) |x\rangle \langle x|. \quad (1.1)$$

Within a reasonable range of parameters with not too large values of V and a one can use the Landau-Zener model [8, 9] to approximate this Hamiltonian. In [10] this model is reviewed and analyzed with a focus on the predicted tunneling time between the two adiabatic states of the Landau-Zener model, see section 2.6. The adiabaticity of a system can be characterized within Landau-Zener theory by the parameter $\frac{V^2}{a}$, which is then proportional

1. Introduction

to the logarithm of the probability

$$P_a = e^{-\frac{\pi}{2} \frac{V^2}{a}} \quad (1.2)$$

of remaining in the ground state after each Bloch oscillation, see for example [11]. We will do the calculation with a very close numerical approximation of the Hamiltonian and derive that once the second band is populated, which happens after one Bloch period, phase dependent tunneling from the second band back to the lowest band causes deviations from the Landau-Zener tunneling probability. In a reasonable parameter range, this process accounts for resonances in two parameters that characterize the decay of the system, the long time decay rate γ (previously observed in [12]) and the adiabatic fidelity intercept Z , see section 3.4.1 for the detailed definitions and section 3.4 for the physical explanation of the resonances. Comparison with available experimental data (e.g. Figure 3.5) suggests that the physical setup is well described by our calculation and we can expect to see also the predicted Z resonances (Figure 3.10) in future experiments.

The second part of this thesis was conducted in Berge Englert's group in Singapore and studies the decay of quantum information protected by a decoherence free subspace (DFS) [13]. Such DFS schemes use the symmetries of a system to shield quantum information against a particular decay channel.

In our case the rotational symmetry of a special set of spin states is exploited [14]. The spin state of three spin- $\frac{1}{2}$ -atoms trapped in a triangular optical lattice decays because of exposure to random magnetic fields. The particular states we study can be used to encode a qubit that is invariant under rotation of all 3 atoms around the same angle. Such a rotation is the effect of a homogeneous field on the atoms. Thus only the inhomogeneous part of the B -field causes decoherence. While in the BEC system of part one the decay is due to a deterministic acceleration, we now have to solve a stochastic differential equation. The typical noise sources we have in mind are for example a current in the wires of a lab or a bypassing truck. The frequency of such noise is low and we can assume the fields to be classical. Another cause of decoherence is the internal interaction between the atoms. In total the Hamiltonian for our model is

$$H = H_0 + H_1 + H_i \quad (1.3)$$

consisting of the term

$$H_0 = \frac{\mu_B g_e}{2\hbar} \vec{B} \cdot \sum_j \vec{\sigma}_j \quad (1.4)$$

from an external constant field \vec{B} we apply for stabilization,

$$H_1(t) = \sum_j \frac{\mu_B g_e}{2\hbar} \vec{b}_j(t) \cdot \vec{\sigma}_j \quad (1.5)$$

caused by random fluctuation fields $\vec{b}_j(t)$ at each atom site j and a term

$$H_i = \frac{\mu_0}{4\pi r^3} \left[\vec{\mu}_A \cdot \vec{\mu}_B - 3(\vec{\mu}_A \cdot \hat{r})(\hat{r} \cdot \vec{\mu}_B) \right] \quad (1.6)$$

due to the atom-atom interaction. This study only cares about the effect of the Hamiltonian (1.3) on the system and is a first step for a realistic description of the experiment. In a real experiment there will in addition be other causes for decoherence, such as the center of mass motion, which have to be considered for a more detailed description.

In our study we derive a white noise limit master equation for the system in section 5.1 and develop a numerical scheme in section 5.5 to verify the analytical result. We analyze different methods to stabilize the setup, calculate the fidelity decay rates and compare the 3-atom case to similar setups with a different number of atoms.

In the first part of the thesis we studied an effective one particle problem. In the second part we have more particles and in our system the initial state is entangled. We got interested in the question which master equations can generate entanglement and which ones can not. We answer this question for two examples in chapter 6. The first example studies master equations with operators of the structure

$$H_1 \otimes H_2. \tag{1.7}$$

In the second example we start with an arbitrary master equation, which could in principle generate entanglement, and show that adding enough noise to the equation can completely suppress the creation of entanglement.

In the next chapter we start with the first part of the thesis. We introduce the experimental setup, sum up some preliminaries we need for our theory and give a review of two previous papers.

Teil I.

**Landau-Zener tunneling in an optical
lattice**

2. Preliminaries

In this chapter we give an abstract in 2.1, introduce the Arimondo group's experimental setup in section 2.2, rephrase some well known theoretical facts in sections 2.3-2.5 and give a review of two papers ([10, 7] describing similar physical situations in section 2.6 and 2.7.

2.1. Abstract

In the system we are studying a Bose-Einstein condensate is loaded into the ground state of a one dimensional optical lattice. Acceleration of the lattice causes Landau-Zener like tunneling to higher energy bands at avoided crossings. This tunneling is the process we want to study. After the first Bloch period the condensate also populates higher bands and can tunnel back to the ground state, causing a difference between the short time and long time decay rate. We establish a Floquet theory based model to describe and manipulate this difference for various parameters of the lattice acceleration and the potential depth.

2.2. Experimental setup

Before we develop the theoretical description, let us introduce the physical setup we want to study. For this information we quote and sum up the data given in the previous paper of Zenesini et al. [2].

In the experiment built by the group of Ennio Arimondo in Pisa a Bose-Einstein condensate of 5×10^4 rubidium-87 atoms is loaded into an optical dipole trap with a mean trap frequency of about 80 Hz along the longitudinal direction, creating a narrow momentum distribution of the condensate. In the next step a one dimensional optical lattice is switched on adiabatically within 100ms. The condensate should have enough time to adiabatically relax to the energy ground state. The lattice is created using two counter propagating lasers with wavelength $\lambda = 842nm$, leading to a sinusoidal potential with lattice constant $d_L = \frac{\lambda}{2} = 421nm$. A small tunable frequency difference between the lasers is used to control the acceleration of the lattice. This corresponds to an effective acceleration of the condensate in the rest frame of the lattice [3].

The experiment aims to measure the survival probability of the condensate to remain in a given state. This state can be defined either in a diabatic or in an adiabatic basis. In the diabatic basis the survival probability is defined as the probability of the condensate to stay in the momentum eigenstates of the first Brillouin zone in the lab system, normalized by the total number of atoms. The adiabatic survival probability is the probability to stay in the

2. Preliminaries

lowest energy band of the reference frame that moves with the lattice. If this probability is high, the condensate performs Bloch oscillations. More elaborate definitions and the details of the measuring protocol will be described in section 3.2, as we first need to introduce some notation to explain the protocol. There are some subtleties involving the measurement in adiabatic basis which are discussed in section 3.2.6.

So let us now start to rephrase some basic definitions from physics literature.

2.3. The quasi free particle model for periodic lattices

As we are interested in the behavior of a dilute BEC we can neglect atom-atom interaction by using a one particle model for our description. The quasi free particle model can be found in all books on solid state physics, for example [15, 16]. In case of a constantly accelerated one dimensional lattice with fixed wavelength and lattice depth, the Hamiltonian H in the reference frame of the lattice is

$$H = \int_{-\infty}^{\infty} dp \frac{1}{2m} (p + mat)^2 |p\rangle \langle p| + \int_{-\infty}^{\infty} dx V_0 \cos(2k_L x) |x\rangle \langle x|. \quad (2.1)$$

Here p is momentum, m is the atomic mass, a is the lattice acceleration, V_0 is the lattice depth and k_L is the wavenumber of the laser. Setting

$$\hbar = m = 2k_L = 1 \quad (2.2)$$

we can do the calculations in the dimensionless units of the system, the Schrödinger equation now reads

$$i\partial_t = H = \int_p dp \frac{1}{2} (p + at)^2 |p\rangle \langle p| + \int_x dx V_0 \cos(x) |x\rangle \langle x|. \quad (2.3)$$

Using Fourier transform to rewrite the second term of H in the momentum basis we get

$$H = \int_p dp \left(\frac{1}{2} (p + at)^2 \cdot |p\rangle \langle p| + \frac{l}{2} V_0 (|p\rangle \langle p+1| + |p+1\rangle \langle p|) \right). \quad (2.4)$$

After setting the lattice length $l = 1$ this simplifies to

$$H = \int_p dp \left(\frac{1}{2} (p + at)^2 \cdot |p\rangle \langle p| + \frac{V_0}{2} (|p\rangle \langle p+1| + |p+1\rangle \langle p|) \right). \quad (2.5)$$

Note: While $|p\rangle$ denotes the momentum eigenstate in the lab system, the prefactor $p + at$ is the momentum in the lattice system. One observes that there are only transitions between states with $\Delta p = p - p' \in \mathbb{Z}$. This allows to decompose the Hamiltonian: We rename the eigenstates and put them into groups with label $\kappa \in \left[-\frac{1}{2}, \frac{1}{2}\right) \subset \mathbb{R}$ and index $z \in \mathbb{Z}$ within each group:

$$p \longleftrightarrow z + \kappa. \quad (2.6)$$

Now we arrive at the decomposition

$$H = \int_{-0.5}^{0.5} d\kappa H_\kappa \quad (2.7)$$

with

$$H_\kappa = \sum_{z \in \mathbb{Z}} \left(\frac{1}{2} (\kappa + z + at)^2 \cdot |\kappa + z\rangle \langle \kappa + z| + \frac{V_0}{2} (|\kappa + z\rangle \langle \kappa + z + 1| + |\kappa + z + 1\rangle \langle \kappa + z|) \right). \quad (2.8)$$

To calculate the time evolution of any momentum eigenstates $|p_0\rangle = |z_0 + \kappa_0\rangle$ we only need the corresponding H_{κ_0} as there are no transitions between states with different κ , i.e. our Hilbert space \mathcal{H} can be written as

$$\mathcal{H} = \oplus_\kappa \mathcal{H}_\kappa \quad (2.9)$$

with independent time evolution for each \mathcal{H}_κ , which can be represented by a time dependent $\mathbb{N} \times \mathbb{N}$ matrix. The Hamiltonian for a given κ_0 then reads

$$H_\kappa = \frac{1}{2} \begin{pmatrix} \cdot & V_0 & 0 & 0 & 0 & 0 & 0 & 0 \\ V_0 & \cdot & V_0 & 0 & 0 & 0 & 0 & 0 \\ 0 & V_0 & (\kappa_0 - 1 + at)^2 & V_0 & 0 & 0 & 0 & 0 \\ 0 & 0 & V_0 & (\kappa_0 + at)^2 & V_0 & 0 & 0 & 0 \\ 0 & 0 & 0 & V_0 & (\kappa_0 + 1 + at)^2 & V_0 & 0 & 0 \\ 0 & 0 & 0 & 0 & V_0 & \cdot & V_0 & 0 \\ 0 & 0 & 0 & 0 & 0 & V_0 & \cdot & V_0 \end{pmatrix} \quad (2.10)$$

in the momentum eigenbasis of the lab. The matrix (2.10) is the basis for our further study. The eigenvalues and eigenvectors of the corresponding time independent matrix are referred to as energy bands in literature. In this study we will sloppily refer also to the energy eigenstates of the time dependent Hamiltonian (2.10) as energy bands, but we have to keep in mind that now there is coupling between those bands.

2.4. Comparison to 2×2 matrix model

To calculate the time evolution of a state which is in the lowest energy band one can approximate the Hilbert space with the two states with lowest kinetic energy and use the Hamiltonian (2.10) for those states only. This approximation is good, as long as the potential energy is small, i.e. $V_0 \ll E_{\text{rec}}$ and one only simulates one Bloch period. During this time one only needs the two states with lowest kinetic energy to represent the two states with lowest overall energy. The 2×2 Landau-Zener matrix with initial condition in the lowest band then corresponds to the Hamiltonian

$$H_{\text{LZ}} = \frac{1}{2} \begin{pmatrix} (\kappa_0 - 1 + at)^2 & V \\ V & (\kappa_0 + at)^2 \end{pmatrix} \quad (2.11)$$

which is equivalent to

$$H_{\text{LZ}} = \frac{1}{2} \begin{pmatrix} (\kappa_0 - 1)^2 - 2at & V \\ V & \kappa_0^2 \end{pmatrix} \quad (2.12)$$

2. Preliminaries

because the time evolution of the system only depends on the difference ΔE of the diagonal terms of $H_{LZ}(t)$ and not on their absolute value. This is a 2×2 matrix with $\Delta E \propto t$ and constant V , i.e. the well known Landau Zener model [8, 9] with finite initial time.¹

This finite initial time is one of the reasons why the transition probabilities in the Wannier Stark system may differ from the asymptotic² Landau-Zener probabilities, which only depended on $\frac{V^2}{F}$. Another reason is the existence of more than two bands in reality, which becomes important for large values of V . A detailed discussion of these differences can be found in section 3.

Let us briefly explain the choice of entries for the 2×2 matrix: One might wonder why the state with kinetic energy $(\kappa_0 + 1 + at)^2$ is not included in this model, as it has the same kinetic energy as $(\kappa_0 - 1 + at)^2$ at $t = 0$. But while $(\kappa_0 + 1 + at)^2$ and $(\kappa_0 - 1 + at)^2$ become degenerate at $t = 0.5$ and the $(\kappa_0 + 1 + at)^2$ -state is the lowest kinetic energy state after one period the energy of $(\kappa_0 + 1 + at)^2$ grows even further and has little contribution to the state with lowest overall energy during the whole time considered. So we only need those states to describe the dynamics in our regime. The validity of this statement will become clearer in section 3.

2.5. Floquet's Theorem

As we will later use the monodromy operator (sometimes also referred to as "one-cycle Floquet operator") U from Floquet's Theorem for the analysis of the solution of our differential equation in the adiabatic basis, we briefly quote it here:

Floquet's Theorem Let $t \in \mathbb{R}$, E a Banach space over \mathbb{C} , $A(t) \in L(E, E)$ a continuous function of time with period T . For the linear differential equation

$$\dot{x} = A(t)x \tag{2.13}$$

there exist T -periodic functions $Q \in C^1(\mathbb{R}, GL(E, E))$ and $B \in L(E, E)$ such that the time evolution operator $U(t)$ which is a solution to the linear equation for initial condition $x(0) = \mathbf{I}$ can be represented as

$$U(t) = Q(t)e^{tB}. \tag{2.14}$$

There exists also $\tilde{B} \in L(E, E)$ so that the monodromy operator $U(T)$ can be expressed as

$$U(T) = e^{T\tilde{B}}. \tag{2.15}$$

For details see for example [17].

¹see 2.6 for details of the Landau-Zener model.

²time evolution from $t \rightarrow -\infty$ to $t \rightarrow \infty$.

2.6. Vitanov's paper

Vitanov [10] analyzes some properties of the Landau-Zener model, which corresponds to our 2×2 model introduced in 2.4. Vitanov's paper gives some results on the applicability of the Landau-Zener model in various situations, for example a series of multiple avoided crossings, which we want to study. He studies the limits of the LZ model which are due to the finite tunneling times in real systems. Another limitation for its use is the assumption of a two-level system, which we discuss in section 3. Raizen uses the Landau-Zener 2×2 -model for the description of a Wannier-Stark-system in a regime (2.32) with limited V . Also equation (2.30) is an interesting result, which would be interesting to check experimentally. That is why we give a short summary of the paper:

Putting the quasimomentum at $t = 0$ to $\kappa_0 = \frac{1}{2}$, which is at the boundary of the Brillouin zone we translate Vitanov's results to our notation from section 2.4. This adjustment is needed to have the maximal adiabatic coupling occur at $t = 0$ in both notations. In the diabatic basis the Hamiltonian can be written as

$$H_d = \frac{1}{2} \begin{pmatrix} -at & V \\ V & at \end{pmatrix}. \quad (2.16)$$

Vitanov also defines the scaled time τ and scaled coupling ω ,

$$\tau = \sqrt{\frac{a}{2}}t, \quad \omega = \frac{V}{\sqrt{\frac{a}{2}}} \quad (2.17)$$

for his analysis. (Vitanov uses the notation $\beta = \sqrt{\frac{a}{2}}$ and $\Omega = V$, but to make this work consistent we stick with the notation introduced earlier.) The eigenvectors of H_d are

$$|1\rangle_a = \cos \theta |1\rangle_d - \sin \theta |2\rangle_d \quad (2.18)$$

and

$$|2\rangle_a = \sin \theta |1\rangle_d + \sin \theta |2\rangle_d \quad (2.19)$$

with

$$\tan 2\theta = \frac{\omega}{\tau}. \quad (2.20)$$

The adiabatic Hamiltonian then has the form

$$H_a = \begin{pmatrix} -\sqrt{\tau^2 + \omega^2} & -\frac{\omega}{2(\tau^2 + \omega^2)} \\ -\frac{\omega}{2(\tau^2 + \omega^2)} & \sqrt{\tau^2 + \omega^2} \end{pmatrix}. \quad (2.21)$$

The analytical solution of the diabatic and adiabatic survival probability, obtained by Landau and Zener [8, 9] are

$$P_d(\tau) = \frac{\omega^2}{2} \exp\left(-\pi\omega^2/4\right) \left| D_{-1+i\omega^2/2} \left(\tau\sqrt{2} \exp(3i\pi/4) \right) \right|^2 \quad (2.22)$$

2. Preliminaries

and

$$P_a(\tau) = \exp\left(-\pi\omega^2/4\right) \left| D_{i\omega^2/2}\left(\tau\sqrt{2}\exp(3i\pi/4)\right) \cos(\theta(\tau)) - \left(\omega/\sqrt{2}\right) \exp(-i\pi/4) D_{-1+i\omega^2/2}\left(\tau\sqrt{2}\exp(3i\pi/4)\right) \sin(\theta(\tau)) \right|^2. \quad (2.23)$$

From (2.21) we can see that the coupling in the adiabatic basis is a Lorentzian Function of time and the unitless coupling time τ_c , which is the time at which the probabilities of $|1\rangle_a$ and $|2\rangle_a$ change the most, is proportional to ω ,

$$\tau_c \propto \omega. \quad (2.24)$$

On a side note, which is not in Vitanov's paper but interesting for our further study, we also calculate also the behavior of the coupling time in units of T_{Bloch} : As $t \propto \sqrt{\frac{1}{a}}\tau$ and $T_{Bloch} \propto \frac{1}{a}$ we get for the coupling time t_c in units of T_{Bloch}

$$\frac{t_c}{T_{Bloch}} \propto \sqrt{\frac{1}{a}}\omega a \propto V. \quad (2.25)$$

Looking at the adiabatic survival probability

$$P_a = \exp(-\pi\omega^2) \quad (2.26)$$

we see that ω can also be interpreted as the adiabaticity parameter and P_a is only a function of ω . Now I will state the new important results of Vitanov that we are interested in.

He defines the adiabatic jump time for $\omega \ll 1$ as

$$\tau_a^{\text{jump}} = \frac{P_a(-\infty) - P_a(\infty)}{P'_a(0)} \quad (2.27)$$

which has the simple geometric interpretation of the fidelity gap divided by the slope at $t = 0$. As the time evolution of P_a is a monotonic function of time in this regime, the definition can be applied and the jump time is just like the coupling time proportional to ω . The result

$$\tau_a^{\text{jump}} = 2\omega \exp(-\pi\omega^2/2) \approx 2\omega \quad (2.28)$$

is in good agreement with what one would expect. For large values of ω however the time evolution of P_a does not look like a jump, but there is a peak at $t = 0$ and after the peak P_a decreases again. (2.27) clearly does not make sense in this regime, as $P'_a(0)$ cannot be interpreted as the jump speed anymore, as can be seen in Figure 3 of his paper. Vitanov introduces the new definition

$$\tau_a^{\text{jump}} = \tau_a^{\text{jump,f}} - \tau_a^{\text{jump,i}} \quad (2.29)$$

with $\tau_a^{\text{jump,i}}$ defined as the initial time of the jump, where P_a crosses $\epsilon P_a(\infty)$ for the first time, where ϵ is to be chosen small. The final time $\tau_a^{\text{jump,f}}$ of the jump is defined in an analogous way. For $\omega \gg 1$ this results in an ω^2 -exponentially growing jump time,

$$\tau_a^{\text{jump}} \approx \left(\frac{4}{\epsilon}\right)^{\frac{1}{6}} \omega^{\frac{1}{3}} \exp(\pi\omega^2/6), \quad (2.30)$$

which one would not expect on the first look at the Lorentzian coupling (2.21). Note however, that the time of coupling of course still scales as ω , because the change of adiabatic probabilities is still only related to the Lorentzian function. As the jump time is defined relative to the jump probability, its exponential increase is only due to the exponential decrease of the jump probability with increasing ω .

2.7. Niu and Raizen's paper

2.7.1. Introduction

This section analyzes the steps of Niu and Raizen's theory [7] for Landau-Zener tunneling. The starting point is the same Hamiltonian

$$H = \int_p dp \left(\frac{1}{2} (p + at)^2 \cdot |p\rangle \langle p| + \frac{V_0}{2} (|p\rangle \langle p+1| + |p+1\rangle \langle p|) \right), \quad (2.31)$$

in natural units as (2.5). Raizen's initial condition is a uniform full occupation of the lowest energy band. He assumes that transitions from the first to the second band are almost adiabatic i.e. the survival probability in the adiabatic basis after one Bloch period is high, while the transition probability from the second to the third band and the probabilities of all higher transitions are nearly 1 after each Bloch period. According to [18] this corresponds to the condition

$$a'_c < a < a_c \quad (2.32)$$

for the acceleration a . In the same units as above $a_c = \pi V_0^2/2$ is the critical acceleration for the first gap and $a'_c = \pi V_0^4/4$ for the second gap.

A second condition for the validity of this theory is

$$V_0 < 1 \quad (2.33)$$

as otherwise one would have to consider more than two momentum eigenstates just to reproduce the lowest band. This result can be obtained by first order perturbation theory for the eigenstates. Both conditions can be graphically represented by Figure 1 in [7]. While it is clear that V should be small for the 2 band model to be approximately valid, choosing the boundary at $V = 1$ is the author's choice.

2.7.2. Basic calculation

We do the derivation of Raizen's theory in a slightly different order than in the original paper, as this will make clearer the connection to the theory introduced in section 3. Let us first realize that the 2×2 matrix theory is quite good in the regime $V_0 < 1$. Thus it can already be used for the simulation of one Bloch period (see 3.3.1). Let us denote the eigenstates of the 2×2 matrix as $|0\rangle(t)$ and $|1\rangle(t)$ with energies $E_0 < E_1$.

For $t < T_{\text{Bloch}}$ we only need 2 states if we are within the regime of validity for V (see

2. Preliminaries

(2.33)) and a good approximation of the time evolution of a state in the lowest band with quasimomentum κ is the expansion

$$|\psi^\kappa(t)\rangle = \sum_{n=0}^1 b_n^\kappa(t) \exp\left(-i \int_0^t dt' E_n^\kappa(t')\right) |n^\kappa\rangle(t) \quad (2.34)$$

with initial condition

$$\begin{aligned} b_0^\kappa &= 1 \\ b_1^\kappa &= 0. \end{aligned} \quad (2.35)$$

For better readability we drop the κ and t dependencies for now. Applying Schrödinger's equation to this expansion in energy eigenstates

$$i\partial_t \sum_{n=0}^1 b_n \exp\left(-i \int_0^t dt' E_n\right) |n\rangle = \sum_{n=0}^1 E_n b_n \exp\left(-i \int_0^t dt' E_n\right) |n\rangle \quad (2.36)$$

we get the time evolution of b_0 and b_1 at time t .

$$\sum_{n=0}^1 \dot{b}_n \exp\left(-i \int_0^t dt' E_n\right) |n\rangle = - \sum_{n=0}^1 b_n \exp\left(-i \int_0^t dt' E_n\right) |\dot{n}\rangle \quad (2.37)$$

Projection on $\langle 0|\dot{0}\rangle$ yields

$$\dot{b}_0 \exp\left(-i \int_0^t dt' E_0\right) = -b_1 \exp\left(-i \int_0^t dt' E_1\right) \langle 0|\dot{1}\rangle + \underbrace{0}_{\propto \langle 0|\dot{0}\rangle}. \quad (2.38)$$

We used $\langle 0|\dot{0}\rangle = 0$ which is due to $\langle 0|0\rangle \equiv 1$. Solving for \dot{b}_0 we get

$$\dot{b}_0 = -b_1 \exp\left(-i \int_0^t dt' (E_0 - E_1)\right) \langle 0|\dot{1}\rangle \quad (2.39)$$

and the analogous result

$$\dot{b}_1 = -b_0 \exp\left(-i \int_0^t dt' (E_1 - E_0)\right) \langle 1|\dot{0}\rangle \quad (2.40)$$

for \dot{b}_1 . Next we integrate (2.40) with initial condition $b_1(0) = 0$

$$b_1 = 0 - \int_0^t dt' b_0(t') \exp\left(-i \int_0^{t'} dt'' (E_1 - E_0)\right) \langle 1|\dot{0}\rangle \quad (2.41)$$

and using $\langle 1|\dot{0}\rangle = -\langle 0|\dot{1}\rangle$ we plug it into (2.39) and integrate again to get

$$\dot{b}_0(t) = - \int_0^t dt' \exp\left(i \int_{t'}^t dt'' (E_0 - E_1)\right) \langle 1|\dot{0}\rangle_{t'} \langle 0|\dot{1}\rangle_t b_0(t') \quad (2.42)$$

2.7.3. First approximation

Now Raizen uses the slowly varying amplitude approximation $b_0(t) \approx b_0(t')$, which is applicable as long as b_0 does not change too much.

$$\dot{b}_0(t) = - \int_0^t dt' \exp \left(\underbrace{i \int_{t'}^t dt'' (E_0 - E_1)}_{:=\tilde{W}^\kappa(t,t')} \right) \langle 1|\dot{0}\rangle_{t'} \langle 0|\dot{1}\rangle_t b_0(t). \quad (2.43)$$

For each κ we now have a kernel \tilde{W}^κ for the amplitude b_κ that can be used to solve the approximate differential equation for one Bloch period for initial condition $b_0^\kappa(0) = 1$ with

$$b_0^\kappa(t) = \exp \left(- \int_0^t dt' \int_0^{t'} dt'' \tilde{W}^\kappa(t', t'') \right). \quad (2.44)$$

We can write the squared amplitude as

$$\begin{aligned} (b_0^\kappa(t))^2 &= \exp \left(- \int_0^t dt' \int_0^{t'} dt'' (2\Re(\tilde{W}^\kappa) + 2\Im(\tilde{W}^\kappa))(t', t'') \right) \\ &= \exp \left(- \int_0^t dt' \int_0^{t'} dt'' 2\Re(\tilde{W}^\kappa)(t', t'') \right) \exp \left(- \int_0^t dt' \int_0^{t'} dt'' 2\Im(\tilde{W}^\kappa)(t', t'') \right) \end{aligned} \quad (2.45)$$

and because the second factor in this expression is only a phase we get

$$P_\kappa = |b_0^\kappa(t)|^2 = \exp \left(- \int_0^t dt' \int_0^{t'} dt'' W^\kappa(t', t'') \right) \quad (2.46)$$

with kernel $W^\kappa = 2\Re(\tilde{W}^\kappa)$ for the survival probability P_κ . To find the survival probability for a uniformly populated lowest band at $t = 0$ we integrate κ over its full range $[-0.5, 0.5]$:

$$P_{\text{tot}} = \int_{-0.5}^{0.5} d\kappa P_\kappa = \int_{-0.5}^{0.5} d\kappa \exp \left(- \int_0^t dt' \int_0^{t'} dt'' W^\kappa(t', t'') \right). \quad (2.47)$$

Taking the time derivative we see that P_{tot} is the solution of the differential equation

$$\dot{P}_{\text{tot}} = - \int_{-0.5}^{0.5} d\kappa \left(\int_0^t dt' W^\kappa(t, t') \right) P_\kappa. \quad (2.48)$$

2.7.4. Second approximation

To simplify the further calculation another approximation is used and the κ integral is drawn into the exponent:

$$P = \exp \left(- \int_{-0.5}^{0.5} d\kappa \int_0^t dt' \int_0^{t'} dt'' W^\kappa (t', t'') \right). \quad (2.49)$$

Taking again the time derivative we see that the approximation solves the different differential equation

$$\dot{P} = - \left(\int_{-0.5}^{0.5} d\kappa \int_0^t dt' W^\kappa (t, t') \right) P. \quad (2.50)$$

This second approximation can be summed up as replacing a differential equation of the form

$$\dot{P} = - \int_{-0.5}^{0.5} d\kappa b^\kappa(t, t') P_\kappa \quad (2.51)$$

by

$$\dot{P} = - \int_{-0.5}^{0.5} d\kappa \int_{-0.5}^{0.5} d\kappa' b^\kappa(t, t') P_{\kappa'} \quad (2.52)$$

i.e., averaging a_κ over all possible quasimomenta. That is why in Raizen's approximation the steplike substructure on the time scale of Bloch oscillations, which is superposed on the long term exponential decay is not present. Thus Raizen's theory is only valid on a longer timescale, the discreteness of steps in the tunneling processes [12, 2] cannot be seen.

Equation (2.49) can only describe one Bloch oscillation, as there is only one avoided crossing in this 2×2 matrix approximation. To get the equation

$$P = \exp \left(- \int_{-\infty}^{0.5} d\kappa \int_0^t dt' \int_0^{t'} dt'' W^\kappa (t', t'') \right) \quad (2.53)$$

for tunneling also after one period we have to extend the κ -integration to $-\infty$. To get an equation that is mathematically better to handle we also extend the integral to $+\infty$, which does not modify the tunneling rate too much, as long as V is small, but introduces a nice temporal symmetry for the expression

$$P = \exp \left(- \int_0^t dt' \int_0^{t'} dt'' \int_{-\infty}^{\infty} d\kappa W^\kappa (t', t'') \right) \quad (2.54)$$

which we want to use in the next section at (2.61).

2.7.5. Simplification of the integral

We now show that the expression

$$W(t', t'') = \int_{-\infty}^{\infty} d\kappa W^\kappa(t', t'') \quad (2.55)$$

in

$$P = \exp \left(- \int_0^t dt' \int_0^{t'} dt'' W(t', t'') \right) \quad (2.56)$$

can be written as a one dimensional function of the time difference $\tilde{t} = |t' - t''|$ only. This enables us to simplify the two dimensional integration in (2.56) to a one dimensional one. For this purpose, let us write down $\tilde{W}^\kappa(t', t'')$ very explicitly as

$$\tilde{W}^\kappa(t', t'') = \exp \left(i \int_{t''}^{t'} dt''' (E_0(\kappa + at''') - E_1(\kappa + at''')) \right) \langle 1|0 \rangle_{\kappa+at''} \langle 0|1 \rangle_{\kappa+at'}. \quad (2.57)$$

In the next step we use

$$a \frac{d}{d\kappa} = \frac{d}{dt} \quad (2.58)$$

and rewrite the time integration as a κ integration in the exponent. The derivative of a function f with respect to κ will be denoted as f' and write

$$\tilde{W}^\kappa(t', t'') = \exp \left(i \int_{\kappa+at''}^{\kappa+at'} d\kappa' \frac{E_0(\kappa') - E_1(\kappa')}{a} \right) a^2 \langle 1|0' \rangle_{\kappa+at''} \langle 0|1' \rangle_{\kappa+at'}. \quad (2.59)$$

Now we introduce the new variable $\tilde{t} = t' - t''$ and use it to replace all dependencies of t' .

$$\tilde{W}^\kappa(t', t'') = \exp \left(i \int_{\kappa+at''}^{\kappa+at''+a\tilde{t}} d\kappa' \frac{E_0(\kappa') - E_1(\kappa')}{a} \right) a^2 \langle 1|0' \rangle_{\kappa+at''} \langle 0|1' \rangle_{\kappa+at''+a\tilde{t}}. \quad (2.60)$$

As we will finally integrate κ from $-\infty$ to ∞ anyway, see (2.55), we can just as well shift the integration in κ , rename

$$\kappa + at'' + a \frac{\tilde{t}}{2} \rightarrow \kappa \quad (2.61)$$

and get rid of all t'' to arrive at

$$\tilde{W}^\kappa(\tilde{t}) = \exp \left(i \int_{\kappa-a\frac{\tilde{t}}{2}}^{\kappa+a\frac{\tilde{t}}{2}} d\kappa' \frac{E_0(\kappa') - E_1(\kappa')}{a} \right) a^2 \langle 1|0' \rangle_{\kappa-a\frac{\tilde{t}}{2}} \langle 0|1' \rangle_{\kappa+a\frac{\tilde{t}}{2}}. \quad (2.62)$$

For the survival probability we need to take twice the real part of this expression to obtain $W^\kappa = 2\Re(\tilde{W}^\kappa)$. The real part of the exponential is a cosine and the real part of

$$\langle 1|0' \rangle_{\kappa-a\frac{\tilde{t}}{2}} \langle 0|1' \rangle_{\kappa+a\frac{\tilde{t}}{2}} \quad (2.63)$$

2. Preliminaries

can be calculated by diagonalizing the Hamiltonian (2.12), which is now of the form

$$H = \begin{pmatrix} z & \frac{V_0}{2} \\ \frac{V_0}{2} & 0 \end{pmatrix} \quad (2.64)$$

with z set to either $z_1 = \kappa - a\frac{\tilde{t}}{2}$ or $z_2 = \kappa + a\frac{\tilde{t}}{2}$ respectively. We calculate the normalized eigenvectors $|0\rangle$ and $|1\rangle$ for all values of κ . Taking derivatives and plugging everything in we get

$$\langle 1|0'\rangle_{\kappa-a\frac{\tilde{t}}{2}} \langle 0|1'\rangle_{\kappa+a\frac{\tilde{t}}{2}} = \frac{z'_1 z'_2 V_0^2}{4(E_{10}(z_1)E_{10}(z_2))^2} \quad (2.65)$$

after a long but straight forward calculation. Here we used the notation $E_{10} := E_1 - E_0$. We now have

$$W^\kappa(\tilde{t}) = \cos \left(i \int_{\kappa-a\frac{\tilde{t}}{2}}^{\kappa+a\frac{\tilde{t}}{2}} d\kappa' \frac{E_0(\kappa') - E_1(\kappa')}{a} \right) \frac{z'_1 z'_2 V_0^2 a^2}{2(E_{10}(z_1)E_{10}(z_2))^2} \quad (2.66)$$

which corresponds to equation (6) in Raizen's paper [7]. Using $z' \equiv 1$ and $E_{10}^2 = V_0^2 + z^2$ we can now write W^κ explicitly as

$$W^\kappa(\tilde{t}) = \cos \left(i \int_{\kappa-a\frac{\tilde{t}}{2}}^{\kappa+a\frac{\tilde{t}}{2}} d\kappa' \frac{E_0(\kappa') - E_1(\kappa')}{a} \right) \frac{V_0^2 a^2}{2((V_0^2 + z_1^2)(V_0^2 + z_2^2))^2}. \quad (2.67)$$

Measure transformation: Having shown that $W = W(\tilde{t})$ we now prove that

$$P = \exp \left(- \int_0^t dt' \int_0^{t'} dt'' W(t', t'') \right) = \exp \left(- \int_0^t d\tilde{t} (t - \tilde{t}) W(\tilde{t}) \right). \quad (2.68)$$

For this purpose we introduce new time variables

$$\begin{pmatrix} \tilde{t} \\ \tilde{z} \\ \tilde{t} \end{pmatrix} = \varphi \begin{pmatrix} t' \\ t'' \end{pmatrix} \quad (2.69)$$

with

$$\varphi = \begin{pmatrix} 1 & -1 \\ 0 & \frac{\sqrt{2}}{2} \end{pmatrix} \quad (2.70)$$

and

$$\det(\varphi) = \frac{\sqrt{2}}{2}. \quad (2.71)$$

This yields

$$P = \exp \left(- \int_0^t d\tilde{t} \int_0^{\sqrt{2}(t-\tilde{t})} d\tilde{t} W(\tilde{t}) \det(\varphi) \right) = \exp \left(- \int_0^t d\tilde{t} (t - \tilde{t}) W(\tilde{t}) \right). \quad (2.72)$$

2.7.6. Summary: Results obtained

Let us sum up the predictions from Raizen's theory for its regime of validity: On a long time scale the decay rate is proportional to the Landau-Zener tunneling probability multiplied by an unimportant prefactor of $(\frac{\pi}{3})^{2n}$. So the tunneling rate must be adjusted and it cannot resolve resonances as reported by [12]. Because of the replacement of (2.51) with (2.52) the time evolution is always averaged over one Bloch period, as there are no probability amplitudes for each κ but only one for each band. Thus the steplike structure of the fidelity in each Bloch period, as observed for example in [2], is not resolved.

On a short time scale there is not a purely exponential decay of P . Let us explain this within Niu's theory: The overall time derivative is taken as the integral over the coupling from all possible values of κ within the Landau-Zener model (2.54). Most of the coupling in the adiabatic basis takes place in the region of the avoided crossing (2.21). While at $t = 0$ the probability amplitude at the crossing is still equal to 1, for later times the coupling at the crossing converges to a smaller, constant value and the decay rate becomes perfectly exponential. The time scale on which this transition of the amplitude of the crossing takes place is just the Landau-Zener coupling time, which is proportional to $\frac{V}{a}$, as can be obtained for example in Vitanov's paper, see (2.6). This result is visualized in Figure 4 of Raizen's paper. The Landau-Zener model is the basis of Raizen's paper and the correspondence of the time scales within his theory directly follows from it.

While in Raizen's paper the change in decay rate is a finite time effect of the Landau-Zener theory, it is indeed due to the population of the second band, which can beat back to the first band, if the adiabaticity parameter V^2/a is not too small and so the tunneling rate from second to third band is not 100% per Bloch period. This tunneling process from the second to the first band is also responsible for resonances in the long time decay rate, as we will see in the following chapter.

3. Methods, results and comparison to experiment

This chapter is a summary of the results we obtained in our study of the Wannier-Stark system. We introduce a convenient notation in section 3.1 to describe the time evolution of the experiment in section 3.2 and properly define the different measurement bases. In section 3.3 the details of the numerical calculation are documented. Section 3.4 develops a method to describe the resonances in the parameters γ and Z , which will be defined to characterize the behavior of the system. We propose a method to manipulate those resonances in future experiments.

3.1. Notation

In this section we build up on the notation introduced in section 2.3. In order to properly define what is often referred to as "adiabatic" basis in literature we also introduce the energy eigenbasis for a given potential V_0 in both the lab system and in the lattice system. For each Hamiltonian $H(\kappa, V_0, t)$ we can write the time dependent eigenbasis as $\{|\kappa, \tilde{n}\rangle_{V_0}(t)\}$ with $\kappa \in \left[-\frac{1}{2}, \frac{1}{2}\right)$ as the quasimomentum index in the lab frame and $\tilde{n} \in \mathbb{N}$ as the index for the energy level in the lattice frame, i.e.

$$E_0 < E_1 < E_2 < E_3 < \dots \quad (3.1)$$

The index V_0 indicates the dependence of the eigenbasis on the potential strength. These eigenstates correspond to the band structure of the quasi-free particle model in the lattice reference frame, see Figure 3.1 and Figure 3.2 for the band structure from different perspectives.

If $V_0 = 0$ it is simply the momentum eigenbasis in the lattice frame which can be seen in the $V \rightarrow 0$ limit with parabolic energy levels as seen in Figure 3.1. With growing V the eigenstates get more and more localized and the band structure becomes equidistant for the states with $V \gg E_{\text{kin}}$. This limit can be seen from the perspective of Figure 3.2. The tilde was used for the \tilde{n} to indicate that these energies refer to the lattice frame and not the lab frame. From now on we will always use tilde to indicate that a variable refers to the lattice frame, while variables without tilde refer to the lab frame. For example we used κ without tilde in the energy eigenbasis above, because this quasimomentum still refers to the lab frame! Note that transformation between those frames can be done quite easily, for example $\tilde{p} = p + at$ is the momentum in the lattice frame.

3. Methods, results and comparison to experiment

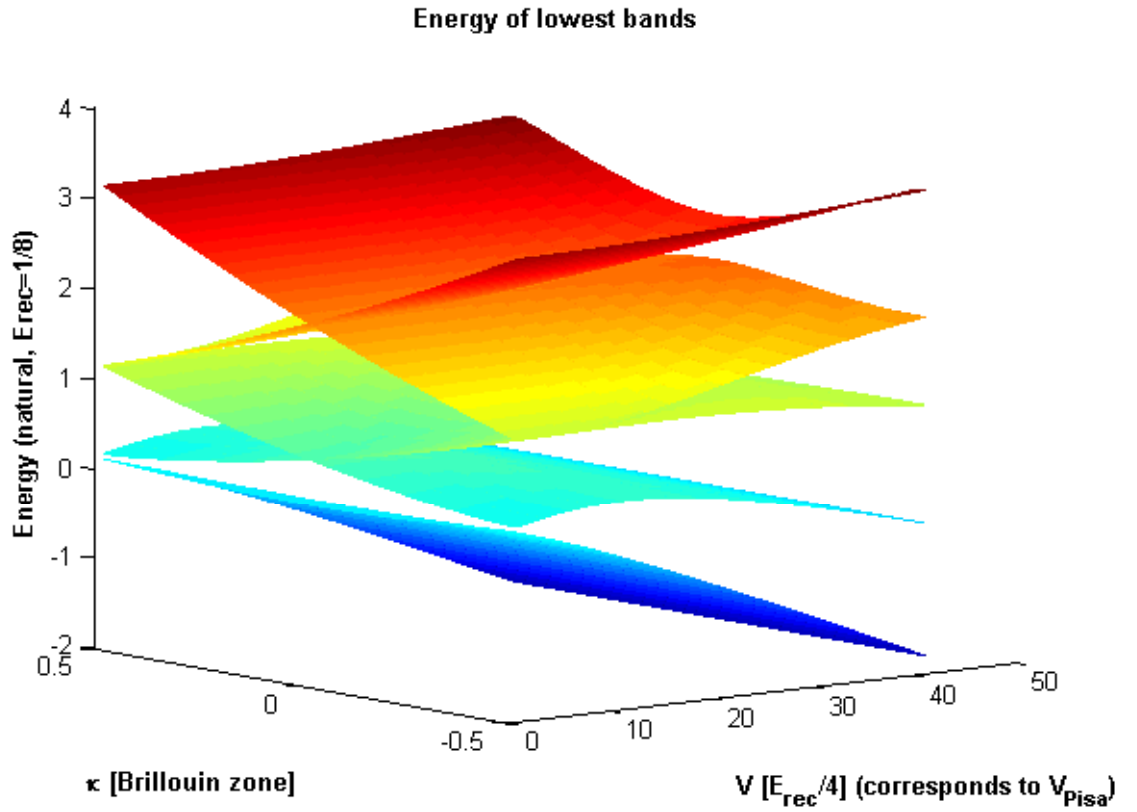


Abbildung 3.1.: Band structure of the system as a function of the potential V , seen from the perspective of small V . We see that for small V already the lowest band is close to a parabola for higher bands the band structure converges to the parabola form of the free particle model.

In the experiment the energy eigenbasis in the lattice frame with quasimomentum index from the lab system, $\{|\kappa, \tilde{n}\rangle_{V_0}(t)\}$, is referred to as the "adiabatic basis". The time independent momentum eigenbasis in the lab system, $\{|\kappa, n\rangle_{V=0}\}$, is referred to as the diabatic basis. The survival probability is defined as the probability for the state to stay in the state with $\tilde{n} = 0$ in the adiabatic case and $n = 0$ for the diabatic case. For our calculation the label $\tilde{\kappa}$ are usually not needed and we stick to κ .

3.2. Comparison to the Pisa experiment

Let us now use the notation from (3.1) to predict the survival probability for the experiment [2]. We will look at what happens in the experiment described in section 2.2 step by step:

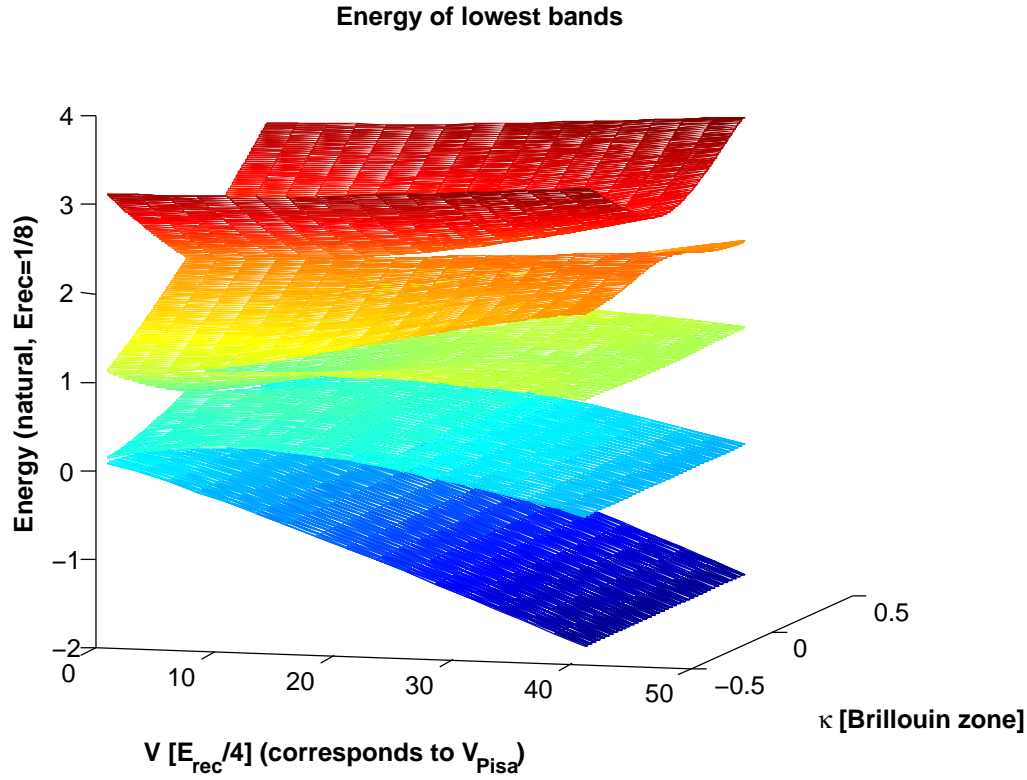


Abbildung 3.2.: Band structure of the system as a function of the potential V , seen from the perspective of large V . We see that for large V the lowest bands are almost flat, and for higher bands the structure is getting closer to a parabola.

3.2.1. Lattice off

At first the lattice is not yet turned on ($V = 0$, $a = 0$) and the BEC is prepared in a state

$$|\psi_1\rangle = \int_{-\infty}^{\infty} dp f(p) |p\rangle_{V=0} \quad (3.2)$$

where f is a density function representing the initial momentum distribution of the BEC, i.e.

$$\int_{-\infty}^{\infty} dp f(p) = 1. \quad (3.3)$$

3.2.2. Switching on the lattice

As a second step the lattice is slowly turned on, while the acceleration a remains 0. Thus the initial state has enough time to relax adiabatically (compare to the adiabatic theorem

3. Methods, results and comparison to experiment

[19]) and each state $|p\rangle_{V=0}$ relaxes to $|p\rangle_{V=V_0}$. We now have¹

$$|\psi_2\rangle = \int_{-\infty}^{\infty} dp f(p) |p\rangle_{V=V_0}. \quad (3.4)$$

3.2.3. Switching on the acceleration

Now acceleration is switched on for some time t_0 . The state evolves according to Schrödinger equation and we get the solution

$$|\psi(t_0)\rangle = |\psi_3\rangle = \lim_{N \rightarrow \infty} \prod_{n=1}^N \exp\left(-iH\left(\frac{t_0}{N}n\right)\frac{t_0}{N}\right) |\psi_2\rangle. \quad (3.5)$$

To do the time integration numerically we just use a large enough N instead of the limit $N \rightarrow \infty$.

3.2.4. Diabatic basis

Finally the survival probability is measured in either the diabatic basis or the adiabatic basis: The survival probability P_d in what was defined as the diabatic basis in the experiment is the probability of the condensate to stay in the momentum eigenstates ($V = 0$ basis) of the first Brillouin zone in the lab(!) system normalized by the total number of atoms:

$$P_d(t_0) = \frac{\int_{-0.5}^{0.5} dp |\langle \psi_3 | p \rangle_{V=0}|^2}{\langle \psi_1 | \psi_1 \rangle}. \quad (3.6)$$

Note that this definition implies that with growing V the fidelity at $t = 0$ decreases and is not equal to 1 anymore, as the lowest overall energy eigenstate deviates more and more from the lowest kinetic energy eigenstate. Figure 3.3 is a comparison of our numerical method to a calculation done by Ghazal Tayebirad using the position basis and published in [2]. The agreement is very good not only in this picture but for all parameters tested we could not see any deviation.

Figure 3.4 compares an experimental data set from the Pisa group with our numerical result. As there are systematic uncertainties in various parameters (V , F_0 , ...) at the Pisa experiment [2], one might have to try using a different parameter set to get better agreement.

3.2.5. Adiabatic basis

For the adiabatic basis the survival probability p_a is defined as the probability for $|\psi_3\rangle$ to be in the energy eigenstate of H of the first Brillouin zone, i.e. the state with lowest energy $E_{\tilde{n}}$ for given κ again normalized by the number of atoms.

$$P_a(t_0) = \frac{\int_{-0.5}^{0.5} d\kappa \left| \langle \psi_3 | \kappa, \tilde{n} = 0 \rangle_{V=V_0}(t_0) \right|^2}{\langle \psi_1 | \psi_1 \rangle} \quad (3.7)$$

¹However there is a remark by Riccardo Mannella in [3] stating that the initial state might be some mixture between the adiabatic and diabatic initial state. This issue is still to be clarified with the experimentalists.

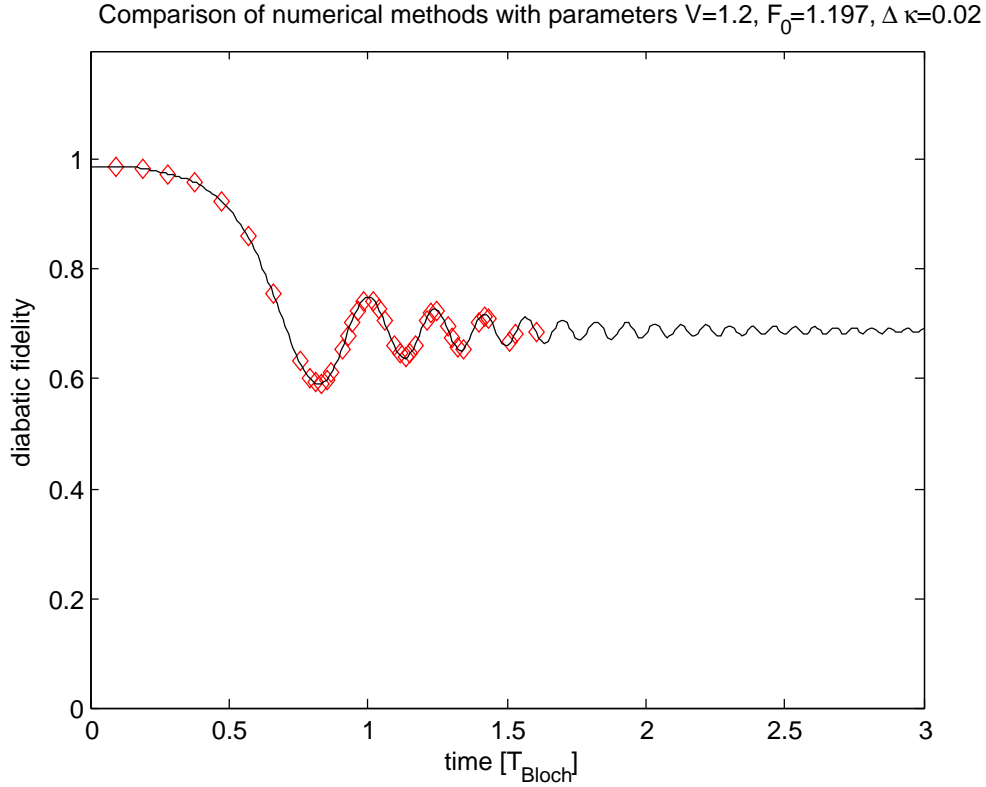


Abbildung 3.3.: Comparison to Ghazal’s numerical result (in diabatic basis): The results of this study for the time evolution in the diabatic basis are plotted as a straight line and compared to the result obtained by Ghazal, who does the calculation in the position basis. Her result is plotted as red diamonds. The agreement is almost perfect. In [2, 3] this data is used to predict the experiment. The initial distribution is a Gaussian with variance $\Delta\kappa = 0.02$ and mean at $\kappa = 0$.

Note that $|\kappa, \tilde{n} = 0\rangle_{V=V_0}(t)$ is time dependent because of the accelerating lattice. As indicated by the tilde of \tilde{n} , this adiabatic survival probability refers to the reference frame of the lattice.

In Figure 3.5 is a plot of a calculation for the adiabatic basis compared to the experimental data. As in the diabatic case also here there are systematic uncertainties in the experimental parameters [2]. These calculations were used for [3] to improve the predictions made by a cut-off method, which is also presented in the paper. There is some ambiguity about what probability is measured in the adiabatic case. See the following section 3.2.6 on this issue.

3. Methods, results and comparison to experiment

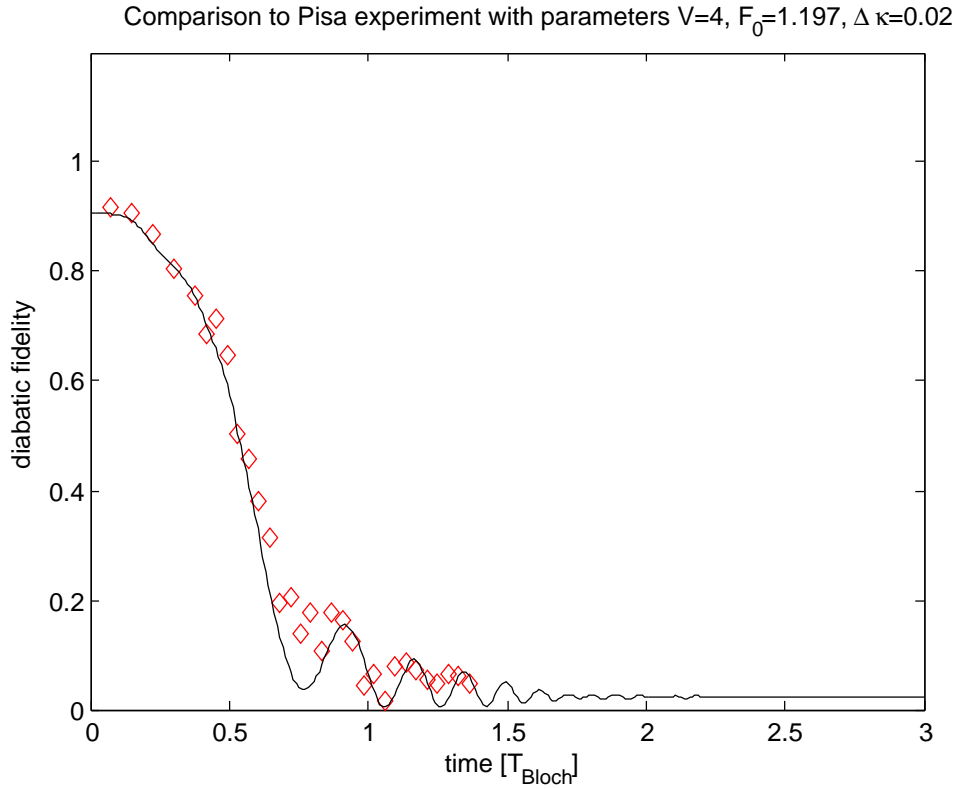


Abbildung 3.4.: Comparison to Pisa experiment (diabatic basis): The result of this study for the diabatic basis is compared to a set of experimental data (red diamonds). The straight line is our prediction. The initial distribution is a Gaussian with variance $\Delta\kappa = 0.02$ and mean at $\kappa = 0$.

3.2.6. Comparability to experiment

While there is a direct correspondence of the experimental measurement in the diabatic basis to our definition (3.6), the adiabatic probability (3.7) is not necessarily what is actually measured in [2]. In [2] the state $|\psi_3\rangle$ is further manipulated using a lattice strength V_{sep} . To make a correct prediction we would have to know more about the time dependence of a and V . What we know from [2] is:

"The acceleration is then suddenly reduced and the lattice depth increased so as to 'freeze' the instantaneous populations in the lowest two bands; finally, further acceleration is used to separate these populations in momentum space."

Assuming a very fast switch from V_0 to V_{sep} and assuming a perfect separation of this lowest

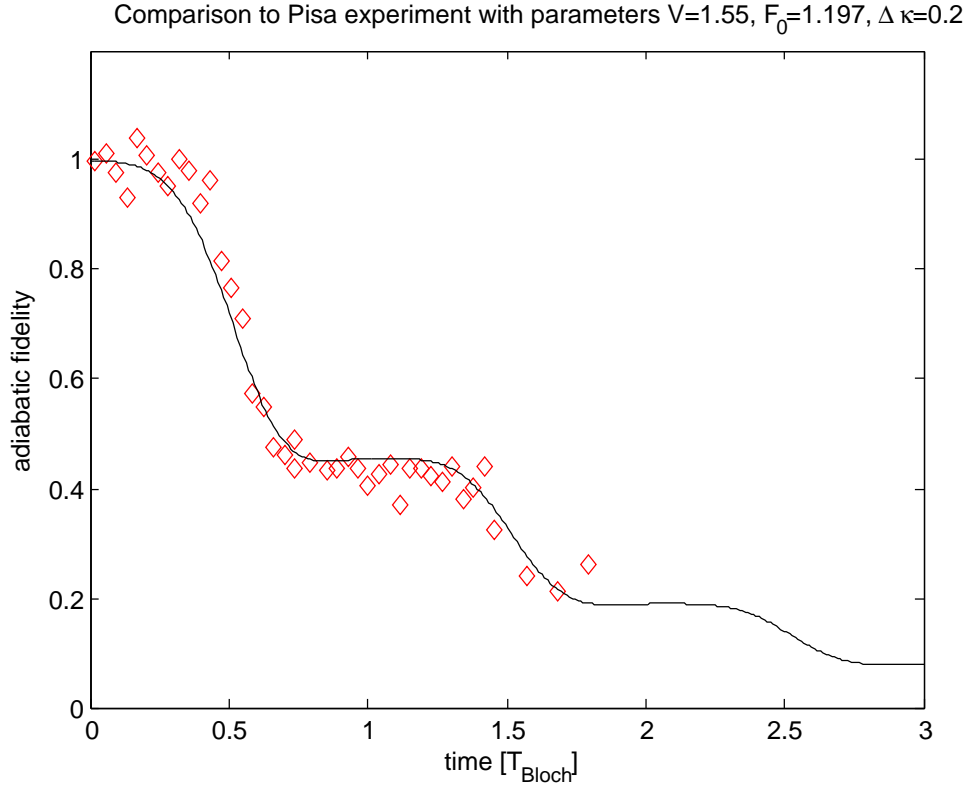


Abbildung 3.5.: Comparison to Pisa experiment (adiabatic basis): The result of this study (straight line) for the adiabatic basis is compared to a set of experimental data (red diamonds). The initial distribution is a Gaussian with variance $\Delta\kappa = 0.2$ and mean at $\kappa = 0$.

energy state from the rest, one would have to project on the V_{sep} eigenstates,

$$P_a = \frac{\int_{-0.5}^{0.5} dp \left| \langle \psi_3 | \kappa, \tilde{n} = 0 \rangle_{V=V_{\text{sep}}} (t_0) \right|^2}{\int_{-0.5}^{0.5} dp \left| \langle \psi_1 | \kappa, \tilde{n} = 0 \rangle_{V=V_{\text{sep}}} (t_0) \right|^2}, \quad (3.8)$$

instead of the V_0 eigenstates of (3.7). If the potential switch takes long enough for $|\psi_3\rangle$ to relax adiabatically but fast enough so that there is no tunneling during the switch process, (3.7) would be valid. The paper states that the switch time t_{ramp} is much smaller than T_{Bloch} , so the second requirement is probably fulfilled, about the first one I am not sure. For a final analysis I would need to know the details of the potential switching process.

An alternative idea to falsify the theory is to use $|\psi_3\rangle$ for a prediction of the momentum distribution. But as the phase between contributions of different momenta gets lost for $|\psi_3\rangle$

3. Methods, results and comparison to experiment

during measurement, one cannot exactly reconstruct the original state from this measurement.

3.3. Numerical Calculation and Implementation in MATLAB

H_κ is an $\mathbb{N} \times \mathbb{N}$ -matrix but we can only use finite dimensional Hilbert spaces for the computer implementation. The basis of the full Hilbert space is the set $\{|\kappa, z\rangle\}$ with $\kappa \in M_1, z \in M_2$, where $M_1 = [-0.5, 0.5)$ and $M_2 = \mathbb{Z}$. For a numerical implementation we have to make both sets M_1, M_2 finite, so we discretize M_1 by a grid and cut off M_2 by using only values with $|z| < |z_{max}|$. The Hamiltonian we use for this restricted system is

$$H_{\text{Num}} = \sum_{\kappa \in M_1} d\kappa H_{\kappa, \text{Num}} \quad (3.9)$$

with

$$\begin{aligned} H_{\kappa, \text{Num}} = & \sum_{z \in M_2} \left(\frac{1}{2} (\kappa + z + at)^2 \cdot |\kappa + z\rangle \langle \kappa + z| \right) \\ & + \sum_{z \in M_2} \left(\frac{V_0}{2} (|\kappa + z\rangle \langle \kappa + z + 1| + |\kappa + z + 1\rangle \langle \kappa + z|) \right). \end{aligned} \quad (3.10)$$

This finite dimensional approximative Hamiltonian has the same structure as the full Hamiltonian (2.7) with countable infinite basis. Of course we can also represent H_{Num} by a block diagonal matrix with $H_{\kappa, \text{Num}}$ on the diagonal. The definitions of adiabatic and diabatic basis for the finite dimensional approximation are also in full analogy to (2.7).

3.3.1. How to choose M_1 and M_2

The requirements for the choice of M_1 depend on the width of the initial momentum distribution in the lowest band. For $\Delta p(t=0) \rightarrow 0$ we can even use $M_1 = \{\kappa_0\}$. If the whole first Brillouin zone is populated we need a larger set. Using $|M_1| = 100$ already gives qualitatively good results for most purposes.

The requirements for M_2 depend on two parameters:

- The number of bands populated during the calculation: As we have to represent each band with one state, $|M_2|$ must be bigger than the number of bands occupied during the time evolution which is:
 $(\text{number of bands at } t=0) + \frac{t_{final}}{t_{Bloch}}$
- The V - ΔE -ratio: With growing V the contributions to each band from different momentum eigenstates will grow. States with higher and higher momentum contribute a considerable amount to the energy ground state. The limiting cases are:
 - $V = 0$: $|\kappa, \tilde{n}\rangle_V = |\kappa, \tilde{n}\rangle_0$
In this case the energy eigenstates correspond to the momentum eigenstates.

$$- V \gg \frac{p_{max}^2}{2m}: |\kappa, \tilde{m}\rangle_V \approx \sum_{\tilde{n}=1}^N \exp\left(i\frac{\tilde{n}}{N}2\pi\right) |\kappa, \tilde{n}\rangle_0$$

In this case the energy eigenstates approximately correspond to location eigenstates $|x\rangle$, so we need more and more momentum eigenstates to represent them.

As for our calculation we use the momentum basis we will need a large $|M_2|$.

As long as the experiment only populates the center of the first Brillouin zone and V is much smaller than the energy of the third band we can use $|M_2| = 2$ to simulate the temporal evolution over one Bloch period. For bigger V one needs more basis states. A good approximation is still achieved, as long as the M_2 is chosen large enough such that at any given time all momentum eigenstates with $E_{kin} \leq \delta V$ are included. Here δ is a parameter indicating the precision of the calculation and can be chosen as for example 10, to be on the safe side.

Side note: 2×2 matrix model revisited The 2×2 Landau-Zener matrix with initial condition in the lowest band corresponds to the two dimensional form of this model for initial states in the lowest band only and can be realized by setting $M_1 = \{\kappa_0\}$ and $M_2 = \{-1, 0\}$. This is the minimal realization of the model. $\kappa_0 \in [-0.5, 0.5]$ is the condition for the model to be physically correct. Now our Hamiltonian is just (see 2.4)

$$H_{LZ} = \frac{1}{2} \begin{pmatrix} (\kappa_0 - 1)^2 - 2at & V \\ V & \kappa_0^2 \end{pmatrix}. \quad (3.11)$$

The splitting between the energy levels of the lowest two bands predicted by this model, see (2.21), is correct for small V . As can be seen in Figure 3.6 the model is unsuitable for larger V . Using the coupling coefficients in adiabatic basis (3.20) which we develop in the next section, we also plot the coupling between the lowest two bands in Figure 3.7. For small values of V and near the crossing it is shaped like the Lorentzian predicted by the Landau-Zener model with only slight relative deviations far away from the crossing, which are due to the avoided crossing located in the neighboring Brillouin zone. For large V however the Landau Zener model coupling is too weak (see the difference between the predicted couplings normalized by the correct coupling strength in Figure 3.8), which is due to the influence of eigenstates with higher kinetic energy.

Another interesting thing to look at is the behavior of the system for $F_0 \rightarrow \infty$ as both γ and Z converge to a finite value, deviating from the Landau-Zener formula. The reason is explained in the following section.

3.4. Resonances of γ and Z

3.4.1. Definition and Calculation of γ and Z

Let us introduce two parameters, γ and Z , which characterize the behavior of our system. On a long time scale the adiabatic survival probability P_a decays approximately exponentially,

3. Methods, results and comparison to experiment

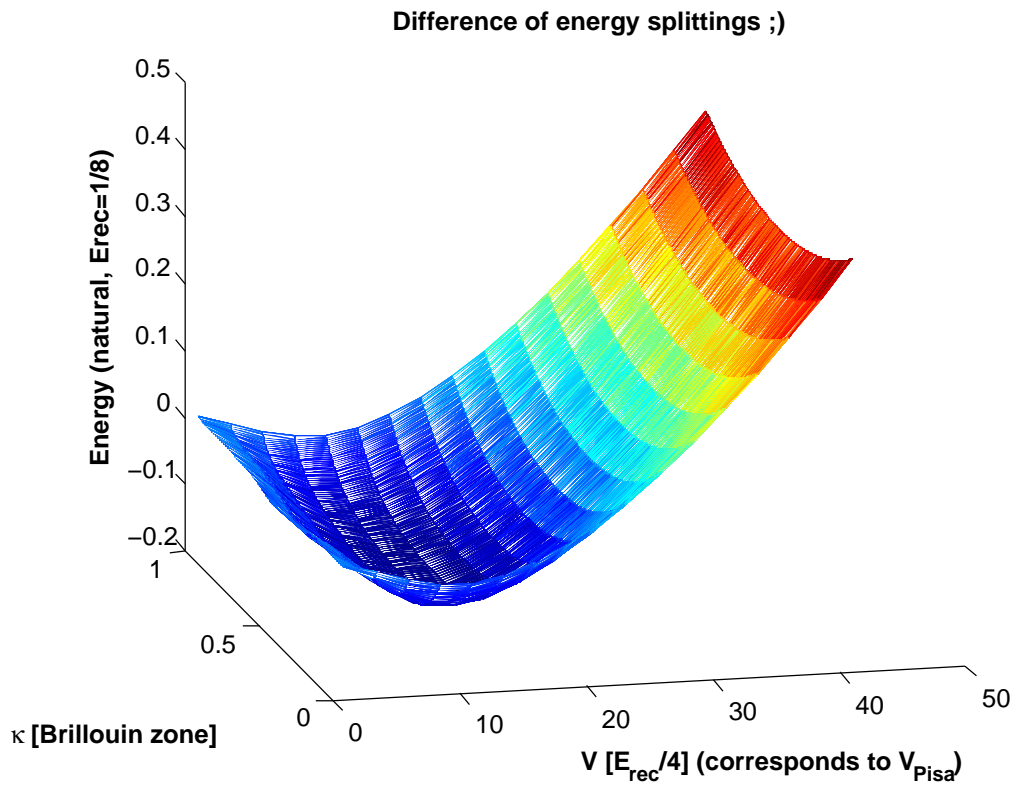


Abbildung 3.6.: Difference of energy gaps: This graph is a plot of the difference $\Delta E_{LZ} - \Delta E_{Num}$ where ΔE_{Num} is the energy difference of the lowest two bands as predicted by Landau-Zener theory and ΔE_{LZ} is the result from our numerical calculation. For $V \rightarrow 0$ both models agree, for larger V the deviation increases. It is interesting that with growing V the difference drops below 0 before it converges to $+\infty$.

and we get the approximate equation

$$P_a(t) \approx Z \exp\left(-\gamma \frac{t}{T_{Bloch}}\right) \quad (3.12)$$

that serves as our definition for γ and Z .

On a short timescale P_A might not decay exponentially. The deviation from the long term exponential decay can be characterized by the parameter Z of (3.12). This parameter was already introduced in [20] to analyze the system with respect to Zeno effect and inverse Zeno effect. They showed for a general system that $Z < 1$ is a sufficient condition for the possibility of generating an inverse Zeno effect with the right frequency of measurement. For $Z > 1$ a measurement frequency that generates an inverse Zeno effect may or may not exist.

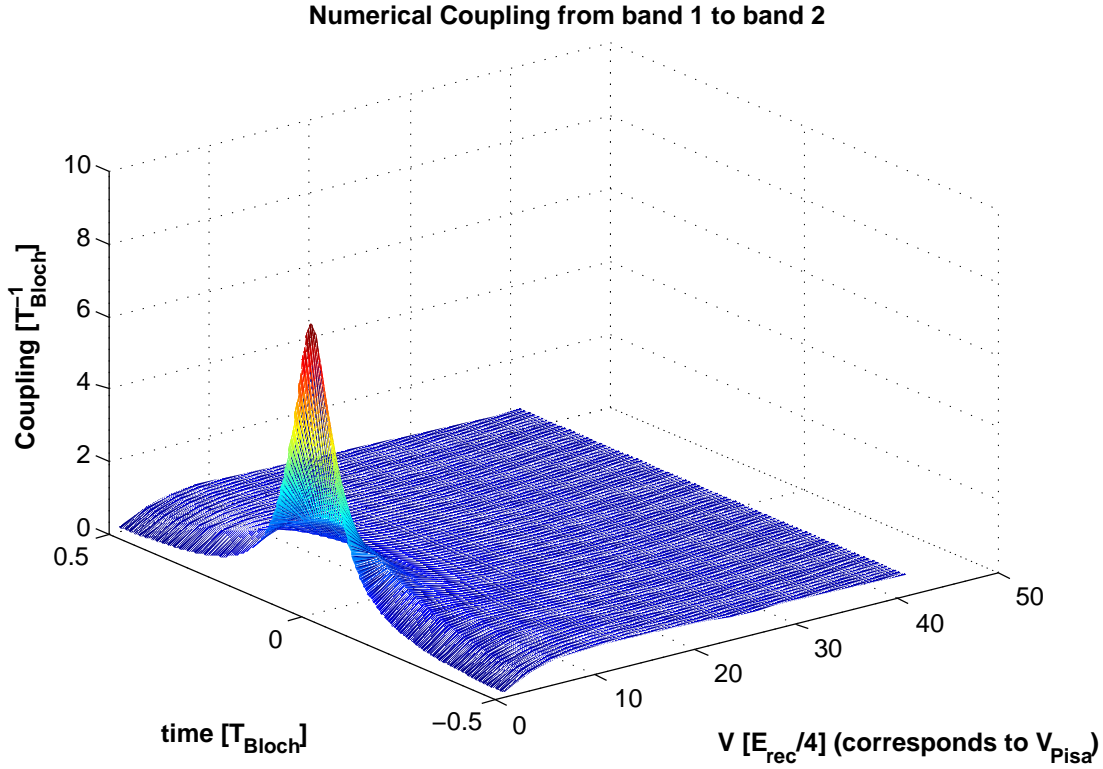


Abbildung 3.7.: Adiabatic coupling between lowest bands: The coupling between the lowest two bands in the energy basis (the first off-diagonal entry of the Hamiltonian in adiabatic basis, i.e. H_{12}^k), as calculated with our numerical method. For small values of V the coupling approaches the Landau-Zener prediction (2.21) and becomes a Lorentzian with width proportional to V . Thus the time of coupling can be approximated as proportional to V in this limit.

For our system even the long time behavior is not purely exponential, but there is a steplike substructure on top of the exponential decay. Thus for our system the definition of Z is a little arbitrary and one must be careful with its interpretation. To get rid of this arbitrariness one could define Z by extrapolation of P_a after every full Bloch periods. If the measurements are also done after full Bloch periods, we will see that $Z < 1$ corresponds to Zeno effect and $Z > 1$ corresponds to inverse Zeno effect. The parameters γ and Z can easily be obtained from our calculation based on definition (3.7) as follows: We fit the adiabatic survival probability at full Bloch times using the least square method with a function of the form

$$P_a^{\text{fit}} = Z \exp\left(-\gamma \frac{t}{T_{\text{Bloch}}}\right), \quad (3.13)$$

Normalized Difference between Lorentzian and numerical Coupling from band 1 to band 2

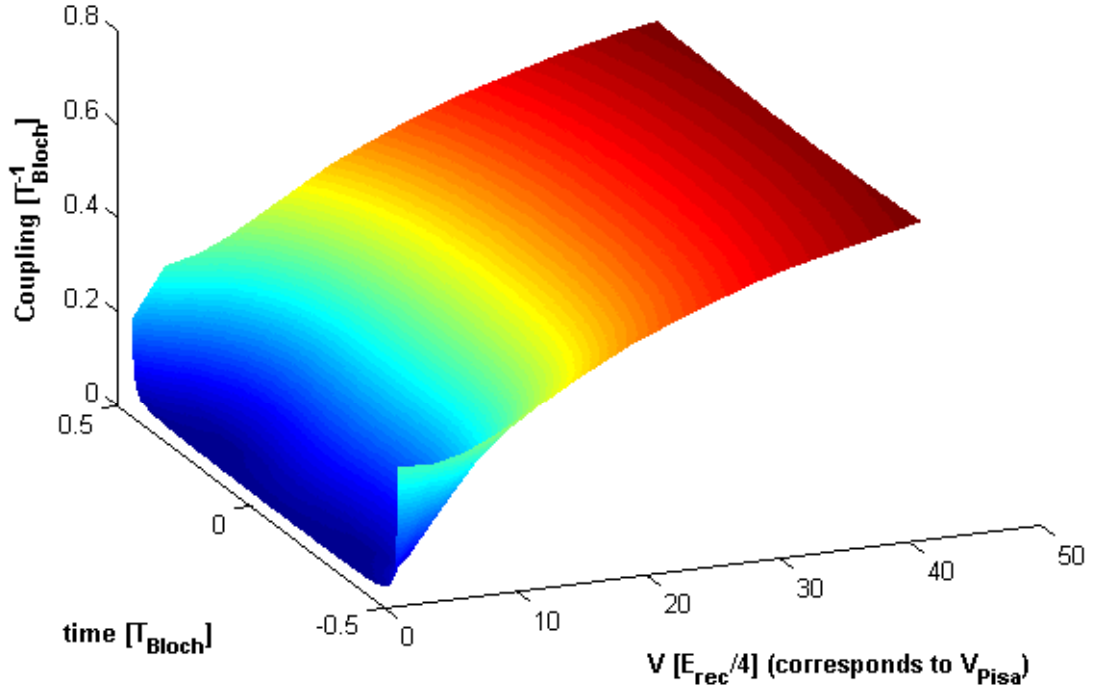


Abbildung 3.8.: Difference in coupling: $(c_{12} - c_{12}^{LZ})/c_{12}$: This picture shows the deviation of the Landau-Zener coupling c_{12}^{LZ} from equation (2.21) between the lowest two bands and the numerical result c_{12} of Figure 3.7. As the coupling rapidly decreases with growing V , we plot the normalized difference $(c_{12} - c_{12}^{LZ})/c_{12}$

where γ and Z are the fit parameters. To get reliable results one has to use roughly 10 Bloch periods for the fit. An example picture for such a fit is plotted in Figure 3.9. For small V there is a long plateau with a constant value for the fidelity after each jump and the fitting process is less arbitrary and Z is indeed well defined as the value of the fidelity at the plateau.

We scan the parameters V and F_0 for resonances in γ and Z . The result of this scanning process can be used to verify the resonances in the Pisa experiment. A prediction for the coming experiment is shown in Figure 3.10. As will be discussed in the following we explain the origin of those resonances and propose a procedure that can manipulate both γ and Z . In Raizen's theory from section 2.7 the parameters γ and Z only depend on $\frac{V^2}{a}$, thus the resonances cannot correctly be resolved and no prediction for Zeno effect is possible.

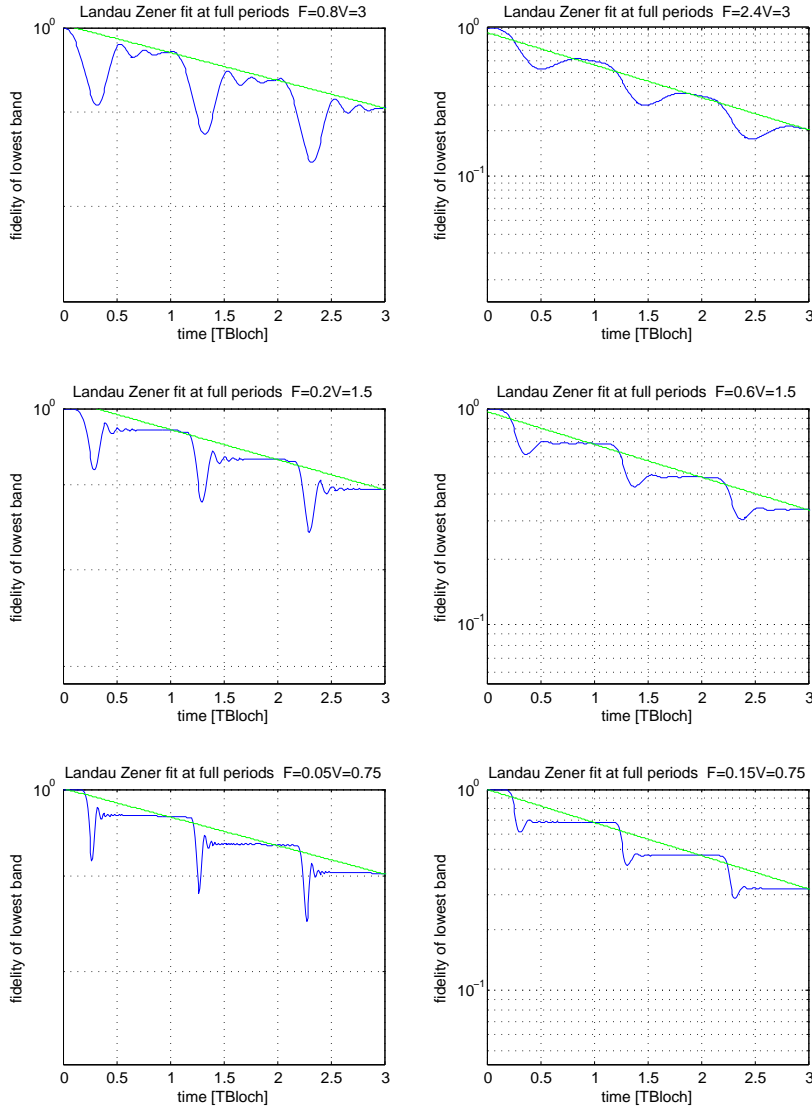


Abbildung 3.9.: Fitting process of Z for different values of V and a : In each row of this picture the ratio $\frac{V^2}{a}$ is constant for better comparability. We see that for smaller V there exists a long plateau of the fidelity $P_a(t)$ of the lowest band and the value of Z becomes independent of the exact location of the fitting procedure, compare Figure 3.7 and equation 2.25 for the time of coupling which is proportional to V if time is measured in Bloch units. In the plots above the initial quasi-momentum is $\kappa = \frac{1}{4}$.

3.4.2. Explanation for the behavior of γ and Z

We can use the calculation from section 3.3 to get some information on the time evolution in the adiabatic basis by calculating a matrix representation of the time evolution for one

3. Methods, results and comparison to experiment

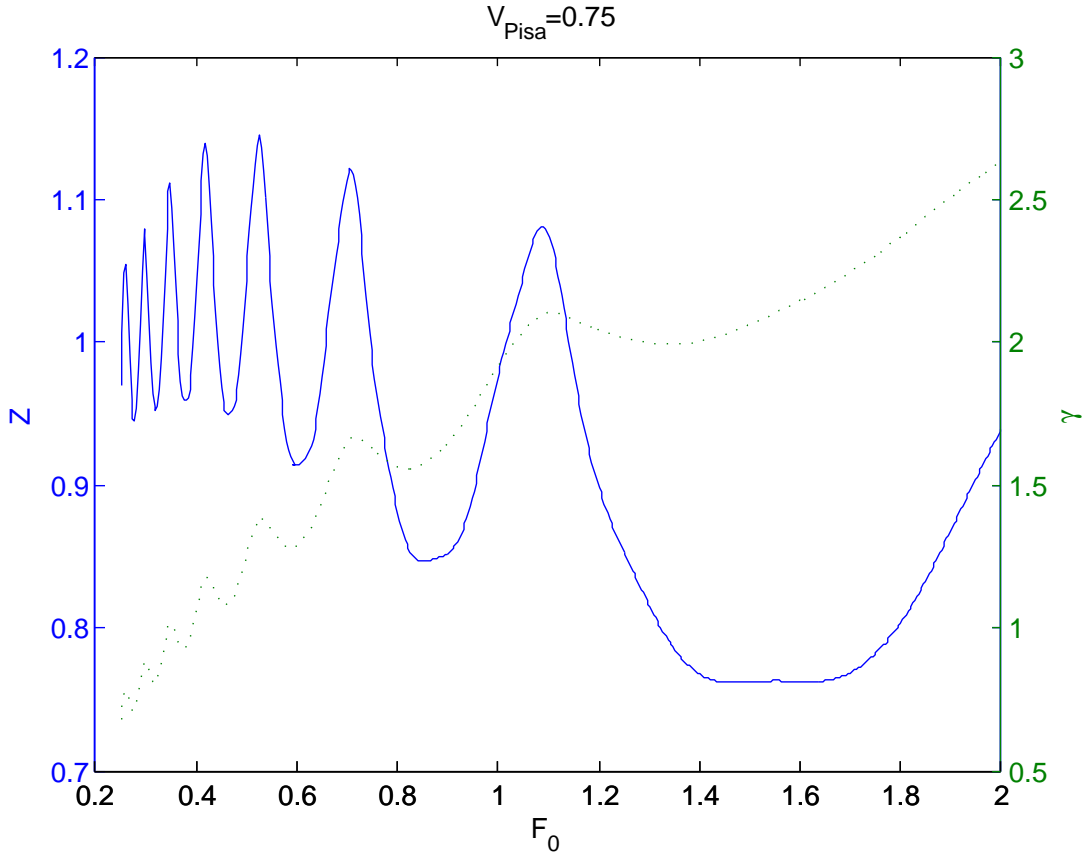


Abbildung 3.10.: Scan of Z and γ for $\kappa_0 = 0.25$.

Bloch period. We calculate the matrix

$$U_\kappa := \lim_{N \rightarrow \infty} \prod_{n=1}^N \exp \left(-i H_{\text{adiabatic}}^\kappa \left(\frac{T_{\text{Bloch}}}{N} n \right) \frac{T_{\text{Bloch}}}{N} \right) \quad (3.14)$$

which we can approximate numerically by using a finite N instead of the limit. U_κ represents the time evolution in the adiabatic basis for one Bloch period for a given value of κ . As the adiabatic Hamiltonian (3.19) is a periodic function of time (see the derivation below), U_κ is time independent(!) in the sense

$$\forall n \in \mathbb{N} : U_\kappa(n \cdot T_{\text{Bloch}} \rightarrow (n+1) \cdot T_{\text{Bloch}}) \equiv U_\kappa. \quad (3.15)$$

Let us now derive $H_{\text{adiabatic}}(t)$, the Hamiltonian in the adiabatic basis: We expand the state in subspace κ in time dependent energy eigenstates of the lattice frame as introduced in (3.1)

$$|\psi^\kappa(t)\rangle = \sum_{\tilde{n}=0}^{\infty} a_{\tilde{n}}^\kappa(t) |\kappa, \tilde{n}\rangle_{V_0}(t) \quad (3.16)$$

and apply Schrödinger's equation

$$i \frac{d}{dt} |\psi^\kappa(t)\rangle = i \sum_{\tilde{n}=0}^{\infty} \left(\dot{a}_{\tilde{n}}^\kappa(t) |\kappa, \tilde{n}\rangle_{V_0}(t) + a_{\tilde{n}}^\kappa(t) \frac{d}{dt} |\kappa, \tilde{n}\rangle_{V_0}(t) \right) = \sum_{\tilde{n}=0}^{\infty} E_{\tilde{n}}^\kappa(t) a_{\tilde{n}}^\kappa(t) |\kappa, \tilde{n}\rangle_{V_0}(t). \quad (3.17)$$

Projecting on $\langle \kappa, \tilde{n} |_{V_0}$ we arrive at

$$\dot{a}_{\tilde{n}}^\kappa = -i E_{\tilde{n}}^\kappa a_{\tilde{n}}^\kappa - \sum_{\tilde{m}=0}^{\infty} \langle \kappa, \tilde{m} | \frac{d}{dt} | \kappa, \tilde{n} \rangle_{V_0} a_{\tilde{m}}^\kappa. \quad (3.18)$$

Thus the Hamiltonian in adiabatic basis is

$$H_{\text{adiabatic}}^\kappa = \sum_{\tilde{n}=0}^{\infty} E_{\tilde{n}}^\kappa |\kappa, \tilde{n}\rangle \langle \kappa, \tilde{n}| - i \sum_{\tilde{m}, \tilde{n}=0}^{\infty} \langle \kappa, \tilde{m} | \frac{d}{dt} | \kappa, \tilde{n} \rangle |\kappa, \tilde{n}\rangle \langle \kappa, \tilde{m}|. \quad (3.19)$$

This is a periodic function of time with period T_{Bloch} , thus Floquet's theorem (2.5) can be applied.

Note that if we measure time in units of Bloch time T_{Bloch} the coupling coefficients

$$\langle \kappa, \tilde{m} | \frac{d}{dt} | \kappa, \tilde{n} \rangle_{V_0} \quad (3.20)$$

are only a function of V . The energies $E_{\tilde{n}}^\kappa$ are a function of V and scale linearly with increasing $T_{\text{Bloch}} = \frac{1}{a}$, if we use units with $T_{\text{Bloch}} = 1$. So in case of a very fast acceleration, these diagonal matrix elements can be neglected on the T_{Bloch} timescale and the tunneling probability converges to a finite value. This deviation from the Landau-Zener tunneling probability is due to the finite time of a Bloch period.

Side note on Numerical Calculation of U_κ

If you are not interested in numerical details you can skip this short side note. Calculating U_κ using $H_{\text{adiabatic}}^\kappa$ is hard to do numerically, as in the limit of a free particle, which occurs for $p^2/2mV \rightarrow \infty$ the time interval Δt in which the coupling is nonzero converges to 0. This is very hard to resolve for the coupling between higher bands, so we use the diabatic Hamiltonian $H_{\text{diabatic}}^\kappa$ to do the calculation as follows: Let $\Lambda_\kappa(t)$ denote the basis transformation matrix between the diabatic and the adiabatic basis, i.e. the matrix with the eigenvectors of $H_{\text{diabatic}}^\kappa(t)$ as column vectors. Then we can also calculate U_κ as

$$U_\kappa = \Lambda_\kappa^{-1}(T_{\text{Bloch}}) \lim_{N \rightarrow \infty} \prod_{n=1}^N \exp \left(-i H_{\text{diabatic}}^\kappa \left(\frac{T_{\text{Bloch}}}{N} n \right) \frac{T_{\text{Bloch}}}{N} \right) \Lambda_\kappa(0) \quad (3.21)$$

and achieve higher precision for the numerical calculation.

2×2 -Matrix model

Let us analyze the matrix U_κ in a regime where there is non-negligible coupling only between neighboring bands and the tunneling probability per Bloch period from third to fourth band

3. Methods, results and comparison to experiment

is much larger than the tunneling probability between the lower bands. If in addition the jump time is small on the scale of a Bloch period and our initial κ is far from an avoided crossing,² we can also assume that after one Bloch period the first two tunneling processes at avoided crossings are complete. These assumptions are for example approximately valid for $V \approx 1$ and $F_0 \approx 1$ in units used by the experimentalists in the Arimondo group. In Figure 3.9 we see that for small V there is a long plateau after the jump. Thus the jump time is indeed small compared to a Bloch period. From Vitanov's paper [10] we know that for small $\frac{V^2}{a}$ the time of coupling is proportional to V , which is also approximately true for our system, compare Figure 3.7.

Under these assumptions we neglect all amplitudes with $\tilde{n} > 2$ and approximate U_κ by the 2×2 -Matrix

$$U_\kappa^{\text{red}} = \begin{pmatrix} a_{11} & a_{12} \\ a_{21} & a_{22} \end{pmatrix}, \quad (3.22)$$

consisting of the first entries of U_κ . This is a good approximation because states with $\tilde{n} > 2$ in this case are already as good as free and transfer to even higher bands. They return to the lowest two bands only with negligible probability, i.e.

$$\forall \tilde{n} > 2 : a_{1n} \approx 0 \wedge a_{2n} \approx 0. \quad (3.23)$$

The simple matrix U_κ^{red} can explain both the behavior of γ and Z :

The survival probability after the first Bloch period is exactly $|a_{11}|^2$. After the second period however there will be a return of the amplitude which had tunneled to the second band in the first time step. Also at later times the same return mechanism is active. The phase ϕ of the returning amplitude is a function of the energy gap ΔE between the lowest bands and the time interval Δt between two crossings, roughly $\phi \approx \Delta t \overline{\Delta E}$, with $\overline{\Delta E} = \int_{-0.5}^{0.5} d\kappa \Delta E(\kappa)$. This ϕ is responsible³ for the resonances of Z and γ we described in section (3.4.1). The returning amplitude can be either constructive or destructive and thus change the survival probability. While the survival probability in the first Bloch period is unaffected by any returning amplitude from the second band, this mechanism changes the long time tunneling probability. This change of tunneling probability after the first Bloch period is the direct cause for the change of the intercept Z : If the returning amplitude is constructive (destructive), the survival probability tends to increase (decrease) after the first Bloch period and thus $Z < 1$ ($Z > 1$). In Figure 3.11 this connection is verified and we see that both resonances occur at the same value of V and a .

Eigenvalues of U^{red}

The matrix U_κ^{red} is not anymore unitary because of our reduction! So the norm of the eigenvalues $e_1 > e_2$ is smaller than 1 and their absolute squares $|e_1|^2$ and $|e_2|^2$ correspond

²The area with maximal amplitude of avoided crossing transitions is located at $\kappa = 0$ if the band with lower energy is odd numbered and at $\kappa = 0.5$ if it is even numbered, if we start counting at $\tilde{n} = 1$. Thus $\kappa_0 = \frac{1}{4}$ is a good choice for an initial state.

³The maxima of γ and Z occur roughly at $\frac{1}{a} \overline{\Delta E} \approx n2\pi$ with $n \in \mathbb{N}$. This corresponds to the RET condition of [21].

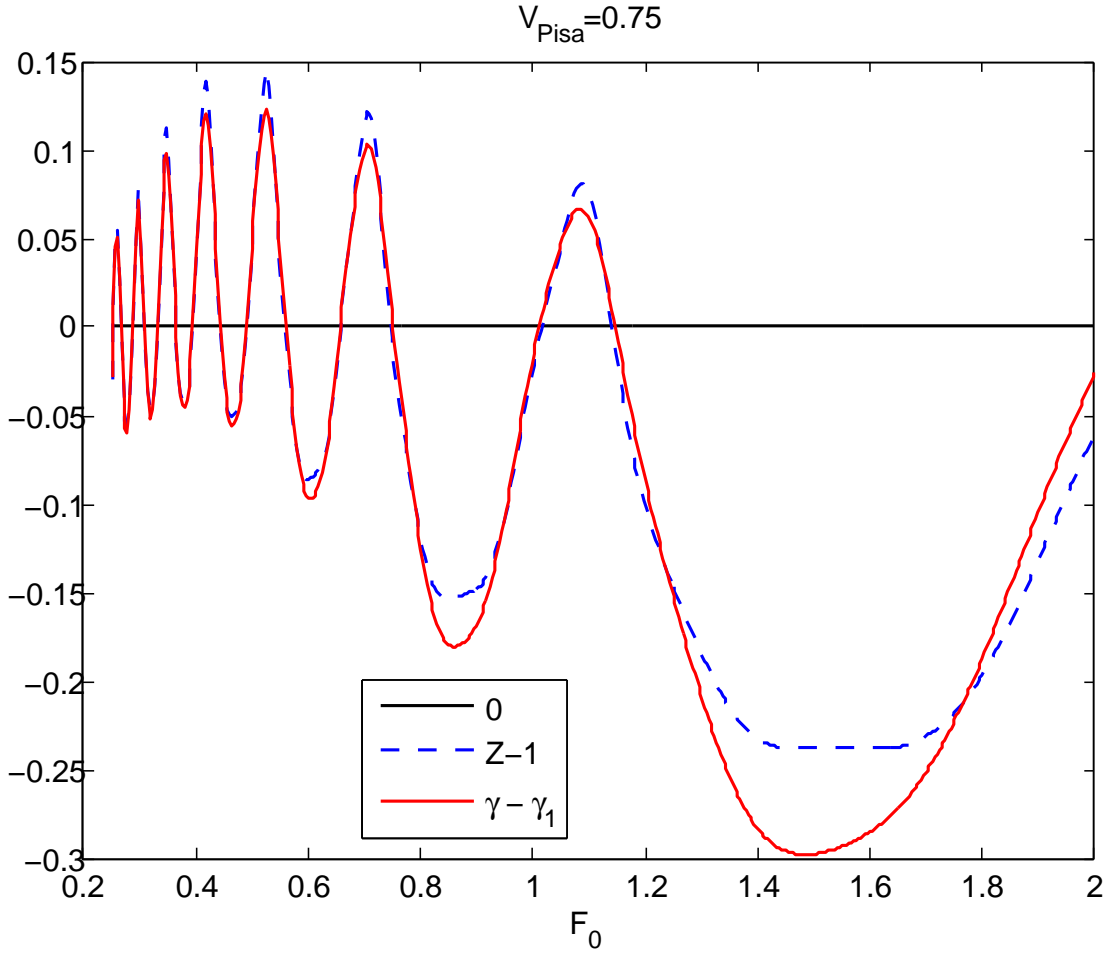


Abbildung 3.11.: $Z - 1$ is compared to the difference of the fitted long time decay rate γ and the decay rate γ_1 after the first Bloch period only ($1 - P_a(1) = e^{-\gamma_1}$). We see that for small F_0 both curves cross 0 at approximately the same value of F_0 . Thus, as long as the jump time is not too long, which is true for small V , Z indeed is smaller (larger) than 1 if the the long time decay rate γ is smaller (larger) than the short time decay rate γ_1 , measured after only one Bloch oscillation.

to the long time decay rate in 3.26 and its modification on a shorter timescale. At $t = 0$ we start in a superposition $|\psi_0\rangle = b_1|e_1\rangle + b_2|e_2\rangle$ of both eigenvectors. After applying t times U_κ^{red} on the initial state, we arrive at

$$|\psi\rangle(t) = \left(U_\kappa^{\text{red}}\right)^t |\psi_0\rangle = b_1 e_1^t |e_1\rangle + b_2 e_2^t |e_2\rangle \quad (3.24)$$

3. Methods, results and comparison to experiment

and

$$\begin{aligned} \langle \psi_0 | \psi \rangle (t) &= \left(|b_1|^2 + b_1 b_2^* \langle e_2 | e_1 \rangle \right) e_1^t + \left(|b_2|^2 + b_2 b_1^* \langle e_1 | e_2 \rangle \right) e_2^t \\ &=: c_1 e_1^t + c_2 e_2^t \end{aligned} \quad (3.25)$$

where $t \in \mathbb{N}$ is an integer and counts the Bloch periods, c_1 and c_2 are defined as the terms in brackets. As the second term $c_2 e_2^t$ can be neglected for large enough t , we obtain in this model

$$\gamma = -\log(|e_1|^2) \quad (3.26)$$

and

$$Z = |c_1|^2. \quad (3.27)$$

Figure 3.12 and 3.13 compare this prediction to the result we obtain by the method that calculates the whole time evolution, as described in section 3.4.1. We see that the simple

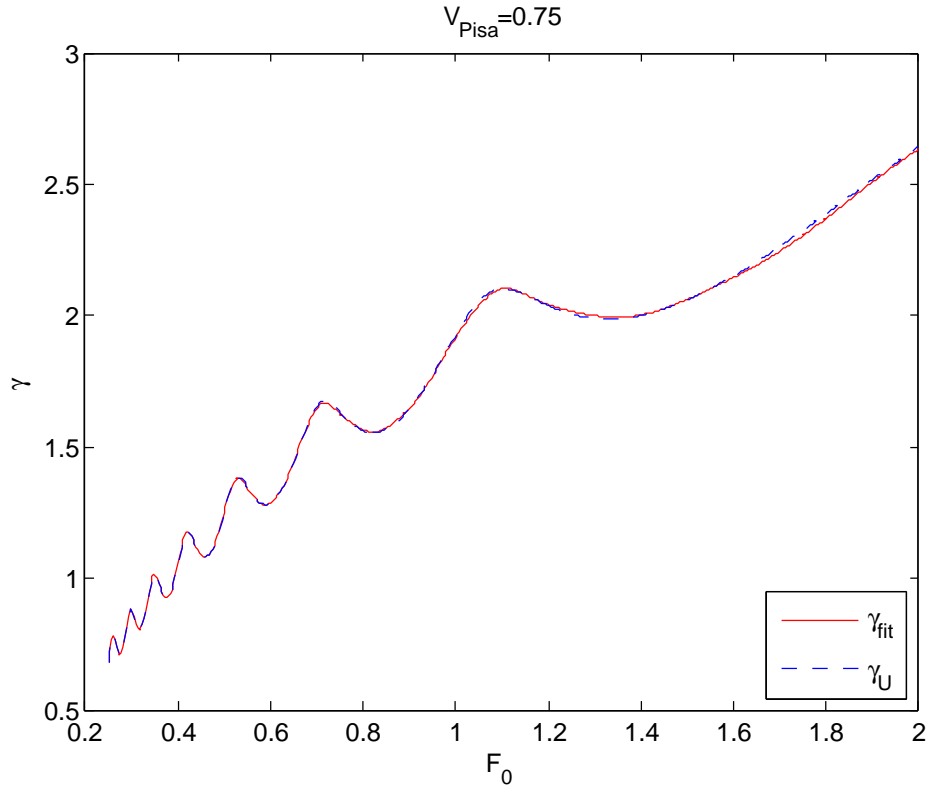


Abbildung 3.12.: The prediction for γ from the 2×2 matrix model, γ_U from equation (3.26), is in good agreement for this range of parameters with γ_{fit} , which is the result obtained by fitting P_a from the numerical simulation of the full time evolution.

2×2 matrix describes both γ and Z very well for small V and a .

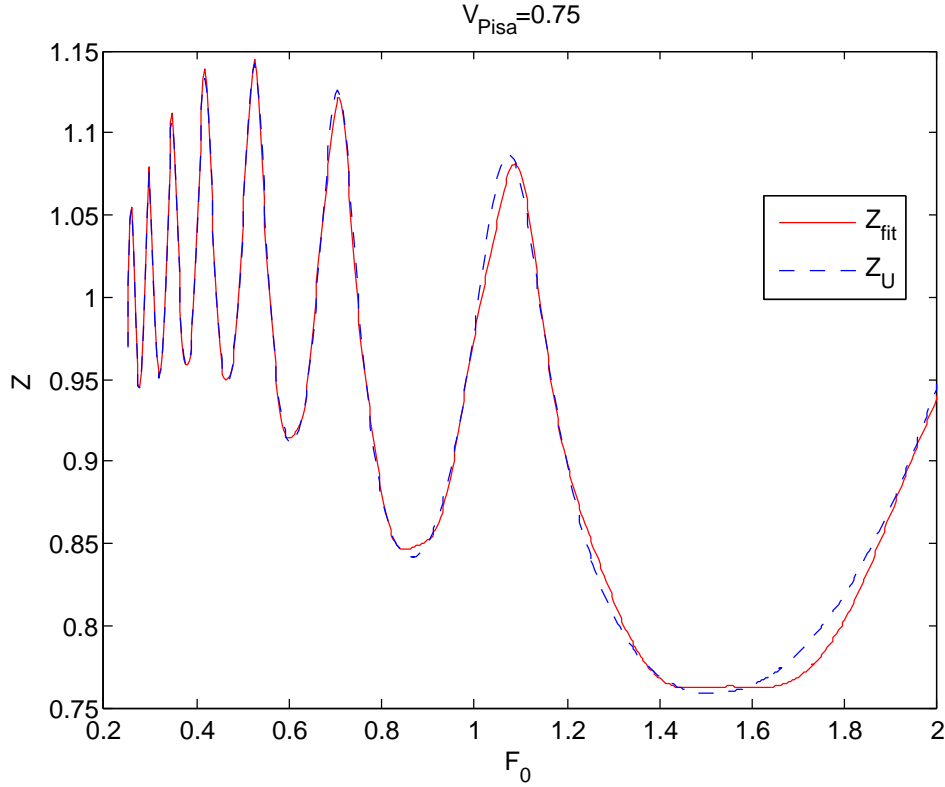


Abbildung 3.13.: The prediction for Z from the 2×2 matrix model, Z_U from equation (3.26), is in good agreement for this range of parameters with Z_{fit} , which is the result obtained by fitting P_a from the numerical simulation of the full time evolution.

3.4.3. Manipulation of the resonances

By abruptly switching off the acceleration after each period and switching it on again abruptly after some time t_{phase} , one could imprint a phase $\phi = \Delta E \cdot t_{\text{phase}}$ on the second band and manipulate the phase of the returning amplitude. It could be changed between destructive and constructive, resulting also in a different value for Z and γ . To calculate the correct value of t_{phase} for this manipulation within this model, we define the matrix

$$U_{\kappa}^{\text{m}} = U_{\kappa}^{\text{red}} \begin{pmatrix} 1 & 0 \\ 0 & e^{i\phi} \end{pmatrix}, \quad (3.28)$$

which is the Floquet operator for the manipulated time evolution. The rigorous way to determine t_{phase} is to optimize the eigenvalues of U_{κ}^{m} as a function of ϕ .

For a less exact but more demonstrative way to optimize ϕ one would only calculate the first band's amplitude after two Bloch periods. Calculating the entry with index (1,1) of

3. Methods, results and comparison to experiment

$U_\kappa^m U_\kappa^{\text{red}}$ we obtain

$$a_{11}^2 + e^{i\phi} a_{21} a_{12}. \quad (3.29)$$

For constructive interference one would choose

$$\phi = \text{angle}(a_{11}^2) - \text{angle}(a_{21} a_{12}) \quad (3.30)$$

and add another phase of π for destructive interference.

Relation to Zeno effect

A nondestructive measurement of the band population can be seen as equivalent to destroying/randomizing the phase relation between the bands, as the respective density matrices are the same: Let us assume that initially the system S is in a superposition

$$|\psi(\phi)\rangle_S = a_1 |1\rangle_S + a_2 e^{i\phi} |2\rangle_S \quad (3.31)$$

of the lowest two bands with a well defined phase relation, e.g. $\phi = 0$. Then we can write the density matrix as

$$\rho_S = \begin{pmatrix} |a_1|^2 & a_1 a_2^* \\ a_2 a_1^* & |a_2|^2 \end{pmatrix} \quad (3.32)$$

After a measurement in this basis with an apparatus A we would get the state

$$|\psi\rangle_{SA} = a_1 |1\rangle_S |1\rangle_A + a_2 |2\rangle_S |2\rangle_A \quad (3.33)$$

and after tracing out the apparatus only the diagonal entries of the density matrix after a measurement,

$$\rho_S^M = \begin{pmatrix} |a_1|^2 & 0 \\ 0 & |a_2|^2 \end{pmatrix}, \quad (3.34)$$

survive. The phase randomized density matrix is

$$\rho_S^R = \frac{1}{2\pi} \int_0^{2\pi} d\phi |\psi(\phi)\rangle_S \langle\psi(\phi)|_S = \begin{pmatrix} |a_1|^2 & 0 \\ 0 & |a_2|^2 \end{pmatrix} \quad (3.35)$$

Thus if a random phase ϕ is imprinted on the state by halting the acceleration for a long and random time, $\rho_S^R = \rho_S^M$ and one gets the same measurement probabilities for the system as after a non-destructive measurement. In the first case the relative phase between the bands is lost by a randomization process, in the second case it is lost by effectively irreversible entanglement to the apparatus.

Depending on whether the returning amplitude was originally constructive or destructive, one could then observe an equivalent to Zeno effect [22, 20] or Anti-Zeno effect. Similar experiments have been conducted by the Raizen group [23] with a broader distribution in κ . Using the optimal value of t_{phase} as derived above instead of a randomized time, the tunneling rate can be changed even more. It would be very interesting to conduct such an experiment. Another interesting thing to do could be to start with an initial state different

from the ground state to enhance or decrease Zeno effect. For example if the initial state is an eigenstate of U_κ we must see $Z = 1$ and the long time and short time decay rate would be the same.

In the next chapter we start with the decoherence study of a spin-qubit that is exposed to random magnetic fields. Also in this setup there is a difference between the short time and long time decay rate, because, as we describe in 4.5.1, the time evolution is equivalent to a random walk on a sphere. While in this first part we study Zeno effect only out of curiosity, in the second part it could be used to achieve our aim and slow down the decay of information.

Teil II.

**Quantum storage in a
decoherence-free subspace**

4. Introduction and Preliminaries

4.1. Abstract

A system of three spin- $\frac{1}{2}$ -atoms allows the construction of a qubit - in the subspace of total angular momentum $j = \frac{1}{2}$ - that is not affected by any magnetic field activity on the magnetic moments of the atoms, provided that all three atoms experience the same magnetic field. If, however, there are stray fields of different direction or strength at the sites of the atoms, the qubit will slowly decohere. It is the objective of this study to examine the decoherence process and to establish the conditions, under which the lifetime of the qubit is sufficiently long for practical uses.

4.2. Motivation

A decoherence-free subspace (DFS) can be used to protect quantum information against a particular kind of noise from the environment, which causes the information to decay non-unitarily. Such a DFS can never cancel all kinds of noise, as there must always exist an interaction to write and read the information into the qubits. The DFS method can be combined with other methods such as error correction codes or dynamical decoupling to achieve a long coherence time, so that the qubits can be used for information processing. The system we have in mind is the spin state of three individual trapped atoms in a triangular optical lattice, the noise we expect is caused for example by the B-field of current wires in the lab or bypassing cars. We use the previously constructed [14] rotational-frame free qubit (rff qubit) to cancel the noise due to the homogeneous part of this random B-field. The inhomogeneity of the field on the scale of the three atoms is the remaining part of the noise, which we want to study.

In the following section we rephrase the construction of the qubit, introduce the Hamiltonian of our system and two methods which could be used to further stabilize the setup.

4.3. Construction of the decoherence-free qubit

The construction of a rotationally invariant qubit has been described by Jun Suzuki et al. [14] in detail. Here we give a short summary for the case of three spin- $\frac{1}{2}$ -atoms and introduce the notation we want to use.

To construct the reference-frame-free qubit (from now on referred to as "rff qubit") one uses the ladder operator

$$J_- = J_x - iJ_y \tag{4.1}$$

4. Introduction and Preliminaries

for the whole three-atom system and defines its two orthogonal lowering partner operators

$$\Omega_-(\lambda) = \frac{1}{\sqrt{3}} \sum_{l=1}^3 \omega^\lambda \sigma_-(l) \quad (4.2)$$

where $\omega = e^{\frac{2\pi i}{3}}$, $\sigma_-(l)$ refers to the lowering operator for only the atom at site l and $\lambda = 1, 2$ labels the state of the rff qubit. For our calculations we will use the following basis in the subspace of total angular momentum $j = \frac{1}{2}$:

$$|j = \frac{1}{2}, m, \lambda\rangle = \Omega_-(\lambda) J_-^{\frac{1}{2}-m} |j = \frac{3}{2}, m = \frac{3}{2}\rangle, \quad (4.3)$$

where m is the value of the z -component of the spin. For the $j = \frac{3}{2}$ subspace we use the ordinary $|j, m\rangle$ -basis.

number	j	m	λ
1	$\frac{3}{2}$	$\frac{3}{2}$	-
2	$\frac{3}{2}$	$-\frac{3}{2}$	-
3	$\frac{3}{2}$	$\frac{1}{2}$	-
4	$\frac{1}{2}$	$\frac{1}{2}$	1
5	$\frac{1}{2}$	$\frac{1}{2}$	2
6	$\frac{3}{2}$	$-\frac{1}{2}$	-
7	$\frac{1}{2}$	$-\frac{1}{2}$	1
8	$\frac{1}{2}$	$-\frac{1}{2}$	2

basis used to describe the rff-qubit

A very similar construction can be done with four atoms, where a qutrit is formed in the subspace of $j = 1$ and a qubit with no degeneracy is formed in the subspace of $j = 0$. In section 5.4.1 we briefly compare the stability of this construction to the setup with three atoms.

4.4. Time evolution of the setup

We are interested in the stability of the rff-qubit. For this study we model the environment by a strong bias field B along the z -axis acting on all 3 atoms with Hamiltonian

$$H_0 = \frac{\mu_B g_e}{2\hbar} \vec{B} \cdot \sum_j \vec{\sigma}_j \quad (4.4)$$

as well as a homogeneous stray field $\tilde{b}(t)$ acting on all three atoms and inhomogeneous stray fields $b_j(t)$ acting only on the individual atom with index $j \in \{1, 2, 3\}$. The time evolution due to stray fields is described by Hamiltonian

$$H_1 = \sum_j \frac{\mu_B g_e}{2\hbar} \vec{b}_j(t) \cdot \vec{\sigma}_j + \sum_j \frac{\mu_B g_e}{2\hbar} \vec{b}(t) \cdot \vec{\sigma}_j. \quad (4.5)$$

In addition there is internal spin-spin-interaction between the atoms of the form:

$$H_i = \frac{\mu_0}{4\pi r^3} \left[\vec{\mu}_A \cdot \vec{\mu}_B - 3(\vec{\mu}_A \cdot \hat{r})(\hat{r} \cdot \vec{\mu}_B) \right]. \quad (4.6)$$

The total Hamiltonian is given by

$$H = H_0 + H_1 + H_i. \quad (4.7)$$

The bias field, which is applied by the experimentalist, is a possibility to stabilize the setup. In the rff-subspace all density matrices commute with H_0 and the homogeneous part of the noise, as they are rotationally invariant states.

For the numerical analysis of the time evolution we will use

$$\vec{\mathbf{B}} := \frac{\mu_B g_e}{2\hbar} \vec{B} \quad (4.8)$$

and

$$\vec{\mathbf{b}}_j := \frac{\mu_B g_e}{2\hbar} \vec{b}_j \quad (4.9)$$

for easier calculations.

Consider the Hamiltonian for atom l with B_z and b in units of energy:

$$H_0(t) + H_1(t) = B_z \sigma_{lz} + b(\sigma_{lx} \xi_{lx}(t) + \sigma_{ly} \xi_{ly}(t) + \sigma_{lz} \xi_{lz}(t)) \quad (4.10)$$

The random variables ξ , which represent the noise, are correlated in space and time. In our setup the atoms will be trapped close together by a laser so we can suppose that the field varies spatially only in first order. The spatial correlation is a result from this first order expansion and restrictions due to Maxwell equations.

We will also use the notation

$$h_0 := \sum_{l=1}^3 \sigma_{lz}, \quad h_1 := \sum_{l=1}^3 (\sigma_{lx} \xi_{lx}(t) + \sigma_{ly} \xi_{ly}(t) + \sigma_{lz} \xi_{lz}(t)) \quad (4.11)$$

and

$$H = B_z h_0 + b h_1. \quad (4.12)$$

In our model the noise is of the form

$$\begin{aligned} \forall t, t' : \\ \text{Cov}(\xi_I(t), \xi_J(t')) &= \Sigma_{IJ} \cdot e^{-\gamma|t-t'|} \\ \overline{\xi_I(t)} &= 0. \end{aligned} \quad (4.13)$$

In this notation the index I labels both the atom number l and the direction of the field (x, y, z) . The time correlation is given by the exponential decay, the spatial correlation is taken care of by the Covariance matrix Σ . Note that time correlation and space correlation are independent.

4. Introduction and Preliminaries

As Σ is a Covariance matrix, it is symmetric and positive semi-definite and can be written as

$$\Sigma = C^T C \quad (4.14)$$

with a real matrix C and

$$\Sigma = U^T D D U \quad (4.15)$$

with an orthogonal matrix U and positive diagonal matrix D . Combining (4.14) and (4.15) we get:

$$C = D U. \quad (4.16)$$

Now $\vec{\xi}$ can be written as

$$\vec{\xi} = C \vec{\zeta} \quad (4.17)$$

where $\vec{\zeta} \sim N(\vec{0}, \mathbb{1})$.

4.5. Methods for stabilization

4.5.1. Zeno effect

As long as we are only concerned with the effects of the random Hamiltonian H_1 the equations are equivalent to a random walk on a sphere with speed b and correlation time $\frac{1}{\gamma}$. The variation of position x for a random walk in one dimension obeys the equation:

$$\begin{aligned} \sigma_x^2(t) &= \overline{\left(\int_0^t b \exp(-\gamma t) dt \right)^2} \\ &= 2 \left(\frac{b}{\gamma} \right)^2 \left(2 \exp\left(-\frac{\gamma t}{\sqrt{2}}\right) - 2 + \sqrt{2} \gamma t \right). \end{aligned} \quad (4.18)$$

In the limit $\gamma t \rightarrow \infty$ the dominant term in the bracket is $\sqrt{2} \gamma t$:

$$\sigma_x^2 \rightarrow 2 \left(\frac{b}{\gamma} \right)^2 (\sqrt{2} \gamma t). \quad (4.19)$$

Thus

$$\sigma_x^2 \propto \frac{b^2}{\gamma} t \quad (4.20)$$

is valid in this case. On the other hand, if $\gamma t \rightarrow 0$ we get

$$\sigma_x^2 \rightarrow b^2 t^2 \quad (4.21)$$

by expanding the exponential function to second order. In analogy to this result our quantum state's decay will be of second order in t as long as $\gamma t \rightarrow 0$ is true. As soon as $\gamma t \gg 1$ the state decoheres in first order of t . This implies that if we want to slow down the decay of the setup using Zeno effect [22], we have to do this before γt becomes too large. So the frequency of measurements f must fulfill $f \gg \gamma$.

4.5.2. Stabilization by overall B-field

Time-constant stray fields As a first approach consider all fields to be constant in time. The effect on the rff qubit by a stray field in the x - y -plane can get suppressed by a large overall field $B_z \gg b_x, b_y$ along the z -axis. However, if the stray field is along z -direction, the overall field B_z has no stabilizing effect at all, as in this situation H_0 and H_1 commute. To analyze the Hamiltonian one can compare the induced time evolution of it to the time evolution for arbitrary two dimensional quantum systems of the form:

$$H = E_1 |1\rangle\langle 1| + E_2 |2\rangle\langle 2| + \lambda |1\rangle\langle 2| + \lambda^* |2\rangle\langle 1|, \quad (4.22)$$

which is given by Rabi's formula [24]

$$|c_2(t)|^2 = \frac{\frac{|\lambda^2|}{\hbar^2}}{\frac{|\lambda^2|}{\hbar^2} + \omega^2/4} \sin^2 \left(\left(\frac{|\lambda^2|}{\hbar^2} + \omega^2/4 \right)^{\frac{1}{2}} t \right) \quad (4.23)$$

where $\omega = \frac{E_1 - E_2}{\hbar}$ and c_2 is the probability to be in state 2 after time t when starting in state 1. For a large energy gap $\omega \gg \lambda$ the factor before the \sin^2 goes to zero and the transition is suppressed for times $t \gg \frac{1}{\omega}$.

In our case we can achieve a suppression of transitions between states with different quantum number m_z by a very strong B_z which can split the energy levels of states with different m_z , as can be seen at the diagonal elements of the Hamiltonian. Those are the transitions caused by inhomogeneities of the x - and y -component of the field. The transition rates between those states are proportional to $\sum_{i,j} c_{ij} b_{ij}$ with some constants $c_{ij} \in \mathbb{C}$, $i \in \{1, 2, 3\}$ and $j \in x, y$ only. In the language of Rabi's model $\omega \propto B_z$ and $\lambda \propto \sum_{i,j} c_{ij} b_{ij}$.

Transitions between states with same m are caused by B-field inhomogeneities of the z -component and can not be suppressed by a field in z -direction as it does not cause an energy gap between those states.

Fluctuating stray fields Expanding (4.23) in a Taylor series one can see that the stabilizing effect of the overall field is of fourth order in t . For very short correlation times τ of the noise only second order effects are important for the time evolution and the fourth order can be neglected. That is why only if $B\tau \gg 1$ a stabilizing effect can be observed. Thus not only $B \gg b$ but also $B \gg \gamma$ is required to stabilize the setup with a homogeneous B-field! If $\gamma > B$ the decay may still be slow, as the decay speed scales with $\frac{1}{\gamma}$ but the bias field would have no significant stabilizing effect.

4.6. Summary

The purpose of this section was to construct the rotational invariant qubits and discuss the physical implementation with spin states of trapped atoms. The notation we will use in the following sections for the time evolution of our setup was introduced. Two ideas for

4. Introduction and Preliminaries

stabilization of the stored information were presented: Application of a bias magnetic field and frequent measurements of the total angular momentum.

5. Methods, results and possible experiment

In the first sections of this chapter (until section 5.6) the internal interaction of the atoms will be neglected and so the Hamiltonian has the form

$$H = H_0 + H_1. \quad (5.1)$$

H_0 is the part of the Hamiltonian which is constant in time and H_1 is the fluctuating part following a Gaussian distribution. We use two methods for this analysis and compare the results: A master equation for the case of $\gamma \gg b$ is derived and solved for various situations and compared to the results of a numerical simulation.

The decay resulting from interaction between the atoms will be discussed in section 5.6. In the following section 5.1 we derive our master equation.

5.1. Master equation method

From [25] we know the limiting case $\Gamma \rightarrow \infty$ of the equation

$$\frac{dx}{dt} = Ax + \sum_{i=1}^N B_i x \cdot \alpha_i(t) \quad (5.2)$$

with linear operators A , B_i and Gaussian noise α of the form

$$\begin{aligned} \forall t, i : \overline{\alpha_i(t)} &= 0 \\ \forall t > 0, \forall i, j \in \{1, \dots, N\} : \overline{\alpha_i(t) \alpha_j(0)} &= \Gamma \cdot \delta_{ij} e^{-\Gamma t}. \end{aligned} \quad (5.3)$$

Using the notation from section 4.4, the corresponding equation we want to study can be written as

$$\begin{aligned} \frac{d\rho}{dt} &= -iB_0[h_0, \rho] - ib \sum_{i=1,2,3} \sum_{j=x,y,z} [\sigma_{ij}, \rho] \xi_{ij}(t) \\ &= -iB_0[h_0, \rho] - ib \sum_{i=1,2,3} \sum_{j=x,y,z} \sum_{k=1}^9 [\sigma_{ij}, \rho] C_{(ij),k} \zeta_k(t). \end{aligned} \quad (5.4)$$

In its general form, (5.2) has the Itô equation [25]

$$dx = (Axdt + \sum_i B_i^2 x \cdot dt + \sum_i B_i x \cdot dW_i) \quad (5.5)$$

as the limit case $\Gamma \rightarrow \infty$. Here W_i is a Brownian motion.

Let us translate this result to our equation: We use dimensionless units with $b = 1$ so that

5. Methods, results and possible experiment

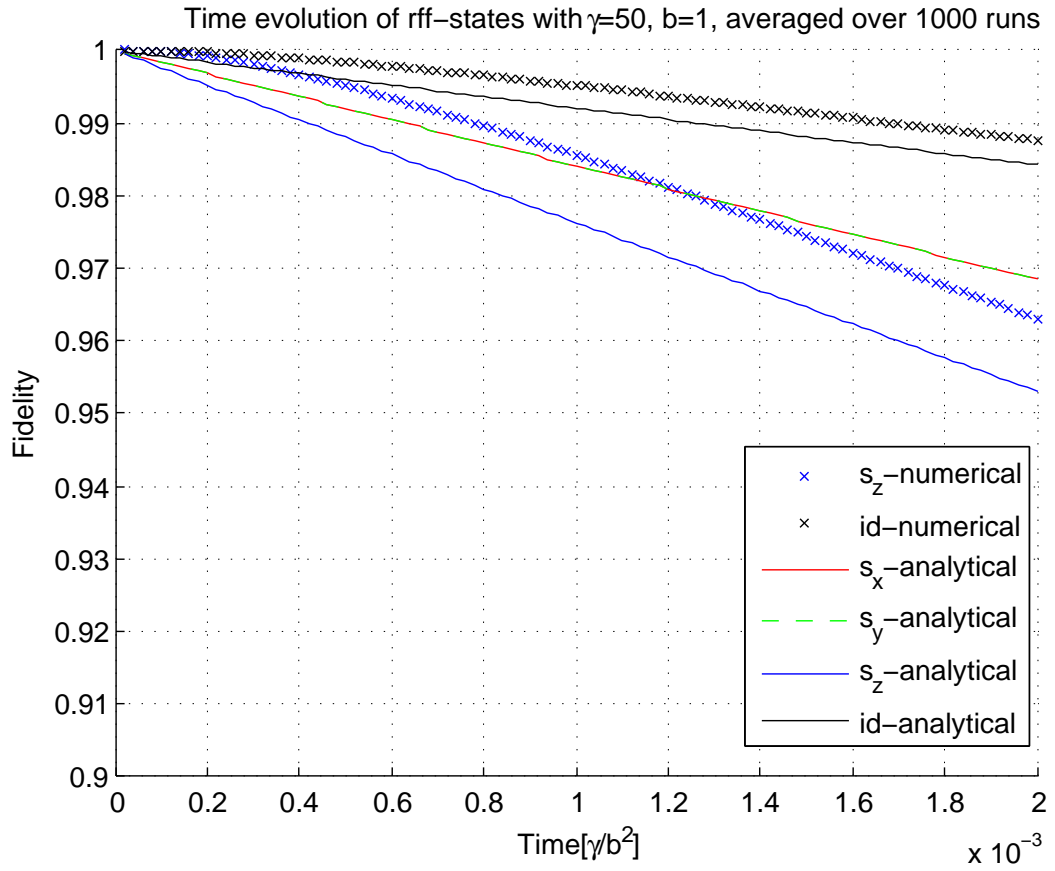


Abbildung 5.1.: For $\gamma \rightarrow \infty$ the numerical result (crosses) converges to the white noise limit analytical result. (solid line) in this figure $\gamma = 50$ and a large deviation can still be seen. The same result for $\gamma = 500$ is plotted in figure 5.2 and shows a very small deviation from the $\gamma \rightarrow \infty$ case on the relevant timescale.

$\gamma = \Gamma$, then adjust the time units according to $t \propto \frac{\gamma}{b^2}$ and take the limit $\Gamma \rightarrow \infty$, which is

graphically visualized in Figure 5.1 to obtain:

$$\begin{aligned} d\rho = & -iB_0[h_0, \rho]dt \\ & - \frac{b^2}{\gamma} \sum_{i,j,m,n,k} C_{(ij),k} C_{(mn),k} [\sigma_{ij}, [\sigma_{mn}, \rho]] dt \\ & - ib \sum_{i,j,k} [\sigma_{ij}, \rho] C_{(ij),k} dW_k \end{aligned} \quad (5.6)$$

Equation (5.6) still describes a unitary time evolution of a pure state subject to a particular realization of the noise. Averaging over all possible noise realizations of the ensemble we will get the time evolution of the density matrix on average, which is what we are interested in. The last term of the sum vanishes when this average is taken, as its mean value is zero:

$$\overline{\sum_{i,j,k} [\sigma_{ij}, \rho] C_{(ij),k} dW_k} = 0. \quad (5.7)$$

We use the notation $\Sigma = C^T C$ and $I = ij$ from section 4.4 to finally write our master equation as

$$\begin{aligned} d\rho = & -iB_0[h_0, \rho]dt - \frac{b^2}{\gamma} \sum_{i,j,m,n,k} C_{(ij),k} C_{(mn),k} [\sigma_{ij}, [\sigma_{mn}, \rho]] dt \\ = & -iB_0[h_0, \rho]dt - \frac{b^2}{\gamma} \sum_{I,J} \Sigma_{IJ} [\sigma_I, [\sigma_J, \rho]] dt. \end{aligned} \quad (5.8)$$

For example in the special case of a spatially uncorrelated inhomogeneous noise and another spatially constant part this is simply:

$$d\rho = -iB_0[h_0, \rho]dt - \frac{b^2}{\gamma} \sum_{i,j} [\sigma_{ij}, [\sigma_{ij}, \rho]] dt - \frac{\tilde{b}^2}{\tilde{\gamma}} \sum_{i,j,k,l} [\sigma_{ij}, [\sigma_{kl}, \rho]] dt. \quad (5.9)$$

Here $\frac{b^2}{\gamma}$ describes the inhomogeneous noise, $\frac{\tilde{b}^2}{\tilde{\gamma}}$ describes the homogeneous part of the noise. An alternative way to write the noise term of equation (5.8) is:

$$\begin{aligned} & \sum_{i,j,m,n,k} C_{(ij),k} C_{(mn),k} [\sigma_{ij}, [\sigma_{mn}, \rho]] \\ = & \sum_{i,j,m,n,k,l} C_{(ij),k} C_{(mn),l} [\sigma_{ij}, [\sigma_{mn}, \rho]] \delta_{kl} \\ = & \sum_{i,j,m,n,k,l} C_{(ij),k} C_{(mn),l} [\sigma_{ij}, [\sigma_{mn}, \rho]] \overline{\zeta_k \zeta_l} \\ = & \overline{\sum_{i,j,m,n,k,l} [C_{(ij),k} \sigma_{ij} \zeta_k, [C_{(mn),l} \sigma_{mn} \zeta_l, \rho]]} \\ \equiv & \overline{[h_1, [h_1, \rho]]}, \end{aligned} \quad (5.10)$$

and this should define $h_1 = \frac{H_1}{b}$. Now our master equation can also be written in the convenient form

$$\rho(t + dt) = \rho(t) - i[H_0, \rho]dt + 2 \frac{b^2}{\gamma} \overline{[h_1 \rho h_1]} - \frac{1}{2} \overline{h_1^2 \rho} - \frac{1}{2} \overline{\rho h_1^2} dt \quad (5.11)$$

5. Methods, results and possible experiment

which is equivalent to

$$\rho(t + dt) = \rho(t) - i[H_0, \rho]dt + 2 \frac{1}{\gamma} (\overline{H_1 \rho H_1} - \frac{1}{2} \overline{H_1^2} \rho - \frac{1}{2} \rho \overline{H_1^2}) dt. \quad (5.12)$$

The bars indicate averaging over the probability distribution.

In the following sections we will apply these results to different kinds of noise environments. For example in the limit of white noise it is assumed that

$$\gamma \gg b, B_z, f. \quad (5.13)$$

Given this inequality we know from equation (5.8) that we cannot expect the bias field or the Zeno measurements to have any stabilizing effect in the white noise limit. If

$$B_z \gg b, \gamma, \quad (5.14)$$

the B-field does have a stabilizing effect. The same is true for a large value of the measurement frequency f of the total angular momentum.

Equation (5.11) is a Lindblad form master equation and can be solved analytically using the corresponding Lindblad superoperator [25] \mathcal{L} :

$$\rho(t) = e^{\mathcal{L}t} \rho(0). \quad (5.15)$$

5.2. Spatially uncorrelated noise

In this section we solve the master equation for spatially uncorrelated noise, which would be a good model, if the atoms were far apart from each other.

5.2.1. Unstabilized setup

If $H_0 = 0$, the resulting operator \mathcal{L} has only real Eigenvalues and all of them are smaller than or equal to zero. The kernel of \mathcal{L} is spanned only by the totally mixed state. We are especially interested in the time evolution of states that are used for encoding the rff-qubit. To solve the master equation \mathcal{L} must be expanded as $e^{\mathcal{L}t}$. This can be done by diagonalizing

$$\mathcal{L} = ADA^{-1} \quad (5.16)$$

with a diagonal matrix D and solving for

$$e^{\mathcal{L}t} = Ae^{Dt}A^{-1}. \quad (5.17)$$

Starting in an arbitrary state in the rff-subspace at time 0 the state will have the following time development in the spin $\frac{1}{2}$ subspace:

$$\rho(t) = \frac{1}{2} \left(s_{\mathbf{I}}(t) \mathbf{I}^{\text{rff}} + s_x(t) \sigma_x^{\text{rff}} + s_y(t) \sigma_y^{\text{rff}} + s_z(t) \sigma_z^{\text{rff}} \right) \otimes \mathbf{I}_{\text{Idler}} \quad (5.18)$$

with coefficients $s_i(t)$ as functions of their initial value and t :

$$\begin{aligned} s_{\mathbf{I}}(t) &= \frac{1}{2} + \frac{1}{2} \cdot e^{-\lambda_0 t}, & s_x(t) &= s_x(0) \cdot e^{-\lambda_x t} \\ s_y(t) &= s_y(0) \cdot e^{-\lambda_y t}, & s_z(t) &= s_z(0) \cdot e^{-\lambda_z t} \end{aligned} \quad (5.19)$$

with

$$\lambda_0 = \lambda_x = \lambda_y = 16 \frac{b^2}{\gamma}, \lambda_z = 24 \frac{b^2}{\gamma}. \quad (5.20)$$

So the calculations predict that the z -component of the rff state is the most unstable one compared to x - and y -components.

The fraction $\frac{2}{3}$ between the decay constants is plausible when looking at the explicit forms of the rff-operators given in equation (12) in [14]: While σ_x^{rff} and σ_y^{rff} consist of scalar products of 2 physical qubit operators, σ_z^{rff} is the triple product of all 3 physical qubits. Each physical qubit has a decay rate of $\lambda_{\text{atom}} = 8 \frac{b^2}{\gamma}$ independent of direction. As in this model the decay is independent for each atom also, we get the decay rates

$$\lambda_x = 2 \cdot \lambda_{\text{atom}}, \lambda_y = 2 \cdot \lambda_{\text{atom}}, \lambda_z = 3 \cdot \lambda_{\text{atom}}. \quad (5.21)$$

5.2.2. Zeno effect

By constantly measuring the quantum number j one can suppress transitions between states with different j -value, if the measuring frequency f is much bigger than the inverse correlation time of the noise: $f \gg \gamma$. This is possible because the state only decays in second order for times $t \ll \frac{1}{\gamma}$. However we do not know how such a continuous measurement of j could be implemented in a real experiment.

To take care of the Zeno effect in our master equation formalism we use equation (5.11) with a modification. For this purpose we define

$$h_{kj} = P_j h_k P_j \quad (5.22)$$

where $k \in \{0, 1\}$ and $j \in \{\frac{1}{2}, \frac{3}{2}\}$. P_j is the Projector on the subspace with total angular momentum j . The master equation with Zeno measurements then reads:

$$\rho(t + dt) = \rho(t) + \sum_{j=\frac{3}{2}, \frac{1}{2}} \left(-i[H_{0j}, \rho] dt + 2 \frac{b^2}{\gamma} (\overline{h_{1j} \rho h_{1j}} - \frac{1}{2} \overline{h_{1j}^2} \rho - \frac{1}{2} \rho \overline{h_{1j}^2}) dt \right) \quad (5.23)$$

Now we get a slowed down decay when starting in the rff-subspace: The coefficients of equation (5.18) evolve according to

$$\begin{aligned} s_{\mathbf{I}}(t) &\equiv 1, & s_x(t) &= s_x(0) \cdot e^{-\lambda_x t} \\ s_y(t) &= s_y(0) \cdot e^{-\lambda_y t}, & s_z(t) &= s_z(0) \cdot e^{-\lambda_z t} \end{aligned} \quad (5.24)$$

with

$$\lambda_x = \lambda_y = 8 \frac{b^2}{\gamma}, \lambda_z = 16 \frac{b^2}{\gamma}. \quad (5.25)$$

Note that $s_{\mathbf{I}} \equiv 1$ because nothing can leak out of the spin- $\frac{1}{2}$ -sector.

5. Methods, results and possible experiment

5.2.3. Bias magnetic field

We use a similar modification of the master equation when a strong bias-field in z -direction stabilizes the setup by suppressing m -transitions. We apply the field in z -direction because we also want to suppress the internal (see section 5.6) interaction. This modification is valid in the regime $B \gg b, \tilde{b}, \gamma$. Using the same procedure as in section 5.2.2 we obtain the master equation:

$$d\rho = -iB_0[h_0, \rho]dt - \frac{b^2}{\gamma} \sum_i [\sigma_{iz}, [\sigma_{iz}, \rho]]dt - \frac{\tilde{b}^2}{\tilde{\gamma}} \sum_{i,k} [\sigma_{iz}, [\sigma_{kz}, \rho]]dt. \quad (5.26)$$

For the time evolution of the coefficients we get:

$$\begin{aligned} s_{\mathbf{I}}(t) &= \frac{2}{3} + \frac{1}{3} \cdot e^{-\lambda_{\mathbf{I}}t}, \quad s_x(t) = s_x(0) \cdot \left(\frac{1}{3} + \frac{2}{3} \cdot e^{-\lambda_x t}\right) \\ s_y(t) &= s_y(0) \cdot \left(\frac{1}{3} + \frac{2}{3} \cdot e^{-\lambda_y t}\right), \quad s_z(t) = s_z(0) \cdot e^{-\lambda_z t} \end{aligned} \quad (5.27)$$

with

$$\lambda = \lambda_x = \lambda_y = \lambda_z = \lambda_{\mathbf{I}} = 8 \frac{b^2}{\gamma}. \quad (5.28)$$

It is remarkable that in this limit the steady state is not totally mixed. Some of the σ_x and σ_y phase information remains. When projected onto the $j = \frac{1}{2}$ subspace we even get

$$\sigma_x \rightarrow \frac{1}{2} \sigma_x \quad (5.29)$$

and

$$\sigma_y \rightarrow \frac{1}{2} \sigma_y \quad (5.30)$$

for $t \rightarrow \infty$. Another interesting property is the emergence of coherences with the $|6\rangle$ -state in the notation introduced in section 4.3. The full time evolution starting in an rff-state with $m = -\frac{1}{2}$ in the notation of (4.3) is:

$$\begin{aligned} \rho(t) &= s_x \left(\left(\frac{1}{3} + \frac{2}{3} e^{-\lambda t}\right) \cdot (|7\rangle \langle 8| + |8\rangle \langle 7|) + \left(\frac{1}{3} - \frac{1}{3} e^{-\lambda t}\right) \cdot (-|6\rangle \langle 8| - |8\rangle \langle 6| + |7\rangle \langle 6| + |6\rangle \langle 7|) \right) \\ &+ i s_y \left(\left(\frac{1}{3} + \frac{2}{3} e^{-\lambda t}\right) \cdot (|7\rangle \langle 8| - |8\rangle \langle 7|) + \left(\frac{1}{3} - \frac{1}{3} e^{-\lambda t}\right) \cdot (|6\rangle \langle 8| - |8\rangle \langle 6| - |7\rangle \langle 6| + |6\rangle \langle 7|) \right) \\ &+ s_z e^{-\lambda t} \cdot (|7\rangle \langle 7| - |8\rangle \langle 8|) \\ &+ \frac{1}{3} \left((1 - e^{-\lambda t}) \cdot |6\rangle \langle 6| + (1 + \frac{1}{2} e^{-\lambda t}) \cdot (|7\rangle \langle 7| + |8\rangle \langle 8|) \right). \end{aligned} \quad (5.31)$$

Possibly the coherences in the density matrix that occur with $|6\rangle$ for σ_x^{rff} and σ_y^{rff} could be useful for error correction.

If however $B < \tilde{b}$ we would have to add a term

$$-\frac{\tilde{b}^2}{\tilde{\gamma}} \sum_{i,k} [\sigma_{ix}, [\sigma_{kx}, \rho]]dt - \frac{\tilde{b}^2}{\tilde{\gamma}} \sum_{i,k} [\sigma_{iy}, [\sigma_{ky}, \rho]]dt \quad (5.32)$$

in the equation which would again result in a totally mixed state as the steady state. In the $B < b$ case we even have to use the noise model without stabilization from section 5.2.1. Finally if both Zeno effect and a strong bias-field are applied we get the equation:

$$\begin{aligned} s_{\mathbf{I}}(t) &\equiv 1, & s_x(t) &= s_x(0) \cdot e^{-\lambda_x t} \\ s_y(t) &= s_y(0) \cdot e^{-\lambda_y t}, & s_z(t) &= s_z(0) \cdot e^{-\lambda_z t} \end{aligned} \quad (5.33)$$

with

$$\lambda_x = \lambda_y = 2 \frac{b^2}{3 \gamma}, \quad \lambda_z = 5 \frac{1}{3} \frac{b^2}{\gamma}. \quad (5.34)$$

So if we want to avoid a totally mixed state as steady state the Zeno measurement cannot be applied.

5.2.4. Conclusion

Applying a B -field that is much stronger than both the homogeneous and the inhomogeneous part of the noise helps to stabilize the setup by making the decay constants smaller and even restore some coherence in the $t \rightarrow \infty$ limit. Finally the state decays with a speed depending on the $\frac{b}{B}$ ratio, this happens on a much longer timescale which is irrelevant for our purpose. If we also continuously monitor the value of the total angular momentum, we get somewhat smaller decay rates but lose all coherence for the steady state. In a real experiment it is much easier to implement only a B -field, so it is the method to be favored.

5.3. Spatially correlated noise

So far the spacial correlations of the inhomogeneous noise part have been neglected. If the atoms are close together a linear approximation of the field is reasonable. In this section we derive the solution of the master equation for this case.

5.3.1. The gradient

In our study of the effect of spatial correlations we assume that the three atoms form an equilateral triangle in the x - y -plane and that the strong bias field is perpendicular to that plane. As the atoms are very close together we assume that the field only changes in first order of \vec{x} :

$$\vec{B}_{\text{approx}}(\vec{x}) = \vec{B}(\vec{x}_0) + \frac{\partial \vec{B}}{\partial \vec{x}}[\vec{x}_0] \cdot (\vec{x} - \vec{x}_0). \quad (5.35)$$

Using this ansatz we also demand that Maxwell equations have to be fulfilled:

$$\nabla \cdot \vec{B} = 0, \quad \nabla \times \vec{B} = 0. \quad (5.36)$$

So $G := \frac{\partial \vec{B}}{\partial \vec{x}}$ must be traceless and symmetric. Together with the demand for rotational invariance the form of the correlation matrix Σ of section 4.4 is uniquely determined:

5. Methods, results and possible experiment

The variance of diagonal elements of G must be independent of the specific vector a . This yields a normalization condition with normalization constant g^2 :

$$\overline{a^T G(t) a a^T G(t') a} = g^2 |a|^4 e^{-\gamma|t-t'|}. \quad (5.37)$$

A general entry of G must be linear in each vector and can only consist of scalars. Thus we use the ansatz

$$\overline{a^T G(t) b c^T G(t') d} = \lambda_1 a^T b c^T d + \lambda_2 a^T c b^T d + \lambda_3 a^T d b^T c. \quad (5.38)$$

To determine the individual λ_i we use the symmetry condition to obtain $\lambda_2 = \lambda_3$. The traceless condition yields $\lambda_1 = -\frac{2}{3}\lambda_2$. Inserting the chosen normalization condition (5.37) we arrive at:

$$\overline{a^T G(t) b c^T G(t') d} = \frac{1}{4} \left(-2a^T b c^T d + 3a^T c b^T d + 3a^T d b^T c \right) g^2 e^{-\gamma|t-t'|}. \quad (5.39)$$

In any orthonormal basis $\{x_1, x_2, x_3\}$ we get the covariances:

$$\begin{aligned} \overline{x_i^T G(t) x_j x_i^T G(t') x_j} &= \left(\frac{3}{4} + \delta_{ij} \frac{1}{4} \right) g^2 e^{-\gamma|t-t'|} \\ \overline{x_i^T G(t) x_j x_j^T G(t') x_i} &= \left(\frac{3}{4} + \delta_{ij} \frac{1}{4} \right) g^2 e^{-\gamma|t-t'|} \\ \overline{x_i^T G(t) x_i x_j^T G(t') x_j} &= -\frac{1}{2} g^2 e^{-\gamma|t-t'|}, \quad \forall i \neq j \end{aligned} \quad (5.40)$$

and

$$\overline{x_i^T G(t) x_j x_k^T G(t') x_l} = 0 \quad (5.41)$$

for all other combinations. The time independent spatial covariance matrix Σ_{∇} for the random variables $\left\{ \frac{\partial B_x}{\partial x}, \frac{\partial B_y}{\partial y}, \frac{\partial B_z}{\partial z}, \frac{\partial B_x}{\partial y}, \frac{\partial B_y}{\partial x}, \frac{\partial B_y}{\partial z}, \frac{\partial B_z}{\partial y}, \frac{\partial B_z}{\partial x}, \frac{\partial B_x}{\partial z} \right\}$ can thus be written as:

$$\Sigma_{\nabla} = g^2 \begin{pmatrix} 1 & -\frac{1}{2} & -\frac{1}{2} & 0 & 0 & 0 & 0 & 0 & 0 \\ -\frac{1}{2} & 1 & -\frac{1}{2} & 0 & 0 & 0 & 0 & 0 & 0 \\ -\frac{1}{2} & -\frac{1}{2} & 1 & 0 & 0 & 0 & 0 & 0 & 0 \\ 0 & 0 & 0 & \frac{3}{4} & \frac{3}{4} & 0 & 0 & 0 & 0 \\ 0 & 0 & 0 & \frac{3}{4} & \frac{3}{4} & 0 & 0 & 0 & 0 \\ 0 & 0 & 0 & 0 & 0 & \frac{3}{4} & \frac{3}{4} & 0 & 0 \\ 0 & 0 & 0 & 0 & 0 & \frac{3}{4} & \frac{3}{4} & 0 & 0 \\ 0 & 0 & 0 & 0 & 0 & 0 & 0 & \frac{3}{4} & \frac{3}{4} \\ 0 & 0 & 0 & 0 & 0 & 0 & 0 & \frac{3}{4} & \frac{3}{4} \end{pmatrix}. \quad (5.42)$$

As we expect possible noise sources to change only with a low frequency noise, the situation can be described as quasistatic and we do not need to use the time dependent Maxwell equations. Also the magnetic fields which are due to the laser trapping can be neglected.

5.3.2. Limitations of the linear model

To derive the covariance matrix for the B-field at different places we would like to assume the gradient to be constant in space and the noise to be completely isotropic.

However in this section we show, that it is not possible to fulfill both conditions, i.e. a linear model that fulfills Maxwell's equations cannot be isotropic. Thus there is no natural choice for a model to be used. Let us restate the conditions in a more elaborate way that leads to a set of equations, which we then show to be *not* simultaneously fulfillable.

1. The distance between the atoms is small enough to consider the gradient as constant in space:

$$\frac{\partial \vec{B}}{\partial \vec{x}}[\vec{x}_0] \equiv \frac{\partial \vec{B}}{\partial \vec{x}} \quad (5.43)$$

2. The noise is completely isotropic.

- a) Thus the covariance matrix for the fields $\{B_x, B_y, B_z\}$ at any individual spot j must be proportional to identity with the same coefficient B^2 :

$$\Sigma_j = B^2 \begin{pmatrix} 1 & 0 & 0 \\ 0 & 1 & 0 \\ 0 & 0 & 1 \end{pmatrix}. \quad (5.44)$$

- b) Let B_{ij} denote the field at point i pointing from point i to point j . Then $\text{Cov}(B_{ij}, B_{ji})$ is independent of i and j , because the distance between each pair is the same.

$$\forall i \neq j, k \neq l : \text{Cov}(B_{ij}, B_{ji}) = \text{Cov}(B_{kl}, B_{lk}). \quad (5.45)$$

- c) Let $B_{ij\perp}$ denote a field at point i perpendicular to the vector pointing from point i to point j . Then

$$\text{Cov}(B_{ij\perp}, B_{ji}) = 0 \quad (5.46)$$

must hold due to isotropy.

Let N denote the number of atoms. We observe that the random variables

$$\vec{d}_j := \vec{B}_j - \vec{B}_{j+1}, \quad j \in 1, \dots, N-1 \quad (5.47)$$

are independent of the overall field. Thus, using assumption 1, their covariance matrix $\Sigma_{\text{diff}} = \Sigma(\vec{d}_1, \vec{d}_2, \vec{d}_3)$ can be derived from the gradient (5.42) and

$$\vec{d}_N := \vec{B}_N - \vec{B}_1 = - \sum_{j=1}^{N-1} \vec{d}_j \quad (5.48)$$

is a linear combination of the remaining field differences. We write Σ_{diff} in the order $\{d_{1x}, d_{1y}, d_{1z}, d_{2x}, \dots, d_{3z}\}$ and define a (not to be confused with the arbitrary vector variable on the previous page) as the spacing between the individual atoms:

5. Methods, results and possible experiment

$$\Sigma_{\text{diff}} = g^2 a^2 \begin{pmatrix} \frac{13}{16} & -\sqrt{\frac{3}{256}} & 0 & -\frac{1}{2} & \sqrt{\frac{27}{64}} & 0 & -\frac{5}{16} & -\sqrt{\frac{75}{256}} & 0 \\ -\sqrt{\frac{3}{256}} & \frac{15}{16} & 0 & -\sqrt{\frac{3}{16}} & -\frac{3}{8} & 0 & \sqrt{\frac{75}{256}} & -\frac{9}{16} & 0 \\ 0 & 0 & \frac{3}{4} & 0 & 0 & -\frac{3}{8} & 0 & 0 & -\frac{3}{8} \\ -\frac{1}{2} & -\sqrt{\frac{3}{16}} & 0 & 1 & 0 & 0 & -\frac{1}{2} & \sqrt{\frac{3}{16}} & 0 \\ \sqrt{\frac{27}{64}} & -\frac{3}{8} & 0 & 0 & \frac{3}{4} & 0 & -\sqrt{\frac{27}{64}} & -\frac{3}{8} & 0 \\ 0 & 0 & -\frac{3}{8} & 0 & 0 & \frac{3}{4} & 0 & 0 & -\frac{3}{8} \\ -\frac{5}{16} & \sqrt{\frac{75}{256}} & 0 & -\frac{1}{2} & -\sqrt{\frac{27}{64}} & 0 & \frac{13}{16} & \sqrt{\frac{3}{256}} & 0 \\ -\sqrt{\frac{75}{256}} & -\frac{9}{16} & 0 & \sqrt{\frac{3}{16}} & -\frac{3}{8} & 0 & \sqrt{\frac{3}{256}} & \frac{15}{16} & 0 \\ 0 & 0 & -\frac{3}{8} & 0 & 0 & -\frac{3}{8} & 0 & 0 & \frac{3}{4} \end{pmatrix} \quad (5.49)$$

As we want to determine the fields and not only their differences we introduce the random variable \vec{B}_1 and relate it to \vec{d}_1 and \vec{d}_2 . As \vec{d}_3 can be reconstructed from the latter two, we replace it by \vec{B}_1 and get a covariance matrix

$$\Sigma(\vec{d}_1, \vec{d}_2, \vec{B}_1) = g^2 a^2 \begin{pmatrix} \frac{13}{16} & -\sqrt{\frac{3}{256}} & 0 & -\frac{1}{2} & \sqrt{\frac{27}{64}} & 0 & c_{17} & c_{18} & c_{19} \\ -\sqrt{\frac{3}{256}} & \frac{15}{16} & 0 & -\sqrt{\frac{3}{16}} & -\frac{3}{8} & 0 & c_{27} & c_{28} & c_{29} \\ 0 & 0 & \frac{3}{4} & 0 & 0 & -\frac{3}{8} & c_{37} & c_{38} & c_{39} \\ -\frac{1}{2} & -\sqrt{\frac{3}{16}} & 0 & 1 & 0 & 0 & c_{47} & c_{48} & c_{49} \\ \sqrt{\frac{27}{64}} & -\frac{3}{8} & 0 & 0 & \frac{3}{4} & 0 & c_{57} & c_{58} & c_{59} \\ 0 & 0 & -\frac{3}{8} & 0 & 0 & \frac{3}{4} & c_{67} & c_{68} & c_{69} \\ c_{17} & c_{27} & c_{37} & c_{47} & c_{57} & c_{67} & c & c_{78} & c_{79} \\ c_{18} & c_{28} & c_{38} & c_{48} & c_{58} & c_{68} & c_{78} & c & c_{89} \\ c_{19} & c_{29} & c_{39} & c_{49} & c_{59} & c_{69} & c_{79} & c_{89} & c \end{pmatrix} \quad (5.50)$$

with some coefficients c_{ij} that we will now determine. First we transform to the basis of the individual fields to obtain

$$\Sigma(\vec{B}_1, \vec{B}_2, \vec{B}_3) = T^T \Sigma(\vec{d}_1, \vec{d}_2, \vec{B}_1) T, \quad (5.51)$$

where the matrix T corresponds to the inverse of the mapping

$$\begin{aligned} \vec{B}_1 &\rightarrow \vec{B}_1 - \vec{B}_2 \\ \vec{B}_2 &\rightarrow \vec{B}_2 - \vec{B}_3 \\ \vec{B}_3 &\rightarrow \vec{B}_1. \end{aligned} \quad (5.52)$$

In this basis we can read of the equations imposed by 2.a). For example we find:

$$c_{89} = c_{78} = c_{79} = 0. \quad (5.53)$$

Similarly we can transform Σ to suitable basis to read of conditions 2.b) and 2.c). Finally we obtain the result:

$$\begin{aligned} c_{69} = c_{67} = c_{68} = c_{49} = c_{59} = c_{37} = c_{38} = c_{19} = c_{29} = c_{58} = 0 \\ c_{39} = \frac{3}{8}, c_{17} = \frac{13}{32}, c_{28} = \frac{15}{32}, c_{57} = \frac{3\sqrt{3}}{8}, c_{48} = -\frac{\sqrt{3}}{4}, c_{27} = -\frac{11\sqrt{3}}{32}, \\ c_{18} = \frac{9\sqrt{3}}{32}. \end{aligned} \quad (5.54)$$

All of the conditions 2.a-c) are necessary for isotropy. However there are even more conditions to be fulfilled for isotropy: For example if we use the resulting coefficients to calculate the covariance matrix

$$\Sigma(\vec{B}_2 - \vec{B}_3, \vec{B}_2 + \vec{B}_3) = g^2 a^2 \begin{pmatrix} 1 & 0 & 0 & 0 & \frac{5}{24}\sqrt{3} & 0 \\ 0 & \frac{3}{4} & 0 & -\frac{5}{24}\sqrt{3} & 0 & 0 \\ 0 & 0 & \frac{3}{4} & 0 & 0 & 0 \\ 0 & -\frac{5}{24}\sqrt{3} & 0 & -1 + 4c & 0 & 0 \\ \frac{5}{24}\sqrt{3} & 0 & 0 & 0 & -\frac{3}{4} + 4c & 0 \\ 0 & 0 & 0 & 0 & 0 & -\frac{3}{4} + 4c \end{pmatrix}, \quad (5.55)$$

we find that it has non-zero off-diagonal elements, which should not be the case! We conclude that in order to make an approximation with a spatially constant, isotropic gradient, we can never fulfill all consistency conditions. Although we just showed that no model can be completely consistent, we can still try some reasonable methods to do the calculation and compare their result.

5.3.3. Expansion point method

Assuming the magnetic field $B(x)$ to be an analytical function of space, we can write it at the individual sites at a given time in a Taylor series around some expansion point x_0 (for better readability we omit the vector sign):

$$B(x) = B(x_0) + \frac{\partial B}{\partial x}[x_0](x - x_0) + \frac{1}{2} \frac{\partial^2 B}{\partial x^2}[x_0](x - x_0, x - x_0) + \dots \quad (5.56)$$

In leading order the Euclidean error of a linear approximation of the B -field is thus:

$$\|B_{\text{approx}}(x) - B(x)\| \approx \epsilon \|x - x_0\|^2 \quad (5.57)$$

with some constant $\epsilon > 0$. This error estimate is justified for small errors which we have already assumed to justify the approximation in the first place. The sum of errors at the individual sites in $\|\cdot\|$ -norm is

$$\sum_j \|B_{\text{approx}}(x_j) - B(x_j)\| \approx \epsilon \sum_j \|x_j - x_0\|^2 \quad (5.58)$$

and is minimized by the mean position

$$x_0 = \sum_{j=1}^N \frac{x_j}{N}, \quad (5.59)$$

5. Methods, results and possible experiment

which is therefore a natural choice for the expansion point. The B-fields at the individual sites don't have an isotropic distribution with this method of expansion, see equation (5.56). For example the variance of the field pointing towards the expansion point is bigger than the variance in other directions. In section 5.3.2 we showed that all linear models have some problem like this.

5.3.4. 2-point-correlation model

If we look at two atoms only, it is possible to use a linear and isotropic model with the help of the gradient from section 5.3.1. The best model for one atom is always a covariance matrix proportional to identity and for any two atoms it is natural to assume that gradient and average field are independent of each other. In this way one would get covariance matrices $\Sigma(\vec{B}_1, \vec{B}_2)$, $\Sigma(\vec{B}_2, \vec{B}_3)$ and $\Sigma(\vec{B}_3, \vec{B}_1)$. With the notation $\alpha = g^2 a^2$ and $\alpha' = c\alpha$ we use the entries from these matrices directly as a definition for:

$$\Sigma(\vec{B}_1, \vec{B}_2, \vec{B}_3) = \begin{pmatrix} \alpha' & 0 & 0 & \alpha' - \frac{13}{32}\alpha & \frac{1}{32}\alpha\sqrt{3} & 0 & \alpha' - \frac{13}{32}\alpha & \frac{1}{32}\alpha\sqrt{3} & 0 \\ 0 & \alpha' & 0 & \frac{1}{32}\alpha\sqrt{3} & \alpha' - \frac{15}{32}\alpha & 0 & -\frac{1}{32}\alpha\sqrt{3} & \alpha' - \frac{15}{32}\alpha & 0 \\ 0 & 0 & \alpha' & 0 & 0 & \alpha' - \frac{3}{8}\alpha & 0 & 0 & \alpha' - \frac{3}{8}\alpha \\ \alpha' - \frac{13}{32}\alpha & \frac{1}{32}\alpha\sqrt{3} & 0 & \alpha' & 0 & 0 & \alpha' - \frac{1}{2}\alpha & 0 & 0 \\ \frac{1}{32}\alpha\sqrt{3} & \alpha' - \frac{15}{32}\alpha & 0 & 0 & \alpha' & 0 & 0 & \alpha' - \frac{3}{8}\alpha & 0 \\ 0 & 0 & \alpha' - \frac{3}{8}\alpha & 0 & 0 & \alpha' & 0 & 0 & \alpha' - \frac{3}{8}\alpha \\ \alpha' - \frac{13}{32}\alpha & -\frac{1}{32}\alpha\sqrt{3} & 0 & \alpha' - \frac{1}{2}\alpha & 0 & 0 & \alpha' & 0 & 0 \\ -\frac{1}{32}\alpha\sqrt{3} & \alpha' - \frac{15}{32}\alpha & 0 & 0 & \alpha' - \frac{3}{8}\alpha & 0 & 0 & \alpha' & 0 \\ 0 & 0 & \alpha' - \frac{3}{8}\alpha & 0 & 0 & \alpha' - \frac{3}{8}\alpha & 0 & 0 & \alpha' \end{pmatrix}. \quad (5.60)$$

The advantage of this method is that by construction the covariance matrix for any 2 atoms is not affected by the total number of atoms one wants to model. However it is not in full agreement with the starting point of the derivation, the assumption of a spatially constant, isotropic gradient. We transform $\Sigma(\vec{B}_1, \vec{B}_2, \vec{B}_3)$ to $\Sigma\left(\frac{\partial\vec{B}}{\partial x}, \frac{\partial\vec{B}}{\partial y}\right)$ and obtain

$$\Sigma\left(\frac{\partial\vec{B}}{\partial x}, \frac{\partial\vec{B}}{\partial y}\right) = \frac{1}{a^2} \begin{pmatrix} \alpha & 0 & 0 & 0 & \frac{\alpha}{8} & 0 \\ 0 & \frac{3}{4}\alpha & 0 & \frac{\alpha}{8} & 0 & 0 \\ 0 & 0 & \frac{3}{4}\alpha & 0 & 0 & 0 \\ 0 & \frac{\alpha}{8} & 0 & \frac{3}{4}\alpha & 0 & 0 \\ \frac{\alpha}{8} & 0 & 0 & 0 & \alpha & 0 \\ 0 & 0 & 0 & 0 & 0 & \frac{3}{4}\alpha \end{pmatrix}, \quad (5.61)$$

which is unequal to our starting point, the gradient matrix (5.42).

5.3.5. Unstabilized setup

As we just derived there is no linear model that fulfills all the conditions we would like to be fulfilled. However in practice this seems irrelevant for the decay rates of the rff-qubit, as all three of the models above give the same decay rates for large values of the constant c , which

is the ratio of homogeneous noise to inhomogeneous noise. As the atoms are close together this is always fulfilled and we can use the resulting decay rates as very good approximations. For a convenient notation we define $\beta^2 = g^2 a^2$. The resulting solution of the master equation with any of the above models is:

$$\begin{aligned} s_{\mathbf{I}}(t) &= \frac{1}{2} + \frac{1}{2} \cdot e^{-\lambda_{\mathbf{I}} t}, & s_x(t) &= s_x(0) \cdot e^{-\lambda_x t} \\ s_y(t) &= s_y(0) \cdot e^{-\lambda_y t}, & s_z(t) &= s_z(0) \cdot e^{-\lambda_z t} \end{aligned} \quad (5.62)$$

with

$$\lambda_{\mathbf{I}} = \lambda_x = \lambda_y = \frac{20}{3} \frac{\beta^2}{\gamma}, \quad \lambda_z = 10 \frac{\beta^2}{\gamma}. \quad (5.63)$$

5.3.6. Bias magnetic field

We do the same calculation for the setup with an applied bias field perpendicular to the plane in which the atoms form an equilateral triangle. This is the most important case as the experiment is planned to be conducted in this way.

We assume that the bias field is strong enough so that only field components along the z -axis need to be considered. All of the models above have the exact same Σ -matrix in this case, so there is even less need for discussing which is the right method than in the last section. The time evolution of the rff-operators is now:

$$\begin{aligned} s_{\mathbf{I}}(t) &= \frac{2}{3} + \frac{1}{3} \cdot e^{-\lambda_{\mathbf{I}} t}, & s_x(t) &= s_x(0) \cdot \left(\frac{1}{3} + \frac{2}{3} \cdot e^{-\lambda_x t} \right) \\ s_y(t) &= s_y(0) \cdot \left(\frac{1}{3} + \frac{2}{3} \cdot e^{-\lambda_y t} \right), & s_z(t) &= s_z(0) \cdot e^{-\lambda_z t} \end{aligned} \quad (5.64)$$

with

$$\lambda = \lambda_x = \lambda_y = \lambda_z = \lambda_{\mathbf{I}} = 3 \frac{\beta^2}{\gamma}. \quad (5.65)$$

So the decay has exactly the same structure as for spatially uncorrelated noise, but the decay rate is now given in units of β^2 instead of b^2 because we have introduced a distance a . This model is the best one we have for the final physical setup. If we use β^2 to calculate the mean fluctuation b^2 , we find that the correlated noise setup decays slightly faster than the uncorrelated noise setup in these units.

With a rough estimate for $\beta \approx 10^{-13} T$ from experimentalists and $\gamma \approx 50 \text{Hz}$, the frequency of an ordinary current in the lab, we get a decay rate of $\lambda \approx 5 \times 10^{-6} \text{Hz}$, which is by far enough to perform an experiment. This is just a rough estimate and the real decay rate can only be determined experimentally. Still we are confident that λ will be small enough to get a reasonable coherence time to perform operations on the qubit.

5.4. Different number of atoms

5.4.1. Four atoms

An rff-qubit can also be constructed in the subspace with $j = 0$ of a setup of four atoms [14]. In this section this setup is compared to the 3 atom case. The 4-atom setup can also

5. Methods, results and possible experiment

be stabilized by a bias B-field, the steady state is then not totally mixed. With the same approximations as before we do the calculation for this setup first for the case of no spatial correlations and then give the results with included spatial correlations.

The setup with no stabilization and no spatial correlation is solved by:

$$\begin{aligned} s_{\mathbf{I}}(t) &= \frac{1}{8} + \frac{1}{4} \cdot e^{-\lambda_1 t} + \frac{5}{8} \cdot e^{-\lambda_3 t}, & s_x(t) &= s_x(0) \cdot \left(\frac{1}{2} \cdot e^{-\lambda_1 t} + \frac{1}{2} \cdot e^{-\lambda_3 t} \right) \\ s_y(t) &= s_y(0) \cdot \left(\frac{1}{2} \cdot e^{-\lambda_1 t} + \frac{1}{2} \cdot e^{-\lambda_3 t} \right), & s_z(t) &= s_z(0) \cdot e^{-\lambda_2 t} \end{aligned} \quad (5.66)$$

with

$$\lambda_1 = 16 \frac{b^2}{\gamma}, \quad \lambda_2 = 24 \frac{b^2}{\gamma}, \quad \lambda_3 = 32 \frac{b^2}{\gamma}. \quad (5.67)$$

So the decay is slightly faster than in the corresponding 3-atom case.

In the case of spatially correlated noise we again use the same methods (expansion point, 2-point-correlation) to solve the 4-atoms master equation as we did for 3 atoms. Again all methods give the same result, so it doesn't matter which one we use. The resulting solution of the master equation without a stabilizing B-field is:

$$\begin{aligned} s_{\mathbf{I}}(t) &= \frac{1}{8} + \frac{4}{9} \cdot e^{-\lambda_1 t} + \frac{25}{72} \cdot e^{-\lambda_2 t} + \frac{1}{12} \cdot e^{-\lambda_3 t} \\ s_x(t) &= s_x(0) \cdot \left(\frac{3}{8} \cdot e^{-\lambda_4 t} + \frac{5}{90} \cdot e^{-\lambda_2 t} + \frac{35}{72} \cdot e^{-\lambda_1 t} + \frac{1}{12} \cdot e^{-\lambda_3 t} \right) \\ s_y(t) &= s_y(0) \cdot \left(\frac{1}{8} \cdot e^{-\lambda_4 t} + \frac{1}{6} \cdot e^{-\lambda_2 t} + \frac{1}{4} \cdot e^{-\lambda_3 t} + \frac{11}{24} \cdot e^{-\lambda_1 t} \right) \\ s_z(t) &= s_z(0) \cdot e^{-\lambda_3 t} \end{aligned} \quad (5.68)$$

with

$$\lambda_1 = 6 \frac{2b^2}{3\gamma}, \quad \lambda_2 = 26 \frac{2b^2}{3\gamma}, \quad \lambda_3 = 13 \frac{1b^2}{3\gamma}, \quad \lambda_4 = 20 \frac{b^2}{\gamma}. \quad (5.69)$$

If a stabilizing field is applied in z-direction we obtain:

$$\begin{aligned} s_{\mathbf{I}}(t) &= \frac{4}{9} + \frac{2}{9} \cdot e^{-\lambda_1 t} + \frac{1}{9} \cdot e^{-\lambda_2 t} + \frac{2}{9} \cdot e^{-\lambda_3 t} \\ s_x(t) &= s_x(0) \cdot \left(\frac{7}{36} + \frac{5}{9} \cdot e^{-\lambda_1 t} + \frac{1}{9} \cdot e^{-\lambda_2 t} + \frac{5}{36} \cdot e^{-\lambda_3 t} \right) \\ s_y(t) &= s_y(0) \cdot \left(\frac{1}{4} + \frac{1}{3} \cdot e^{-\lambda_1 t} + \frac{1}{3} \cdot e^{-\lambda_2 t} + \frac{1}{12} \cdot e^{-\lambda_3 t} \right) \\ s_z(t) &= s_z(0) \cdot \left(\frac{2}{3} e^{-\lambda_1 t} + \frac{1}{3} e^{-\lambda_2 t} \right) \end{aligned} \quad (5.70)$$

with

$$\lambda_1 = 3 \frac{\beta^2}{\gamma}, \quad \lambda_2 = 6 \frac{\beta^2}{\gamma}, \quad \lambda_3 = 12 \frac{\beta^2}{\gamma}. \quad (5.71)$$

The decay is a little bit faster than in the 3-atoms case, if we assume the edge length to be the same in both cases. In the four atom case σ_x and σ_y have different time evolutions. The probability to stay in the rff-state for $t \rightarrow \infty$ is smaller, but the average fidelity of the operators containing the information divided by the $j = 0$ survival probability is still $\frac{\frac{7}{36} + \frac{1}{4}}{\frac{4}{9}} = \frac{1}{2}$, just as in the 3 atom case.

5.4.2. Two atoms

If a bias B -field is applied in z -direction, which makes the effect of field-inhomogeneities in x - and y -direction negligible, one can also store a decoherence free qubit in the states

$$|0\rangle := |\uparrow\downarrow\rangle, \quad |1\rangle := |\downarrow\uparrow\rangle \quad (5.72)$$

as has been implemented by the Wineland group. With the noise model that takes into account the fluctuation in first order only we get the following fidelities for these states:

$$\begin{aligned} s_x(t) &= s_x(0) \cdot e^{-\lambda t}, & s_y(t) &= s_y(0) \cdot e^{-\lambda t} \\ s_z(t) &= s_z(0), & s_{\mathbf{I}}(t) &= s_{\mathbf{I}}(0) \end{aligned} \quad (5.73)$$

with

$$\lambda = 3 \frac{\beta^2}{\gamma}. \quad (5.74)$$

So this setup decays a little bit faster than the 3-atom setup.

5.5. Numerical analysis

For small γ compared to B_0, b, \tilde{b} the white noise model is no longer valid. To evaluate the small γ case we use a numerical method. This numerical analysis is also compared to the analytical results for the white noise limit to check its validity and we see that both methods are in good agreement.

The numerical method generates time correlated noise and evolves our initial state unitarily with many different realizations of an ensemble of this noise. Then the average over many runs is taken. It is described in more detail below and error estimation is derived.

5.5.1. Method

We use the numerical scheme

$$\begin{aligned} \forall n \in N \\ \zeta_{\text{Num}}(t=0) \sim N(0, 1) \\ \zeta_{\text{Num}}(n \cdot dt + dt) &= e^{-\gamma \cdot dt} \cdot \zeta_{\text{Num}}(n \cdot dt) + \sqrt{1 - e^{-\gamma \cdot 2dt}} \cdot c(n \cdot dt) \end{aligned} \quad (5.75)$$

to simulate the noise. All $c(t)$ are independently Gauss distributed

$$c(t) \sim N(0, 1), \quad \langle c(t), c(t') \rangle = 0. \quad (5.76)$$

Here the index Num of ζ_{Num} stands for numerical. The scheme creates a series with the property

$$\begin{aligned} \forall t = n \cdot dt, t' = n' \cdot dt' : \\ \text{Cov}(\zeta_{\text{Num},ij}(t), \zeta_{\text{Num},kl}(t')) &= \delta_{ik} \delta_{jl} \cdot e^{-\gamma|t-t'|} \\ \overline{\zeta_{\text{Num},ij}(t)} &= 0. \end{aligned} \quad (5.77)$$

5. Methods, results and possible experiment

To get the values for $\vec{\xi}_{\text{Num}}$ we use

$$\vec{\xi}_{\text{Num}} = C\vec{\zeta}_{\text{Num}} \quad (5.78)$$

with the matrix C from 4.4. The vector $\vec{\xi}(t)$ fulfills equation (4.13) for a series of discrete times. The time evolution of the quantum state can then be done using the exact unitary transformation

$$\psi(t + dt) = \exp(-i(Bh_0 + bh_1)dt)\psi(t) \quad (5.79)$$

and $\xi(n \cdot dt)$ as an approximation for $\xi(n \cdot dt + h)$ if $h < dt$ at each time step. Thus the error in this calculation occurs mostly because of the noise simulation.

5.5.2. Error estimation

Let us estimate the error of this scheme for spatially uncorrelated noise to simplify the notation. For spatially correlated noise the resulting choice of time step size is the same.

$\xi(t)$ will denote the true value, $\xi_{\text{Num}}(t)$ is its approximation. At each instance $t = n \cdot dt$ for $n \in N$, when t is equal to one of the times for which the noise value was calculated with equation (5.75), there is no error on $\xi(t)$ at all, because $\xi_{\text{Num}}(n \cdot dt) \equiv \xi(n \cdot dt)$.

We can approximate values of $\xi(n \cdot dt + h)$ with

$$\xi(n \cdot dt + h) \approx \xi(n \cdot dt) \equiv \xi_{\text{Num}}(n \cdot dt). \quad (5.80)$$

If the time step dt is much smaller than the correlation time of the noise $dt \ll \tau = \frac{1}{\gamma}$ and $0 < h < dt$ this approximation is good, as will be shown below. At each instance of time for

$0 < h < dt$ the error is

$$|\xi_{\text{Num}}(t) - \xi(t + h)|, \quad (5.81)$$

as $h < dt$

$$\overline{|\xi_{\text{Num}}(t) - \xi(t + h)|} \leq \overline{|\xi_{\text{Num}}(t) - \xi(t + dt)|} \quad (5.82)$$

on average. Thus we use $\overline{|\xi_{\text{Num}}(t) - \xi(t + dt)|}$ as an upper bound for the average error:

$$\begin{aligned} \overline{|\xi_{\text{Num}}(t) - \xi(t + h)|} &\leq \overline{|\xi_{\text{Num}}(t) - \xi_{\text{Num}}(t + dt)|} \\ &= \overline{|(1 - e^{-\gamma \cdot dt}) \cdot \xi_{\text{Num}}(t) + \sqrt{1 - e^{-\gamma \cdot 2dt}} \cdot c(t)|} \end{aligned} \quad (5.83)$$

Expanding the exponential functions in first order, which is valid for $\sqrt{2\gamma dt} \ll 1$ one obtains:

$$\overline{|\xi_{\text{Num}}(t) - \xi(t + h)|} \leq \overline{|\gamma dt \xi_{\text{Num}}(t) + \sqrt{2\gamma dt} \cdot c(t)|}. \quad (5.84)$$

As ξ_{Num} and $c(t)$ are independently standard normally distributed we get on average:

$$\overline{|\xi_{\text{Num}}(t) - \xi(t + h)|} \leq \sqrt{|\gamma dt|^2 + 2\gamma dt} \xrightarrow{\gamma dt \rightarrow 0} \sqrt{2\gamma dt}. \quad (5.85)$$

Thus the simulation gives reasonable results if the time step $dt \ll \frac{1}{\gamma}$. The error on the noise scales with $\sqrt{2\gamma dt}$. The error on the exponent in the unitary time evolution of equation

(5.79) scales with $b\sqrt{2\gamma dt}$. Taking only the first order error in the exponential the total error of a run for time T can be estimated by

$$\text{error} \approx bT\sqrt{2\gamma dt}. \quad (5.86)$$

For $\gamma = 0$ this method is numerically exact, errors are only do to statistics and the half time of the decoherence-free z-component state is about:

$$T_{1/2} \approx 0.25 \frac{\hbar}{\mu_B b}. \quad (5.87)$$

The approximate equal sign only refers to the numerical prefactor, the scaling with $\frac{\hbar}{\mu_B b}$ is exact. Compared to the white noise limit the half time depends on b only linearly in the small γ case. Combining both formulas to a rough estimation we obtain:

$$T_{1/2} \approx \frac{\hbar}{\mu_B b} \cdot (0.25 + 0.03\gamma \frac{\hbar}{\mu_B b}). \quad (5.88)$$

We want to do the calculation for a time period that is as long as the half life. So we plug our half-life estimation into equation (5.86) and get the condition

$$\sqrt{2\gamma dt} b \frac{\hbar}{\mu_B b} \cdot (0.25 + 0.03\gamma \frac{\hbar}{\mu_B b}) \ll \text{errortolerance} \ll 1 \quad (5.89)$$

for dt , to obtain good results with this method. Note, that equation (5.88) is also an interesting result for a rough half-life estimation on its own without the context of error estimation.

5.5.3. Comparison to analytical equation

To check if the numerical method is consistent with the analytical model, both results are plotted in figures 5.2-5.5 for a big value of γ (white noise limit) and for different setup: no stabilization, stabilization with Zeno effect, bias field and finally with both methods. The notation for $s_x, s_y, s_z, \mathbf{I}$ is the same as in equation (5.18). The good agreement with the analytical result shows that the method is valid for big values of γ . As the error of the numerical method scales with γ we can be even more convinced that it gives reasonable results when γ is small.

The comparison of the effective analytical equations from section 5.2.2 and the numerical results requires $f_{\text{Zeno}} \gg b, \gamma$ and/or $B_z \gg b, \gamma$. Here f_{Zeno} denotes the frequency at which the quantum number j is measured in order to use the Zeno effect. If these conditions are not fulfilled, the stabilization attempt does not work. These plots which include different stabilization scenarios can be seen in the figures 5.3, 5.4 and 5.5.

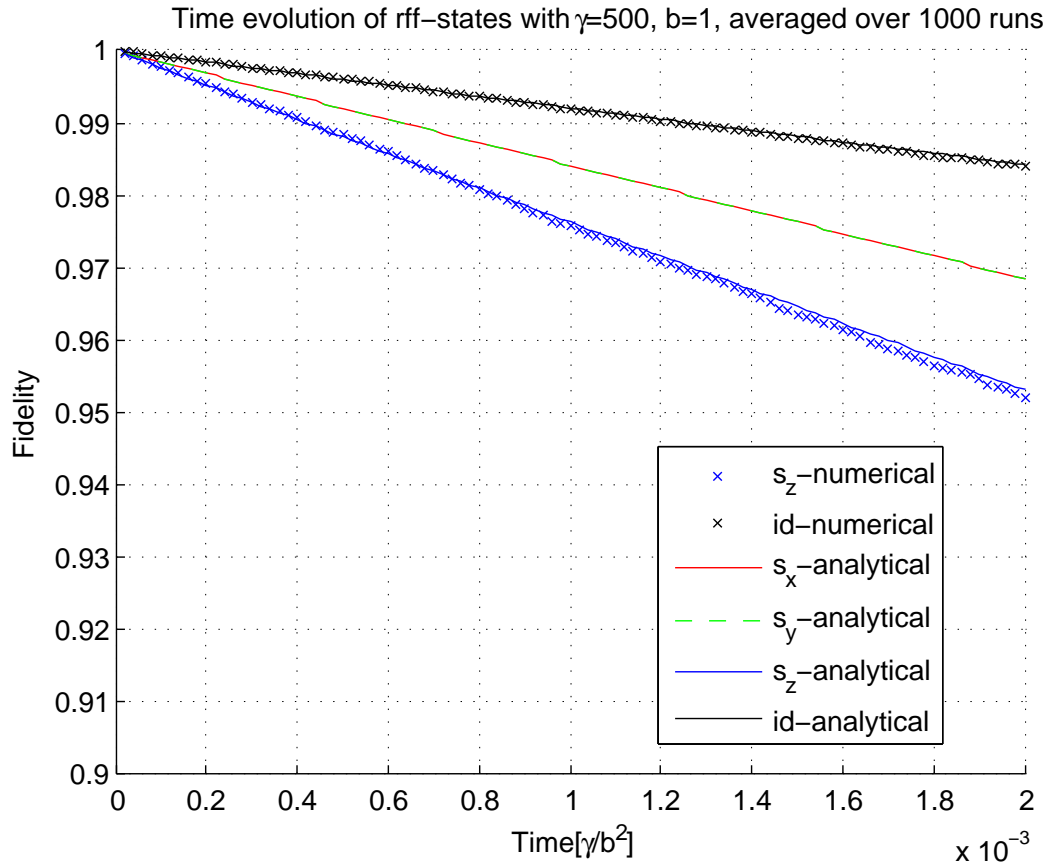


Abbildung 5.2.: Time evolution without any stabilization methods.

5.5.4. Strongly time correlated noise

For very small values of γ the master equation ansatz from (5.11) is not valid anymore. As the numerical scheme agrees with the analytical result for big values of γ we can trust it even more in the small γ case. Figure 5.6 is a plot for the extreme case $\gamma = 0$.

It can be seen that the decay is in second order of t now. With increasing γ it will transform more and more into a decay in first order and the analytical equation will be a good approximation.

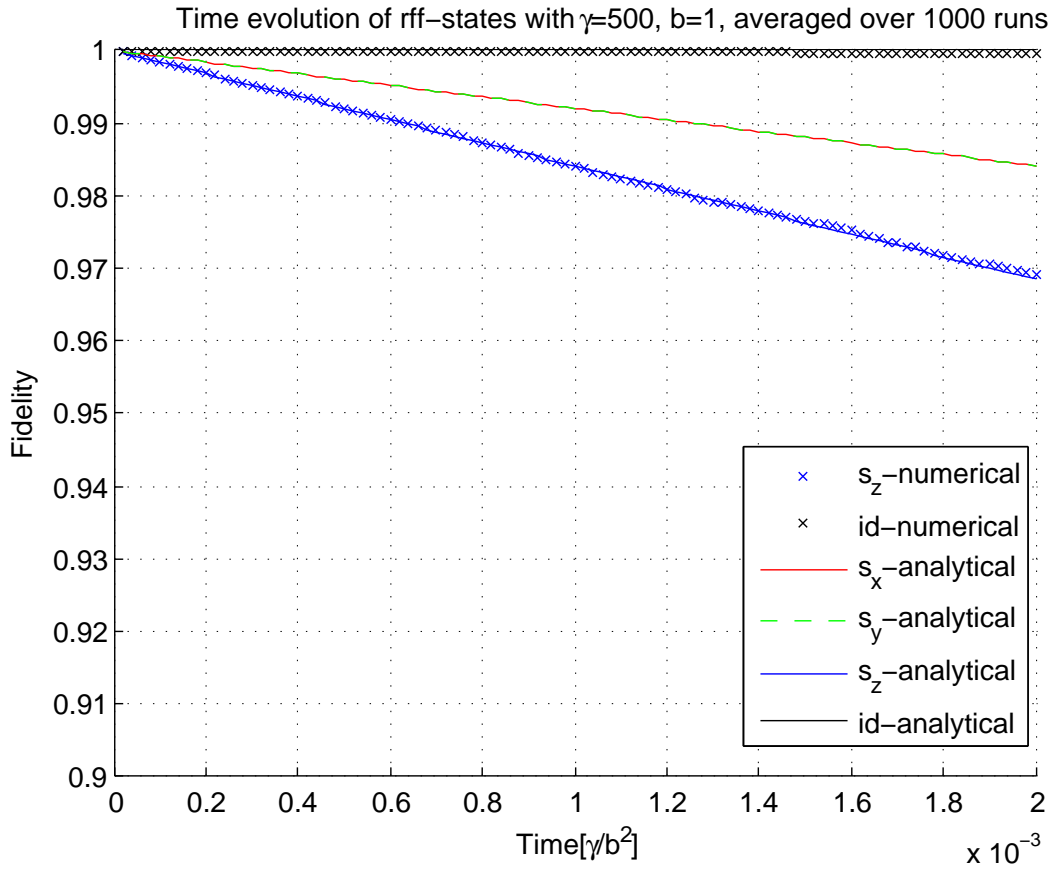


Abbildung 5.3.: Time evolution with stabilization by Zeno effect.

5.6. Internal interaction

In the above models spin-spin interaction between the atoms was ignored. Now we will analyze this part of the Hamiltonian under the assumption that the atoms are trapped by a very strong potential and we can neglect their center of mass motion. In the basis given in section 4.3 the Hamiltonian has the form:

$$H_{\text{internal}} = \frac{\mu_0}{4\pi r^3} \left[\vec{\mu}_A \cdot \vec{\mu}_B - 3(\vec{\mu}_A \cdot \hat{r})(\hat{r} \cdot \vec{\mu}_B) \right]. \quad (5.90)$$

5. Methods, results and possible experiment

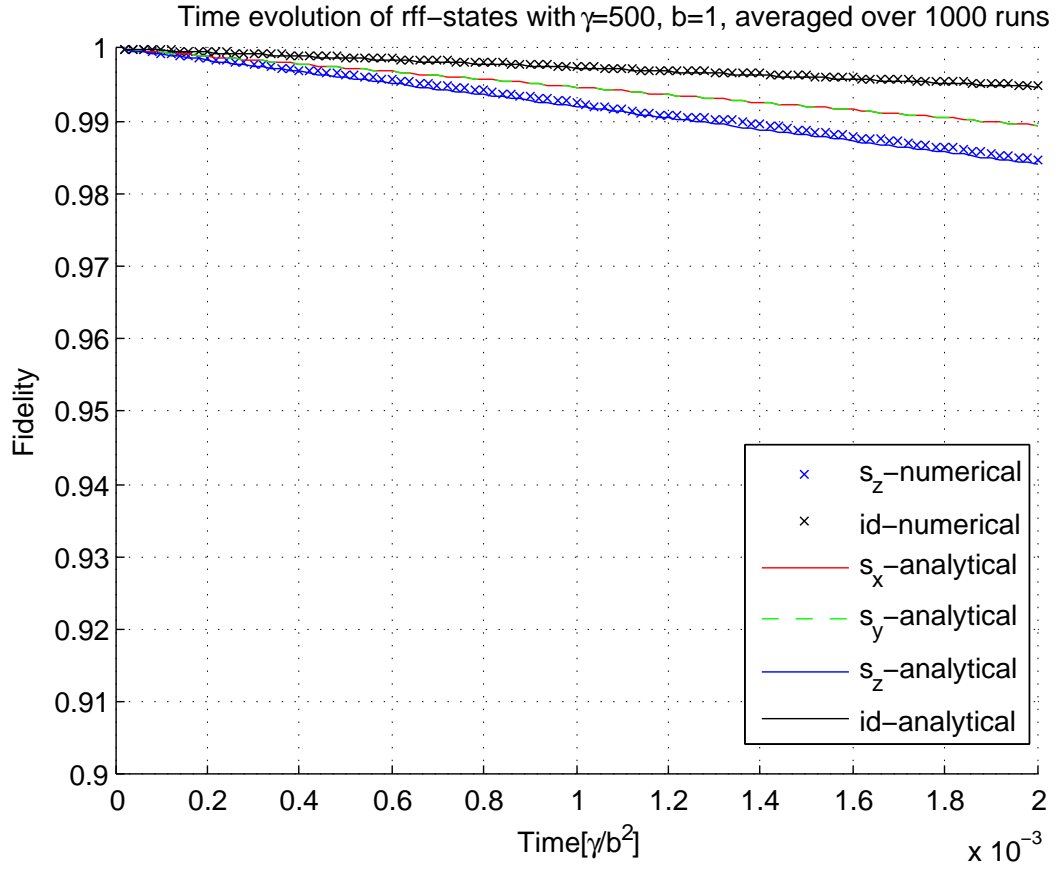


Abbildung 5.4.: Time evolution with stabilization by strong B-field.

and caused by the B-field created by a magnetic dipole:

$$\vec{B}(x, y, z) = \frac{\mu_0}{4\pi} \frac{3\vec{r}(\vec{\mu} \cdot \vec{r}) - \vec{\mu}r^2}{r^5}. \quad (5.91)$$

Here A and B refer to different atoms, r is the distance between them and \hat{r} is the unit vector pointing from one atom to the other. For $\mu = \frac{\mu_B}{2} g_e$ and a setup of the three atoms sitting in a clockwise numbering in an equilateral triangle of distance r in the xy -plane we get the result for H_{internal} :

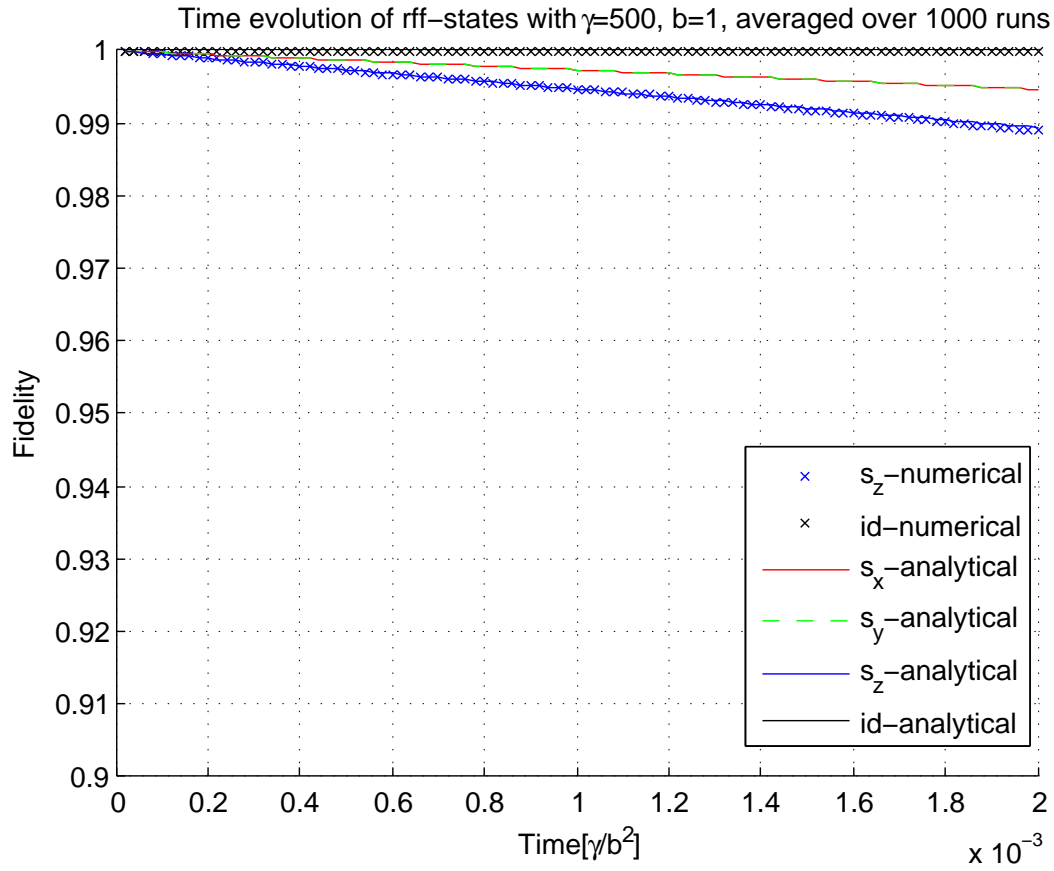


Abbildung 5.5.: Time evolution with stabilization by both methods.

$$H_{\text{internal}} = \frac{\mu_0 \mu_B^2 g_e^2}{16\pi r^3} \begin{pmatrix} 3 & 0 & 0 & 0 & 0 & 0 & 0 & 3\sqrt{3} \\ 0 & 3 & 0 & -3\sqrt{3} & 0 & 0 & 0 & 0 \\ 0 & 0 & -3 & 0 & 0 & 0 & 0 & 0 \\ 0 & -3\sqrt{3} & 0 & 0 & 0 & 0 & 0 & 0 \\ 0 & 0 & 0 & 0 & 0 & 0 & 0 & 0 \\ 0 & 0 & 0 & 0 & 0 & -3 & 0 & 0 \\ 0 & 0 & 0 & 0 & 0 & 0 & 0 & 0 \\ 3\sqrt{3} & 0 & 0 & 0 & 0 & 0 & 0 & 0 \end{pmatrix}. \quad (5.92)$$

5. Methods, results and possible experiment

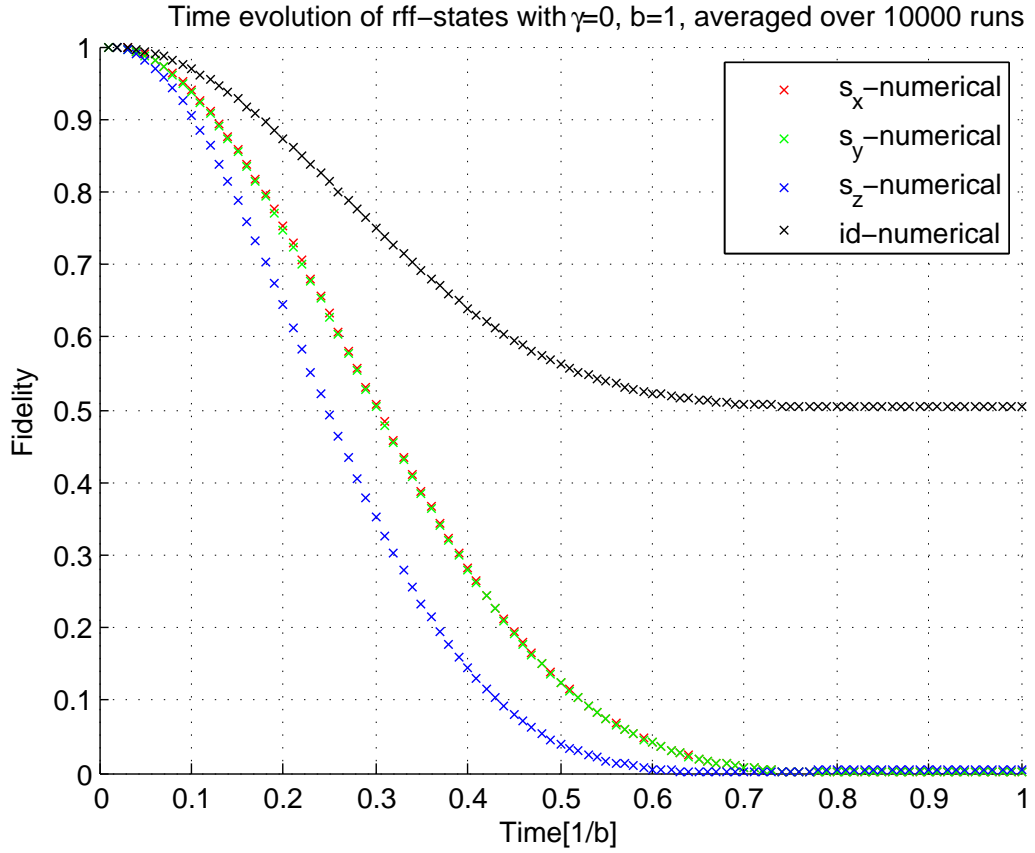


Abbildung 5.6.: Decay with $\gamma = 0$

Inserting the numerical values we get a prefactor

$$E_{\text{internal}} = \frac{\mu_0 \mu_B^2 g_e^2}{16\pi r^3} = 8.6 \cdot 10^{-54} \text{ Jm}^3 \cdot \frac{1}{r^3}. \quad (5.93)$$

A realistic value of r is about an optical wavelength.¹

The matrix is written down in the basis numbered as in section 4.3. In this basis all states in the spin- $\frac{1}{2}$ -subspace, which encodes the qubit, have the same energy and there is no transition between them. Four states of the matrix are eigenstates already and the remaining four

¹E.g. if $r = 100\text{nm}$ we get $E_{\text{internal}}/\hbar = 86\text{Hz}$.

by four matrix can be decomposed into two two-dimensional subspaces with no transitions between them. The time evolution for arbitrary two dimensional quantum systems of this form was already given above in Rabi's equation (4.23).

As there are only transitions between states of different m this can again be suppressed by a strong overall field in z -direction, in analogy to section 4.5.2. In the internal interaction case the decay can even be completely suppressed. Without an external field the transition is strong as the off-diagonal elements are big compared to the diagonal elements. The maximal value of $|c_2|^2$ is $\frac{27}{27.75} \approx 1$ for both transitions in that case. This result shows that we need a bias field to suppress the decay resulting from internal interaction, which would otherwise even be faster than the noise induced decay.

6. Entanglement in 2-qubit master equations

6.1. Motivation

While analyzing the master equation for the rff-qubit, we wondered whether it is possible to see from the structure of a 2-qubit Lindblad form master equation if it can entangle two initially separable qubits or not. As any mixed state is composed of pure states and entanglement monotones are subadditive [26], we may consider only pure states as initial states: If a given master equation cannot entangle any pure initial state, it can't entangle initial mixed states either.

We have not found a general classification of Lindblad equations, but some interesting examples. Let us first remind ourselves of the general form of 2-qubit master equation in Lindblad form:

$$\dot{\rho} = -\frac{i}{\hbar}[H, \rho] - \sum_{n,m=1}^{N^2-1} h_{nm}(\rho L_m^\dagger L_n + L_m^\dagger L_n \rho - 2L_n \rho L_m^\dagger), \quad (6.1)$$

where H is a Hamiltonian, $\{L_m\}$ is some orthonormal operator basis excluding the identity 1, and h_{nm} is a positive matrix. This equation is always trace preserving and completely positive [27]. The equation has a unitary part represented by H and a non-unitary part represented by the Lindblad operator \mathcal{L} , in short we can write:

$$\dot{\rho} = -\frac{i}{\hbar}[H, \rho] - \mathcal{L}\rho. \quad (6.2)$$

6.2. White noise limit of unitary evolution...

6.2.1. ...cannot entangle if:

If $\mathcal{L} = 0$ it is well known [28], that all product states remain product states during an interaction if and only if the full Hamiltonian can be factorised as

$$H(t) = H_1(t) \otimes 1 + 1 \otimes H_2(t). \quad (6.3)$$

So Hamiltonians of the general form

$$H = H_1 \otimes H_2 \quad (6.4)$$

with $H_1 \neq 1$ and $H_2 \neq 1$ are able to produce entanglement for separable initial states suitable with respect to the given Hamiltonian¹ H . But what happens if a Hamiltonian

¹For example the initial state $|\psi\rangle_1 \otimes |\psi\rangle_2$ should not be such that one of the $|\psi\rangle_j$ is an eigenstate of H_j .

6. Entanglement in 2-qubit master equations

$H = H_1 \otimes H_2$ of this form comes with a prefactor that is statistically distributed? From (5.12) we already know that if we have a unitary time evolution with Hamiltonian $\tilde{H}(t)$

$$\tilde{H}(t) = \alpha(t)H, \quad (6.5)$$

with a random variable α that has the properties

$$\begin{aligned} \forall t, i : \overline{\alpha_i(t)} &= 0 \\ \forall t > 0, \forall i, j \in \{1, \dots, N\} : \overline{\alpha_i(t)\alpha_j(0)} &= \Gamma \cdot \delta_{ij} e^{-\Gamma t} \end{aligned} \quad (6.6)$$

and if Γ is sufficiently large, this unitary time evolution can be approximated by the non-unitary Lindblad term

$$\mathcal{L}\rho = 2 \left(H\rho H - \frac{1}{2}H^2\rho - \frac{1}{2}\rho H^2 \right) dt. \quad (6.7)$$

If now H has the property

$$H^2 \propto 1 \quad (6.8)$$

and is of the form (6.4), which is both fulfilled for example by

$$H = \vec{b}_1 \cdot \vec{\sigma} \otimes \vec{b}_2 \cdot \vec{\sigma}, \quad (6.9)$$

we can solve the master equation explicitly. For arbitrary initially separable states ρ_0 we define

$$\rho_1 = \frac{H\rho_0 H}{\text{tr}(H\rho_0 H)} \quad (6.10)$$

and get the equation of motion:

$$\rho(t) = \frac{1}{2} \left(1 + e^{-\kappa t} \right) \rho_0 + \frac{1}{2} \left(1 - e^{-\kappa t} \right) \rho_1. \quad (6.11)$$

By definition ρ_0 is separable and thus $\rho_1 \propto H\rho_0 H$ must also be separable because $H = H_1 \otimes H_2$. We see that $\rho(t)$ is always a mixture of separable states and thus separable itself. To get more understanding for this result we solve the equation again with a different method, which only refers to α and does not involve any approximations. Let

$$A(t) = \int_0^t dt \alpha(t) \quad (6.12)$$

denote the integrated α -distribution and \mathbb{P} denote the probability measure. As $A(t)$ is symmetric, i.e.

$$\forall t : \mathbb{P}(A = x) = \mathbb{P}(A = -x), \quad (6.13)$$

the solution of the master equation can be written as

$$\begin{aligned} \rho(t) &= \int_{-\infty}^{\infty} d\mathbb{P} e^{iA(t)H} \rho(0) e^{-iA(t)H} \\ &= \int_0^{\infty} d\mathbb{P} \left(e^{iA(t)H} \rho(0) e^{-iA(t)H} + e^{-iA(t)H} \rho(0) e^{iA(t)H} \right). \end{aligned} \quad (6.14)$$

With the notation $\rho_j = |j\rangle\langle j|$ we use $H^2 \propto 1$ to conclude

$$\forall x \in \mathbb{R} : e^{-ixH} \rho_0 e^{ixH} = (\cos(x \|H\|) |0\rangle - i \sin(x \|H\|) |1\rangle) (\dots)^\dagger \quad (6.15)$$

and so the relative phases between $|0\rangle$ and $|1\rangle$ in the integrand of (6.14) cancel,

$$e^{-ixH} \rho_0 e^{ixH} + e^{ixH} \rho_0 e^{-ixH} = \cos^2(x \|H\|) \rho_0 + \sin^2(x \|H\|) \rho_1, \quad (6.16)$$

and so $\rho(t)$ is the integral over separable states and thus separable.

6.2.2. ...does entangle:

As equation (6.9) is already a quite general class of Hamiltonians one might want to generalize this result to all 2-qubit-Hamiltonians of the form of equation (6.4). However this is not possible as the following counter example shows:

Consider the Hamiltonian

$$H = (1 + \sigma_x) \otimes (1 + \sigma_x) \quad (6.17)$$

with initial state

$$\psi_0 = |\uparrow\downarrow\rangle. \quad (6.18)$$

Now a Lindblad time evolution of the form (6.7) does create entanglement. We define $\tau := A(t)$, the vectors

$$\begin{aligned} |a\rangle &:= (|\uparrow\uparrow\rangle + |\uparrow\downarrow\rangle + |\downarrow\uparrow\rangle + |\downarrow\downarrow\rangle)/4 \\ |b\rangle &:= (-|\uparrow\uparrow\rangle + 3|\uparrow\downarrow\rangle - |\downarrow\uparrow\rangle - |\downarrow\downarrow\rangle)/4 \\ |\psi(\tau)\rangle &:= e^{i\tau} |a\rangle + |b\rangle, \end{aligned} \quad (6.19)$$

the density matrix $\vartheta_\tau := |\psi(\tau)\rangle\langle\psi(\tau)|$ and the density function $f(t, \tau)$ resulting from the distribution of α . The solution of the master equation can be derived with the same method as before to obtain:

$$\rho(t) = \int_{-\infty}^{\infty} d\tau f(t, \tau) \vartheta_\tau. \quad (6.20)$$

As $f(\tau) \bmod 2\pi$ converges to a uniform distribution for $t \rightarrow \infty$, the phase factor $e^{i\tau}$ in (6.19) becomes random and the steady state is entangled:

$$\rho(\infty) = |a\rangle\langle a| + |b\rangle\langle b|. \quad (6.21)$$

Let us compare this result to section 6.2.1:

In both cases entanglement builds up, (for $\tau \bmod \pi \neq 0$) if there is enough information on the phase $\tau = A(t)$, for example via some ρ -independent measurement on τ . (A more simple case of such knowledge is $\tau = t$, representing ordinary unitary time evolution.) In contrast to section 6.2.1, such knowledge is not crucial for entanglement in our counterexample, where $\tau(\infty)$ is uniformly distributed in $[0, 2\pi]$.

Note that $H = (1 + \sigma_x) \otimes (1 + \sigma_x)$ differs from $H = \sigma_x \otimes \sigma_x$ only by the sum of local (!) Hamiltonians $(1 + \sigma_{1x} + \sigma_{2x})$. With this modification entanglement is possible even if τ is unknown.

6.3. Inhibition of entanglement by noise

Let us look at a different setup: The rotational invariant Hamiltonian

$$H = \omega \sum_{j=x,y,z} \sigma_{1j} \otimes \sigma_{2j} \quad (6.22)$$

can be written in the basis $\{|\uparrow\uparrow\rangle, |\uparrow\downarrow\rangle, |\downarrow\uparrow\rangle, |\downarrow\downarrow\rangle\}$ as a matrix:

$$H = \omega \begin{pmatrix} 1 & 0 & 0 & 0 \\ 0 & -1 & 2 & 0 \\ 0 & 2 & -1 & 0 \\ 0 & 0 & 0 & 1 \end{pmatrix}. \quad (6.23)$$

Thus a unitary time evolution would leave initial states in the $\{|\uparrow\uparrow\rangle, |\downarrow\downarrow\rangle\}$ -sector unentangled and entangle states that have a nonzero amplitude in the $\{|\uparrow\downarrow\rangle, |\downarrow\uparrow\rangle\}$ -sector. If however noise is added to the time evolution in form of the Lindblad term \mathcal{L} with

$$\mathcal{L}\rho = -\gamma(\rho + 1/4) \quad (6.24)$$

the formation of entanglement can be completely inhibited if the ratio $\frac{\gamma}{\omega}$ is sufficiently large. Note that this Lindblad term is also rotationally invariant and we could also write it in a more elaborate way to fit the form of (6.1),

$$\mathcal{L}\rho = -\gamma \sum_j \left(A_j^2 \rho + \rho A_j^2 - 2A_j \rho A_j \right), \quad (6.25)$$

with

$$A_j \in \{\sigma_{ik}, \sigma_{1k} \otimes \sigma_{2l}\}, i \in \{1, 2, 3\}, l, k \in \{x, y, z\}. \quad (6.26)$$

As the resulting master equation is rotationally invariant we can restrict our study to initial states

$$\rho_0 = (a |\uparrow\uparrow\rangle + b |\uparrow\downarrow\rangle) (a \langle\uparrow\uparrow| + b \langle\uparrow\downarrow|) \quad (6.27)$$

with $a, b \in \mathbb{R}$. As the effect of H on $|\uparrow\uparrow\rangle$ is only a relative phase, we can further set $a = 0$ and $b = 1$ for the initial state that reaches the maximum amount of entanglement possible for any ω and γ . The solution of the master equation with this initial state is:

$$\rho(t) = e^{-\gamma t} \begin{pmatrix} 0 & 0 & 0 & 0 \\ 0 & \cos^2(2\omega t) & -i \sin(2\omega t) \cos(2\omega t) & 0 \\ 0 & i \sin(2\omega t) \cos(2\omega t) & \sin^2(2\omega t) & 0 \\ 0 & 0 & 0 & 0 \end{pmatrix} + \frac{1}{4} (1 - e^{-\gamma t}). \quad (6.28)$$

To fulfill the Peres-Horodecki criterion [29, 30] the partial transpose of $\rho(t)$ must have at least one non-zero eigenvalue. As we can read of from $\rho(t)$ it is fulfilled if and only if

$$\frac{1}{4} (1 - e^{-\gamma t}) < e^{-\gamma t} \sin(2\omega t) \cos(2\omega t). \quad (6.29)$$

Thus entanglement will temporarily arise if and only if

$$\omega > \frac{\gamma}{8}, \quad (6.30)$$

while in the limit $t \rightarrow \infty$ the state is totally mixed (and separable) for any $\gamma > 0$.

This result can be generalized:

For any uniformly bounded master equation operator $M_0(t)$ with

$$\begin{aligned} \dot{\rho}(t) &= M_0(t)\rho(t) \\ \exists m \forall t : \|M_0(t)\| &\leq m \end{aligned} \quad (6.31)$$

there exists a $\gamma_0 > 0$ such that for all $\gamma > \gamma_0$ the master equation operator

$$M = M_0 + \mathcal{L} \quad (6.32)$$

with

$$\mathcal{L}\rho = -\gamma \left(\rho + \frac{1}{\text{tr}(1)} \right) \quad (6.33)$$

never entangles initially separable states for all times t .

Proof:

Let M_0 denote the operator of the original master equation and for a given initial state ρ_0 the solution of (6.31) is denoted as $\rho_0(t)$. Now M_0 is a bounded operator and $\rho_0(t)$ is a positive, finite dimensional operators with $\text{tr}(\rho) = 1$ for any time t and thus uniformly bounded by a constant r :

$$\exists r \forall t : \|\rho_0(t)\| \leq r. \quad (6.34)$$

Consequently, using Cauchy-Schwarz inequality, also the derivative $\dot{\rho}_0(t)$ is uniformly bounded,

$$\exists m, r \forall t : \|\dot{\rho}_0(t)\| \leq \|M_0(t)\| \|\rho_0(t)\| \leq mr, \quad (6.35)$$

and we find a time dependent upper bound for $\epsilon(t) = \rho_0(t) - \rho_0(0)$:

$$\exists m, r \forall t : \|\epsilon(t)\| = \left\| \int_0^t \dot{\rho}_0(t) dt \right\| \leq mrt. \quad (6.36)$$

Using triangle inequality we also find a time independent bound:

$$\exists r \forall t : \|\epsilon(t)\| \leq \|\rho_0(t)\| + \|\rho_0(0)\| \leq 2r. \quad (6.37)$$

The solution of the full master equation with operator M is

$$\begin{aligned} \rho(t) &= e^{-\gamma t} \rho_0(t) + \left(1 - e^{-\gamma t}\right) \frac{1}{\text{tr}(1)} \\ &= e^{-\gamma t} \rho_0(0) + e^{-\gamma t} \epsilon(t) + \left(1 - e^{-\gamma t}\right) \frac{1}{\text{tr}(1)}. \end{aligned} \quad (6.38)$$

The first term in the sum is separable by definition. The second two terms of the sum can be written as

$$\left(1 - e^{-\gamma t}\right) \left(\frac{1}{\text{tr}(1)} + f_\gamma(t) \epsilon(t) \right) \equiv \left(1 - e^{-\gamma t}\right) \left(\frac{1}{\text{tr}(1)} + \rho_1(t) \right) \quad (6.39)$$

6. Entanglement in 2-qubit master equations

with

$$f_\gamma(t) = \frac{e^{-\gamma t}}{(1 - e^{-\gamma t})}. \quad (6.40)$$

We now show that

$$\forall \delta > 0 \exists \gamma_0 \forall \gamma > \gamma_0 \forall t : \|\rho_1(t)\| < \delta, \quad (6.41)$$

and so after choosing γ big enough, $\frac{1}{tr(1)} + \rho_1(t)$ is within the separable neighborhood of $\frac{1}{tr(1)}$, which was established in [31].

For a given t_0 we use two upper bounds for f_γ :

As $f_\gamma \xrightarrow{\gamma \rightarrow \infty} 0$ uniformly with respect to $t > t_0$ we can derive an estimate for large values of t :

$$\exists \gamma_0 \forall t > t_0, \gamma > \gamma_0 : f_\gamma(t) < t_0. \quad (6.42)$$

Using the convexity of $e^{-\gamma t}$ we also get an estimate for small times:

$$\forall \gamma > \frac{2}{t_0} \forall t < t_0 : f_\gamma(t) < \frac{t_0}{t}. \quad (6.43)$$

Combining equation (6.36) with equation (6.43) and equation (6.37) with equation (6.42) we get

$$\forall t_0 \exists \gamma_0 \forall \gamma > \gamma_0 \forall t : \|\rho_1(t)\| < \max(2rt_0, mrt_0). \quad (6.44)$$

7. Conclusion and Outlook

In the first part of the thesis we first reviewed the articles on the Landau-Zener jump time by Vitanov [10] in section 2.6 and compared it to the time evolution of the Wannier-Stark system as a function of the parameters a and V in section 3.3. For small values of V and a the Landau-Zener model describes our system very well. However to resolve the resonances in the long time decay rate γ and the Zeno parameter Z we need to consider at least 3 energy bands.

As Niu's paper [7], reviewed in section 2.7, uses a 2 state description, we realized that we cannot use it to describe γ and Z . In addition due to the approximation used in section 2.7.4 we cannot use it to resolve the steplike substructure on the exponential decay.

That is why we decided to start with the full Hamiltonian in section 3.1, adjust it to the Pisa experiment in section 3.2, approximate it with a large but finite number of states for the numerical implementation in section 3.3, and only in the final step, after calculating the Floquet operator $U_\kappa(T_{\text{Bloch}})$, approximate this operator with a 2×2 matrix $U_\kappa^{\text{red}}(T_{\text{Bloch}})$ in section 3.4 within a reasonable set of parameters.

The results obtained in sections 3.1-3.3 were then used to calculate the time evolution, especially in the adiabatic basis, for the Pisa experiment in Tayebirad et al. [3]. However as mentioned in section 3.2.6 a definite statement can only be made as soon as we know the details of the experimental measurement procedure. The matrix U_κ^{red} explains the resonances in γ and Z and can be used to manipulate the resonances with an altered time evolution as described in section 3.4.3. Possibly a further experiment making use of this modification could be done in Pisa. The relation of the resonances to Zeno effect is explained in section 3.4.3.

An idea that could be interesting to study in the future is to modify the time evolution not only by pausing the acceleration in the way we proposed, but to optimize $a(t)$ or $V(t)$ as a function of time to achieve a desired final state $|\psi_f\rangle$. For example Krotov algorithm [32] could be used to calculate the optimal $a(t)$ and $V(t)$ for a given $|\psi_f\rangle$.

While in this first part of the thesis the Hamiltonian $H(t)$ was under our control and we wanted to induce a decay of the ground state fidelity on purpose, in the second part $H(t)$ is a random function of time, as our system was coupled to an uncontrollable environment. Thus instead of a wave function $|\psi\rangle$ we describe the system with a density matrix ρ and the time evolution of the system is described by an effective master equation instead of the Schrödinger equation.

For the decoherence study of the rotation frame free qubit (rff-qubit) we derived this master equation for the white noise limit in section 5.1 and introduced a numerical scheme with error estimation in section 5.5 to simulate the fidelity decay due to random magnetic fields

7. Conclusion and Outlook

in various physical setups of the rff-construction. In the white noise regime the results of both methods are in good agreement and also agree with the perturbation theory based calculations done by Han Rui. The numerical scheme also allows the calculation of strongly time correlated noise. In section 5.3 we checked that the results don't depend the details of incorporating the spatial correlations.

We found that the setup can be stabilized by a bias magnetic field with $B \gg \gamma, b$ and to some extent by monitoring the value of j with a measuring frequency $f \gg \gamma, b$. This stabilization is also needed to suppress the internal interaction of the atoms. The time scale of the decay using estimated noise parameters is sufficient for a physical implementation. Those timescales are also compared to similar setups with 2 or 4 atoms in section 5.4. In a real experiment other noise sources such as the center of mass motion of the atoms also lead to decoherence. Thus further stabilization methods like error correction codes have to be applied to achieve a long coherence time.

The next step in the study of the rff-setup is to come up with a way to encode an rff-state and identify further noise sources. Possibly we could use Rydberg blockade [33] or interaction with single photons to entangle the atoms and thereby produce an rff-state.

In the last part of the thesis we looked at some examples of master equations that can or can not generate entanglement. In section 6.2 we found that the randomization of a crucial phase can prevent the occurrence of entanglement.¹ We show that nonunitary terms in master equation of the form $H = H_1 \otimes H_2$ that seem to generate entanglement on first look, do not entangle if $H^2 = 1$. In section 6.3 we start with an arbitrary master equation and show that adding enough noise will completely inhibit the generation of entanglement. The conditions for this entanglement inhibition can still be slightly generalized. It would be very interesting to find out whether simple criteria exist that can be used to tell whether a given master equation can generate entanglement or not.

We have studied two systems which were out of reach of experimental control only a few years ago. In the future even narrower distributions in momentum space could be achieved for the BEC system and also even better control and shielding of single atoms will be possible, so that the predictions of this thesis can be tested with higher precision.

¹This is a similar mechanism as the phase randomization in section 3.4.3 that simulates a Zeno measurement.

Literaturverzeichnis

- [1] I. Bloch, J. Dalibard, and W. Zwerger, “Many-body physics with ultracold gases,” *Reviews of Modern Physics*, vol. 80, no. 3, pp. 885–964, 2008.
- [2] A. Zenesini, “1. Time-resolved measurement of Landau-Zener tunneling in periodic potentials A. Zenesini, H. Lignier, G. Tayebirad, J. Radogostowicz, D. Ciampini, R. Manella, S. Wimberger, O. Morsch, E. Arimondo *Phys. Rev. Lett.* 103, 090403 (2009)
2. Trap modulation spectroscopy of the Mott-insulator transition in optical lattices, H. Lignier, A. Zenesini, D. Ciampini, O. Morsch, E. Arimondo, S. Montangero, G. Pupillo, R. Fazio,” *Phys. Rev. Lett*, vol. 103, p. 090403, 2009.
- [3] G. Tayebirad, A. Zenesini, D. Ciampini, R. Mannella, O. Morsch, E. Arimondo, N. Lörch, and S. Wimberger, “Time-resolved measurement of landau-zener tunneling in different bases,” *Phys. Rev. A*, vol. 82, p. 013633, Jul 2010.
- [4] J. Feldmann, K. Leo, J. Shah, D. Miller, J. Cunningham, T. Meier, G. Von Plessen, A. Schulze, P. Thomas, and S. Schmitt-Rink, “Optical investigation of Bloch oscillations in a semiconductor superlattice,” *Physical Review B*, vol. 46, no. 11, pp. 7252–7255, 1992.
- [5] K. Leo, P. Bolivar, F. Brüggemann, and R. Schwedler Klaus, “Observation of Bloch oscillations in a semiconductor superlattice,” *Solid State Communications*, vol. 84, no. 10, pp. 943–946, 1992.
- [6] S. Wilkinson, C. Bharucha, M. Fischer, K. Madison, Q. Niu, B. Sundaram, and M. Raizen, “Experimental evidence for non-exponential decay in quantum tunnelling,” *Nature*, vol. 387, pp. 575–577, 1997.
- [7] Q. Niu and M. Raizen, “How Landau-Zener tunneling takes time,” *Physical review letters*, vol. 80, no. 16, pp. 3491–3494, 1998.
- [8] L. Landau, “Zur Theorie der Energieübertragung. II,” *Phys. Z. Sowjetunion*, vol. 2, p. 46, 1932.
- [9] C. Zener, “Non-adiabatic crossing of energy levels,” *Proceedings of the Royal Society of London. Series A, Containing Papers of a Mathematical and Physical Character*, vol. 137, no. 833, pp. 696–702, 1932.
- [10] N. Vitanov, “Transition times in the Landau-Zener model,” *Physical Review A*, vol. 59, no. 2, pp. 988–994, 1999.

- [11] M. Holthaus, “Bloch oscillations and Zener breakdown in an optical lattice,” *Journal of Optics B: Quantum and Semiclassical Optics*, vol. 2, p. 589, 2000.
- [12] C. Sias, A. Zenesini, H. Lignier, S. Wimberger, D. Ciampini, O. Morsch, and E. Arimondo, “Resonantly enhanced tunneling of Bose-Einstein condensates in periodic potentials,” *Physical review letters*, vol. 98, no. 12, p. 120403, 2007.
- [13] D. Lidar and K. Birgitta Whaley, “Decoherence-free subspaces and subsystems,” *Irreversible Quantum Dynamics*, pp. 83–120, 2003.
- [14] J. Suzuki, G. Tabia, and B. Englert, “Symmetric construction of reference-frame-free qudits,” *Physical Review A*, vol. 78, no. 5, p. 52328, 2008.
- [15] M. Marder, “Condensed matter physics,” *Cambridge Monographs on Physics*, 2000.
- [16] H. Ibach and H. Lüth, *Festkörperphysik: Einführung in die Grundlagen*. Springer, 2008.
- [17] H. Amann, *Gewöhnliche Differentialgleichungen*. Walter de Gruyter, 1995.
- [18] Q. Niu, X. Zhao, G. Georgakis, and M. Raizen, “Atomic Landau-Zener tunneling and Wannier-Stark ladders in optical potentials,” *Physical review letters*, vol. 76, no. 24, pp. 4504–4507, 1996.
- [19] D. Griffiths, *Introduction to Quantum Mechanics*. Englewood Cliffs, NJ: Prentice Hall, 1995.
- [20] P. Facchi and S. Pascazio, “Unstable systems and quantum Zeno phenomena in quantum field theory,” in *Fundamental aspects of quantum physics: proceedings of the Japan-Italy Joint Workshop on Quantum Open Systems, Quantum Chaos and Quantum Measurement: Waseda University, Tokyo, Japan, 27-29 September 2001*, p. 222, World Scientific Pub Co Inc, 2003.
- [21] A. Zenesini, C. Sias, H. Lignier, Y. Singh, D. Ciampini, O. Morsch, R. Mannella, E. Arimondo, A. Tomadin, and S. Wimberger, “Resonant tunneling of Bose-Einstein condensates in optical lattices,” *New Journal of Physics*, vol. 10, p. 053038, 2008.
- [22] B. Misra and E. Sudarshan, “The Zeno paradox in quantum theory,” *Journal of Mathematical Physics*, vol. 18, no. 4, p. 756, 1977.
- [23] M. Fischer, B. Gutiérrez-Medina, and M. Raizen, “Observation of the quantum Zeno and anti-Zeno effects in an unstable system,” *Physical Review Letters*, vol. 87, no. 4, p. 40402, 2001.
- [24] J. Sakurai and S. Tuan, *Modern quantum mechanics*. Addison-Wesley Reading (Mass.), 1994.
- [25] C. Gardiner, “Handbook of stochastic methods: for physics, chemistry & the natural sciences,(Series in synergetics, Vol. 13),” 2004.

- [26] G. Vidal and J. Mod, “Opt. 47, 355 (2000),” *Arxiv preprint quant-ph/9807077*.
- [27] R. Alicki and K. Lendi, “Quantum dynamical semigroups and applications,” in *Quantum Dynamical Semigroups and Applications*, vol. 286, 1987.
- [28] T. Durt, “Quantum entanglement, interaction, and the classical limit,” *Arxiv preprint quant-ph/0401121*, 2004.
- [29] A. Peres, “Separability criterion for density matrices,” *Physical Review Letters*, vol. 77, no. 8, pp. 1413–1415, 1996.
- [30] M. Horodecki, P. Horodecki, and R. Horodecki, “Separability of mixed states: necessary and sufficient conditions,” *Physics Letters A*, vol. 223, no. 1-2, pp. 1–8, 1996.
- [31] K. Życzkowski, P. Horodecki, A. Sanpera, and M. Lewenstein, “Volume of the set of separable states,” *Physical Review A*, vol. 58, no. 2, pp. 883–892, 1998.
- [32] V. Krotov, *Global methods in optimal control theory*. Marcel Dekker Inc, 1996.
- [33] H. Weimer, M. Müller, I. Lesanovsky, P. Zoller, and H. Büchler, “A Rydberg quantum simulator,” *Nature Physics*, 2010.

Erklärung:

Ich versichere, daß ich diese Arbeit selbständig verfaßt und keine anderen als die angegebenen Quellen und Hilfsmittel benutzt habe.

Heidelberg, den 30.08.2010

.....

(Unterschrift)